International Pacific Research Center

April 2008–March 2009 Report

School of Ocean and Earth Science and Technology
University of Hawai‘i at Mānoa

CONTENTS

Editor: Gisela E. Speidel, PhD
Japanese Translator: Keiko Tokinaga
Cover Photo: Gisela E. Speidel, PhD
Design: Susan Yamamoto

THE INTERNATIONAL PACIFIC RESEARCH CENTER

Conceived under the "US–Japan Common Agenda for Cooperation in Global Perspective," the International Pacific Research Center (IPRC) was established in 1997 within the School of Ocean and Earth Science and Technology at the University of Hawai'i at Mānoa. The IPRC mission is "To provide an international research environment dedicated to improving mankind's understanding of the nature and predictability of climate variations and change in the Asia-Pacific region, and to developing innovative ways to utilize knowledge gained for the benefit of society." The core support for the IPRC comes from the State of Hawai'i through the University and from the principal supporting agencies: the Japan Agency for Marine-Earth Science and Technology (JAMSTEC), NASA and NOAA. Financial support for our research is also provided by other government agencies in the US and abroad. The IPRC now has an annual budget of roughly 7 million dollars.

Asia and the Pacific region are home to over half the world's people, all of whom are affected by variations in the climate system. IPRC researchers conduct modeling and diagnostic studies to document these variations and understand their causes, whether such causes are purely natural or have a human component. Through advances in basic research, the IPRC contributes to improving environmental forecasting for the Asia-Pacific region. One focus of IPRC investigations is the understanding of key phenomena rooted in the tropics, such as the El Niño-Southern Oscillation of the ocean-atmosphere system, monsoon circulations, interannual variability in the Indian Ocean, intraseasonal oscillations of the tropical atmosphere, and tropical cyclones. Other examples of important issues for IPRC study include the nature of decadal variability in the extratropical North Pacific Ocean, the dynamics of the very strong Kuroshio and Oyashio ocean currents in the western North Pacific and the role of marginal seas in the climate system. Concerns about climate change are addressed through modeling studies of past climate and through assessment of model predictions for future trends in climate.

国際太平洋研究センター

国際太平洋研究センター（IPRC）は、「地球的展望に立った協力のための日米共通課題」のもと、1997年にハワイ大学マノア校の海洋地球科学技術学部内に設立されました。その使命は、「国際色豊かな研究環境を創り、アジア・太平洋地域の気候変動及び変化について、その性質と予測可能性に対する人類の理解を向上させ、そして得られた知見を社会に役立てるために活用する革新的な手段を生み出すこと」です。IPRCの研究費は主に、ハワイ大学を通してハワイ州から、また主要支援機関である海洋研究開発機構、NASA、NOAAから支援されています。内外のその他の政府機関からも支援を受けており、現在およそ七百万ドルの年間予算により運営しています。

アジア・太平洋地域は世界人口の半分以上が居住する地域で、気候系の変動はこれらの人々すべてに影響を及ぼします。そのような気候変動には純粋な自然現象であるものも人類活動が関係したものもありますが、IPRCでは、それらを記述し原因を探るため、モデルによる研究や診断的研究を実施しています。このような基礎研究を進展させることでアジア・太平洋地域の環境予測の改善に大きく貢献しています。現在IPRCでは、エルニーニョ・南方振動、モンスーン循環、インド洋の経年変動、熱帯大気の季節内振動、そして熱帯低気圧といった、熱帯起源の現象に注目して研究を行っています。その他の重要な課題として、北太平洋亜熱帯域における十年規模変動の性質、西部北太平洋の強い海流である黒潮・親潮の力学、気候系での縁辺海の役割に関する研究を行っています。さらに、過去の気候のモデル研究やモデルによる将来予測の評価により、気候変化に関する様々な課題に取り組んでいます。

FOREWORD

This report summarizes the activities of the IPRC for the period April 1, 2008 – March 31, 2009. The IPRC performs research to enhance understanding of the nature and mechanisms of climate variability and change, and to improve the tools for modeling and forecasting the climate system. IPRC activities continue to grow in concert with increasing public interest in understanding the climate system and its impacts on society. The IPRC now has a scientific staff of over 60, consisting of faculty, researchers, postdoctoral fellows and extended-term scientific visitors. IPRC faculty also supervise several graduate students in the Meteorology and Oceanography departments of the University of Hawai'i. Even this extensive *Annual Report* can describe only a fraction of the ongoing research at IPRC. Here I will touch on just a few highlights of the impressive body of research achievements over the past year.

Many of the most important problems in meteorology and oceanography involve strongly nonlinear interactions across a wide range of space and time scales. The range of scales involved makes detailed observational diagnostic study nearly impossible, and the nonlinearity makes simplified theoretical treatments particularly challenging. The availability of ultra-fine resolution models that allow explicit simulation of a wide range of scales of motion provides one approach to studying some of these difficult problems. Interest at IPRC in analyzing ultra-fine resolution simulations of the atmosphere and ocean has coincided with the important model developments in this area by our JAMSTEC partners. In the past year, we have collaborated with JAMSTEC colleagues on a number of studies employing high-resolution simulations conducted on the JAMSTEC Earth Simulator. Some highlights of this work include a detailed study of the lifecycle of tropical cyclones simulated in a very fine resolution simulation with the Non-hydrostatic ICosahedral Atmospheric Model (NICAM). The NICAM results allowed a detailed diagnosis of the interaction between cyclone-scale and larger-scale flow. An analysis of the Madden–Julian Oscillation as it appears in an extended NICAM simulation showed a potential forecast skill with a lead time in the order of one month. This result supports other recent developments at IPRC and elsewhere suggesting that improved modeling of the evolution of organized tropical convection in the Asian and Pacific region may be the key to unlocking extended-range weather predictability. Results from high-resolution simulations of global ocean circulation using the Ocean General Circulation Model for the Earth Simulator (OFES) have helped inspire simpler theoretical studies at the IPRC that deal with the dynamics of the subtropical undercurrent in the South Indian Ocean and the Kuroshio Extension northern recirculation gyre.

We made progress on understanding the dynamics of regional climate features. A diagnostic study was conducted on the Meiyu-Baiu rainband, which is such a prominent circulation feature over China and Japan in late spring and early summer. The results emphasize the role of the mid-tropospheric jet stream flow in forming the rainband and suggest that the seasonal migration of the jet stream may determine the beginning and end of the Maiyu period. Another observational study showed that the state of the tropical Indian Ocean has a systematic effect on the amplitude attained by El Niño events in the Pacific, suggesting that dynamical forecast models for El Niño need to include a realistic representation of air – sea coupling over the entire Indo-Pacific warm pool.

Much of our work is motivated by the ultimate goal of improving forecasts of the long-term response of the climate system to expected human impacts, with a focus on possible climate change in Asia-Pacific. We have analyzed global warming experiments conducted with current coupled climate models to understand the projected changes in the hydrological cycle by diagnosing the perturbations to the oceanic surface energy balance that controls evaporation. We have also analyzed results of global warming simulations to determine the expected changes in thermal and dynamical factors that control maximum tropical cyclone intensity. Since understanding the nature of very significant climate changes that have occurred in the past can provide insights into the natural variability and forced responses of the climate system, an important component of our work is investigation of paleoclimate variations. A study examining the causes of the cycle of dry and humid periods observed in the Sahel/Sahara regions of Africa has identified both orbital-driven variations in summer insolation and the evolution of

Northern Hemisphere ice sheets as key elements in the dynamics of this remarkable climate variation.

Through our Asia-Pacific Data-Research Center (APDRC), we operate a web-based data-server system that makes data resources readily accessible to IPRC researchers, the international climate community and the wider public. Over the last year the APDRC continued to expand its data holdings and server capabilities. The APDRC now derives from extensive ARGO float observations a variety of three-dimensional, monthly mean gridded ocean circulation products, including temperature, salinity and dynamic topography.

The IPRC was founded in 1997 as a US–Japan center of collaboration in climate science. Our Japanese partnership, now focused on joint projects with JAMSTEC, remains central to IPRC's mission. This year marked the completion of the activities under the 2004–2009 IPRC Cooperative Agreement between JAMSTEC and the University of Hawai'i, and the negotiation and implementation of a new Cooperative Agreement covering the next five years (2009–2014). We are grateful to the leadership of JAMSTEC, as well as to our primary U.S. supporting agencies, NOAA and NASA, for their continuing commitment to the IPRC as a center for deep and enduring international collaboration in climate science.

Kevin P. Hamilton, PhD
Interim Director

はじめに

本冊子では、国際太平洋研究センター(IPRC)における、2008年4月1日から2009年3月31日までの活動概要を報告します。IPRCでの研究活動は、気候変動の性質とそのメカニズムに対する理解を深め、気候系のモデル化と予測に必要な道具を改良するという目的のもと行われており、気候系そのものや気候が社会に及ぼす影響に一般の方々の関心が高まるのに応じて、日々発展し続けています。現在総勢60名を超える、教授陣、研究員、博士研究員、長期訪問研究員を擁し、さらに教授陣は、ハワイ大学気象学部や海洋学部の大学院生を指導しています。IPRCの活動は多岐に渡るため、この広範囲に及ぶ報告書でさえ、現在行われている研究の一部しか紹介しておりません。その内から特に目立つものを、以下に簡単に紹介します。

気象学や海洋学の重要な問題には、広範囲の時空間規模にわたる非線形相互作用が絡むものが多々あります。時空間規模の範囲が広いため、詳細な診断的観測研究は概して不可能であり、非線形性のため単純化した理論的な取り扱いは非常に困難になります。最近可能になってきた超高解像モデルは、広範囲な運動規模を陽に再現できるため、この様な難問の解決に有効です。IPRCでは、以前から大気海洋の超高解像再現実験の解析に関心を寄せており、一方で共同研究を進める海洋研究開発機構(JAMSTEC)では重要なモデル開発が進みました。この一年、JAMSTECの研究者と共同で、JAMSTECの地球シミュレータによる高解像再現実験を用い、様々な研究を行ってきました。目立った成果としては、非静力正二十面体大気モデル(NICAM)による超高解像実験で再現された熱帯低気圧のライフサイクルに関する詳細な研究があります。NICAMの再現実験結果によって、熱帯低気圧の規模と大気の大規模場の相互作用に関する詳細な診断解析が可能になったのです。また、高解像度のNICAM実験で再現されたマデン・ジュリアン振動の解析では、1ヶ月予報の精度が明らかに改善していることが分かりました。IPRCや他機関における最近の研究では、アジア・太平洋地域で組織化した熱帯対流の発達をより良くモデル化することが、長期の天候予測可能性を広げる鍵かも知れないことが示唆されていますが、NICAMの結果はこのことを支持するものです。さらに、地球シミュレータで得られた超高解像度全球海洋大循環モデル(OFES)の再現実験の結果を参照することによって、南インド洋における亜熱帯循環や黒潮続流北方再循環の力学に関わる理論的研究が進みました。

地域気候力学の理解も進みました。梅雨降水帯は、夏の初めに中国および日本上の大気循環が作り出す非常に特徴的な現象です。梅雨降水帯の形成について診断的研究を行ったところ、対流圏中層のジェット気流が大きな役割を果たしていること、また、ジェット気流の位置の季節変化が梅雨の開始と終息を決めている可能性があることが分かりました。別の観測研究では、太平洋における発達中のエルニーニョ現象の振幅に、熱帯インド洋の状態が系統的に影響を与えていることを示しました。この研究結果から、エルニーニョの力学的予測モデルには、インド・太平洋暖水塊全域における大気海洋結合を現実的に表現する必要があることが示唆されます。

IPRCの研究のかなりの部分は、将来の人間活動に対する気候系長期的応答の予測精度を向上させることを究極の目標とし、特にアジア・太平洋地域で将来起こり得る気候変化に注目しています。現在使われている結合モデルによる地球温暖化実験について、蒸発を支配している海表面のエネルギー平衡に対する摂動を診断することにより、モデルで予測された将来の水循環の変化の理由を調べました。また、熱帯低気圧の最大強度を支配している熱的および力学的要因が将来どのように変化するか調べるために、温暖化実験の解析を行いました。さらに、過去に起きた大きな気候変化は、気候系の自然変動や強制応答を理解する上での手掛かりとなり得るため、古気候変動の究明にも力をいれています。アフリカのサヘル・サハラ地域で観測された乾燥期と湿潤期の周期性の原因を調べたところ、

軌道変化による夏季太陽放射の変動と北半球の氷床変化の両方が、この変動の力学において重要な要因であることが突き止められました。

IPRC附置のアジア太平洋データ研究センター(APDRC)ではウェブ上にデータサーバを運用しており、IPRC内だけではなく世界中の気候研究者に向けて、さらには広く一般の方が容易に使える形でデータを提供しています。昨年も引き続き保有データ量とサーバ性能は拡張され、現在はアルゴフロートによる大規模な現場観測データを用いて、水温、塩分、力学高度などの、三次元月平均格子海洋データを作成しています。

IPRCは、日米共同の気候科学研究拠点として1997年に設立されました。現在も、日本との協力関係はIPRCの使命の中核を成しており、主にJAMSTECとの共同研究を行っています。今年は、JAMSTECとハワイ大学間の協力協定(2004年から2009年)の下で実施された活動の締めくくりの年であり、また、新たな五年間の協力協定(2009年から2014年)締結の年となりました。奥行きがあり持続的な気候科学の国際協力拠点として、引き続きIPRCを支援してくださるJAMSTEC及びアメリカ側の主たる支援機関であるNOAAとNASAの指導力に深く感謝いたします。

国際太平洋研究センター
暫定所長　ケビン P. ハミルトン

Chapter 1: LARGE-SCALE INDO-PACIFIC CLIMATE

Climate Modes and Predictability

The jet stream and the origin of the Meiyu–Baiu rainband. The Meiyu–Baiu rainband, stretching from central China across Japan and over 1000 miles northeastward into the Pacific, is a prominent climate phenomenon for the highly populated regions of eastern China and Japan. The low-level moist southerly winds blow throughout summer, yet the narrow rainband typically forms only during the Meiyu–Baiu season. Though the band has been known to be collocated with the jet stream during June to mid-July, the reason for this has been unclear. Past research has focused on the low-level circulation for an explanation, but heating by the rainband itself creates a low-level circulation.

This study took a different tack by looking at what is happening in the mid-troposphere. Reanalysis data at 500 hPa show that in May warm air is horizontally advected along the southern flank of the jet stream. During June, the source of warm air migrates northward from Indochina to southern Tibet, and the advection of the warm, moist air now occurs around 30–35°N over China and Japan and begins to form the Meiyu–Baiu band. The advection is downstream of the temperature maximum anchored by the Tibetan Plateau and occurs all along the rainband. It drives the large-scale motion and the low-level moist air upward, triggering heavy rainfall and diabatic heating (see Figure 1.1). The diabatic heating, in turn, favors warm advection and ascending motion downstream along the jet, strengthening the association between the jet and the rainband. Weather disturbances in the jet-stream westerly waveguide increase the probability of convection and contribute to the formation of the rainband. In mid-July the jet stream migrates north into a cooler region, ~45°N, bringing the Meiyu–Baiu season to a close.

Thus, while the summer southerly winds provide the low-level moisture, the jet stream's advection of the mid-level warm air determines the location and timing of the Meiyu–Baiu rainband. This more complete, dynamical picture should improve regional rainfall predictions. [T. Sampe, and S.-P. Xie (IPRC)]

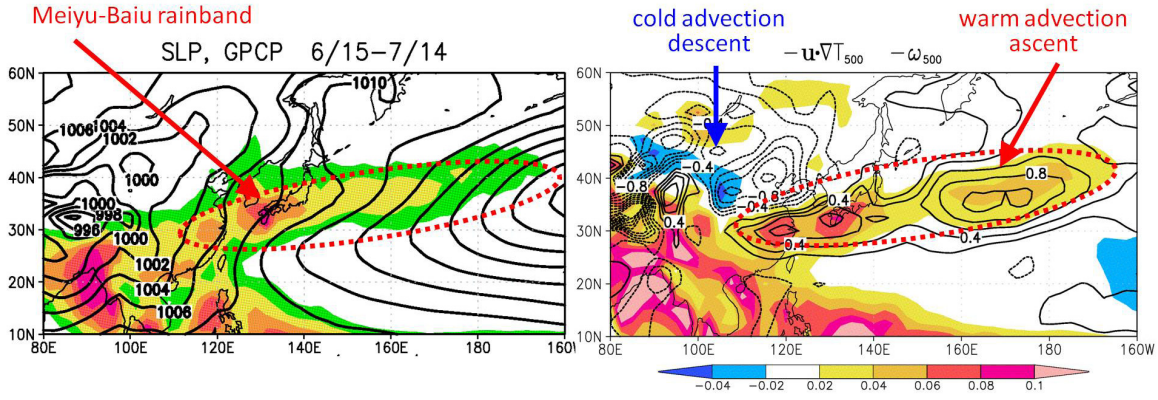

Figure 1.1. Horizontal temperature advection large-scale dynamical forcing of vertical motion. Precipitation (left, color) is associated with upward motion (right, warm colors); in the Meiyu–Baiu season, precipitation and vertical motion closely follow warm horizontal temperature advection at mid-troposphere (right, contours) over East Asia.

Air-Sea Interaction

Tropical Indian Ocean effects on East Asia and Northwest Pacific summer climate. Already in the 1980s, meteorologists noted that the Meiyu–Baiu and summer rainfall in other parts of East Asia correlate not with concurrent sea surface temperature (SST) in the equatorial Pacific but with an El Niño event that occurred two seasons before. El Niño peaks in December and by the following summer the associated SST anomalies have decayed over the equatorial Pacific. What then provides the memory of the El Niño and anchors the summer climate anomalies in East Asia? Past studies have linked these anomalies to an anomalous anticyclone circulation and suppressed atmospheric convection over the subtropical Northwest Pacific.

A 2007 collaborative study between IPRC and the Ocean University of China pointed to basin-wide warming of the tropical Indian Ocean (TIO)—induced by El Niño through teleconnective mechanisms—as the mechanism that sustains these El Niño influences. The study, based on observational analysis and coupled model experiments, proposed that El Niño warms the TIO like a battery charging a capacitor, and after El Niño has dissipated the capacitor releases its energy. Why, however, are the most pronounced anomalies of rainfall and surface circulation observed in the subtropics, not on the equator? Why is the Northern Hemisphere favored for summer anomalies?

The answer was found in tropospheric warming. During the summer following an El Niño, TIO warming heats the troposphere in towering cumulonimbus. This tropospheric warming spreads horizontally in accordance with equatorial wave dynamics discovered by T. Matsuno in 1966: west of the TIO, the warming centers occur off the equator in the form of Rossby waves, while to the east, a wedge-like Kelvin wave, trapped on the equator, penetrates the western Pacific. The tropospheric temperature anomalies resemble the solution of an equatorial wave response to an isolated heating on the equator, first obtained by A. Gill in 1980.

The Kelvin wave induces rainfall anomalies in the subtropics through friction's induced low-level flow. Accompanied by low surface pressure centered on the equator, surface friction drives southwesterly winds on the north flank of the Kelvin wave. The resultant surface divergence acts to suppress atmospheric convection in the subtropical Northwest Pacific, and the reduced latent heat release spins up an anomalous anticyclone circulation, which in turn intensifies surface divergence. The effects are concentrated on the Northwest Pacific because the major rainfall is displaced to the summer hemisphere and the Northwest Pacific is more conducive to feedback between suppressed convection and the surface anticyclone circulation. The combined Kelvin wave-induced Ekman divergence (WIED) and convective feedback explain why the TIO warming causes the reduced convective rainfall and anomalous surface anticyclone in the subtropical Northwest Pacific. Once these anomalies form in the Northwest Pacific, they excite a meridional dipolar teleconnection to affect Meiyu–Baiu, seen in the cyclonic circulation centered over Japan, a pattern called the Pacific-Japan pattern, discovered by T. Nitta in 1987.

The Kelvin WIED adjustment illustrates that because of convective feedback, moist teleconnection in the tropics can take forms very different from those expected from dry wave dynamics. More research into moist teleconnection dynamics is necessary to improve the understanding and prediction of climate variability of tropical origin. [S.-P. Xie, K. Hu, J. Hafner, H. Tokinaga, Y. Du, G. Huang, and T. Sampe, 2009: Indian Ocean capacitor effect on Indo-western Pacific climate during the summer following El Niño. *J. Climate*, **22**, 730–747. Yang, J., Q. Liu, S.-P. Xie, Z. Liu, and L. Wu, 2007: Impact of the Indian Ocean SST basin mode on the Asian summer monsoon. *Geophys. Res. Lett.*, **34**, L02708, doi: 10.1029/2006GL028571]

Clouds over the Kuroshio Extension. IPRC scientists and their colleagues have analyzed the impact of the Kuroshio Extension (KE) on the atmosphere and cloud formation. A synthesis of high-resolution observations from JAMSTEC, JMA, JFA, and SIO ships together with measurements from different satellite instruments reveals the three-dimensional structure of the ocean and atmosphere in detail not seen before.

Sharp differences are visible between the marine atmospheric boundary layer (MABL) and cloud structure on the northern and on the southern flanks of the KE, as well as large differences in these structures between summer and winter. In winter, the warm KE releases huge amounts of latent and sensible heat with a surface flux greater than 450 W/m^2. Under strong surface northwesterlies, the intense turbulent heat flux warms the MABL on the southern flank of the KE front, lowering sea level pressure and causing surface wind convergence. The resulting strong upward motion transports moisture, producing clouds that penetrate above the MABL and reach the mid-troposphere. This band of clouds reach much higher than in the surroundings, and lightning occurs frequently.

In early summer, turbulent heat flux is suppressed over the western North Pacific as the southerly warm/moist advection stabilizes the surface atmosphere. Nevertheless, a weak but significant north–south gradient in surface heat flux remains across the KE front. This meridional gradient of surface heating causes a sharp transition across the KE front, with low clouds, but elevated bases on the southern flank and sea fog on the northern flank. Sea fog occurs frequently on both the northern flank of the subtropical KE and the subarctic fronts as the warm/moist air mass is rapidly cooled by colder SST. On the other hand, sea fog occurs infrequently over the southern KE front as the warm ocean current weakens atmospheric stratification and promotes vertical mixing.

From June to July, a narrow band of surface wind convergence forms at the KE front. This convergence, caused by deceleration of southerly winds associated with the SST-induced near-surface stabilization, helps to support a broad band of upward motion at 700 hPa. The collocation of the KE-induced surface wind convergence and upward motion suggests that the SST front may play a significant role in extending Baiu precipitation east of Japan. [H.Tokinaga, S.-P. Xie, and T. Sampe (IPRC), Y. Tanimoto (Hokkaido Univ.; JAMSTEC); H. Tomita and H. Ichikawa (JAMSTEC)]

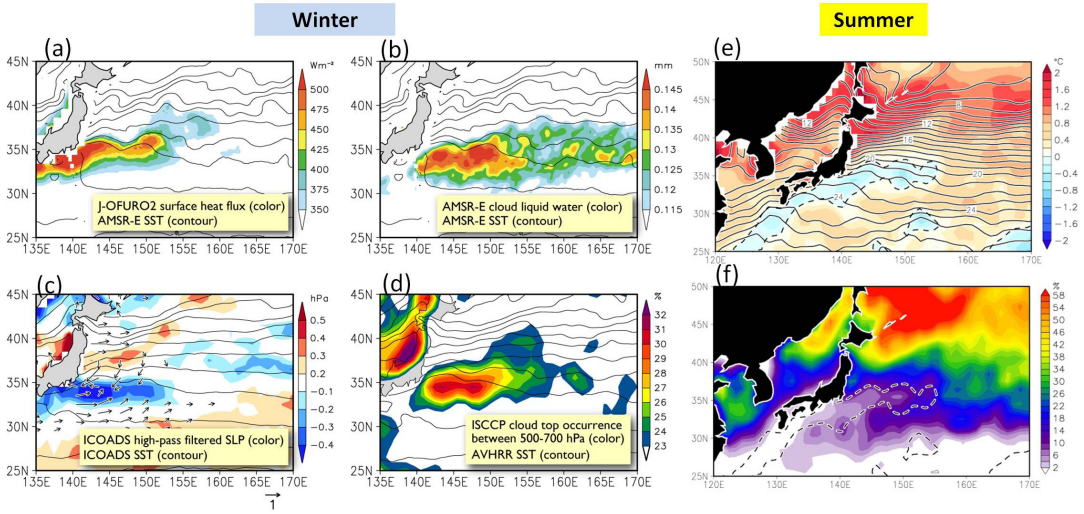

Figure 1.2. Seasonal impact of the Kuroshio on the atmosphere: Winter: (a) Surface heat flux, (b) cloud liquid water, (c) high-pass filtered SLP, and (d) cloud-top occurrence between 500–700 hPa in December–February. Contours are SST at 2°C intervals. Summer: (e) Air-sea temperature difference, and (f) frequency of sea-fog occurrence under the southerly winds in June. Dashed line is 0°C contour of air-sea temperature difference.

Changes in the hydrological cycle with global warming. Both observations and model simulations have suggested that with global warming, atmospheric moisture content increases at a rate of 7% per degree Kelvin, a rate consistent with roughly constant relative humidity. If the general circulation remains unchanged, this would imply an increase in precipitation at the same rate. Model integrations performed for the Fourth Assessment Report (AR4) of the International Panel on Climate Change (IPCC), however, typically produce a rate of merely 1–3%/K, a finding that has been referred to as the "muted precipitation" increase. Observational evidence is unclear: earlier studies suggest that precipitation increase has indeed approximately followed this 7%/K rate, whereas more recent studies suggest a rate that is roughly consistent with the AR4 model results. Thus some doubt remains as to how much rainfall will increase with warming and whether the changes in the hydrological cycle are represented accurately in global climate models.

Since precipitation and evaporation have to balance in the global mean, each can be used to examine changes in the hydrological cycle. Evaporation, though, is more readily analyzed than precipitation as the models have very similar parameterization schemes for each of its components. IPRC scientists have therefore analyzed the surface evaporation in the model outputs from the IPCC AR4 simulations under the A1B greenhouse gas forcing scenario. A 90-year analysis based on a standard bulk formula reveals that the following atmospheric changes slow down the increase in surface evaporation over ice-free oceans: surface relative humidity increases by 1.0%; surface stability, as measured by air-sea temperature difference, increases by 0.2 K; and surface wind speed decreases by 0.02 m/s. With these changes, surface evaporation increases by only 2%/K of surface warming. The increase in surface stability and relative humidity is similar across models. To determine whether the models represent these variables correctly, changes in the surface relative humidity and the air-sea-temperature difference need to be monitored as the planet warms. [I. Richter and S.-P. Xie (IPRC), 2008: The Muted Precipitation Increase in Global Warming Simulations: A Surface Evaporation Perspective. *J. Geophys. Res.-Atmos.*, **113**, D24118, doi:10.1029/2008JD010561.]

Ocean Circulation

A near-real-time model of the near-surface ocean circulation. The surface ocean circulation has a strong impact on the atmosphere and on climate. Realistic simulation of the near-surface circulation should therefore help to improve weather and climate models and their prediction skill. A model of near-surface velocities in near real time is now being developed at the IPRC, and the results are illustrated for velocities at a depth of 15 m in Figure 1.3. The top panel shows the velocities determined from ensemble-averaged direct drifter observations. The bottom panel shows the velocities obtained by combining the mean geostrophic and mean Ekman currents. The mean geostrophic velocities were calculated from the improved mean dynamic topography of Maximenko and Niiler, 2008; the mean Ekman velocities were obtained by combining NCEP reanalysis winds and an improved drifter velocity parameterization.

A comparison of the panels shows that the model simulates well the observed circulation. The geostrophic velocities represent all major fronts and currents. The Ekman velocities illustrate the impact of winds on equatorial upwelling in the Pacific and Atlantic, the coastal upwellings at the eastern boundaries of subtropical oceans, and subtropical convergences. Analyses of the model output reveal that the convergences are responsible for the mid-ocean accumulation of large fields of plastic and other marine debris. The convergences also seem to provide nutrients to bring about episodic chlorophyll blooms without upwellling. [N. Maximenko, O. Melnichenko, and J. Hafner (IPRC), P. Niiler and L. Centurioni (SIO), M.-H. Rio (CLS, France), Wilson (NMFS, NOAA), Chambers (U. of Taxes at Austin), V. Zlotnicki (JPL), B. Galperin

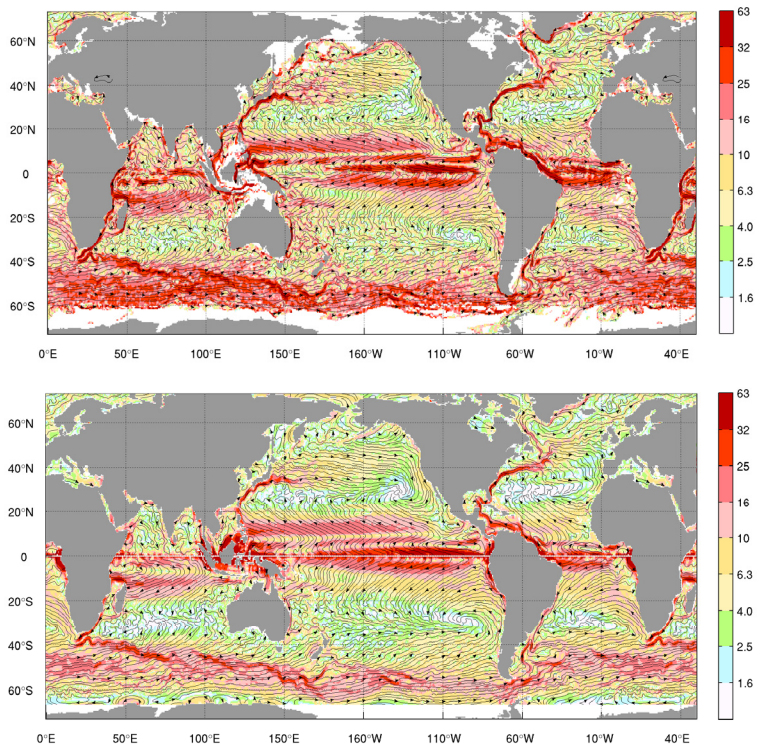

Figure 1.3. Mean streamlines calculated (top panel) from 0.25° ensemble-mean velocities of the drifters drogued at 15 m depth between February 15, 1979, and May 1, 2007, smoothed to 1°; and (bottom panel) from a combination of the mean geostrophic and Ekman velocities with a method described in the text. The choices of streamlines are made in an iterative fashion to cover the ocean at relatively uniform spatial density of several degrees, giving preference to the longest lines. Colors are magnitudes (top) of mean drifter velocity and (bottom) of mean geostrophic plus Ekman velocity used to compute the streamlines (units in cm/s).

(U. of South Florida). Figure is from Maximenko, N., P. Niiler, M.-H. Rio, L. Centurioni, D. Chambers, V. Zlotnicki, and B. Galperin, 2009: Mean dynamic topography of the ocean derived from satellite and drifting buoy data using three different techniques. *J. Atmos. Oceanic Tech.*, IPRC-576 (in press).]

The North Pacific Gyre Oscillation (NPGO) and the El Niño-Southern Oscillation (ENSO). Last year's report described for the first time the NPGO index, an index that is distinct from the Pacific Decadal Oscillation (PDO) index and is more closely related to fluctuations in salinity, nutrients and chlorophyll in the eastern North Pacific than is the PDO. Exploration of the NPGO index this year showed that anomalies occurring in spring tend to persist significantly longer than those in fall. This unexpected property of the oceanic NPGO reflects seasonal variations in atmospheric forcing, as noted in the variances, auto-correlations, and cross-correlations of sea level pressures that form a dipole over Hawaii and the Alaskan Gyre.

As expected, sea level pressure over both locations varies the most in winter. The correlation between sea level pressure over Hawaii and the Alaskan Gyre is greatest in spring and summer. The month-to-month correlation of the Alaskan Gyre sea level pressure is low throughout the year, suggesting that fluctuations in sea level pressure in the Alaskan Gyre are dominated by intrinsic atmospheric variations in the storm track. In contrast, the month-to-month correlation of sea level pressure over Hawaii reaches $r \geq 0.6$ during spring and summer. The correlations between averaged April–June sea level pressure over Hawaii and sea level pressure throughout the Pacific during the seasons in the year before (–1) and same year (0) reveal that spring anomalous sea level pressure over Hawaii is associated with the development of ENSO-like sea level pressure patterns during the following fall. The footprinting mechanism may be the means by which this signal pattern is carried from one season to the next. Thus, we conclude that the North Pacific NPGO forces, and subsequently interacts with, ENSO in the tropical Pacific. [N. Schneider (IPRC), E. Di Lorenzo (Georgia Institute of Technology), A. Miller (SIO)].

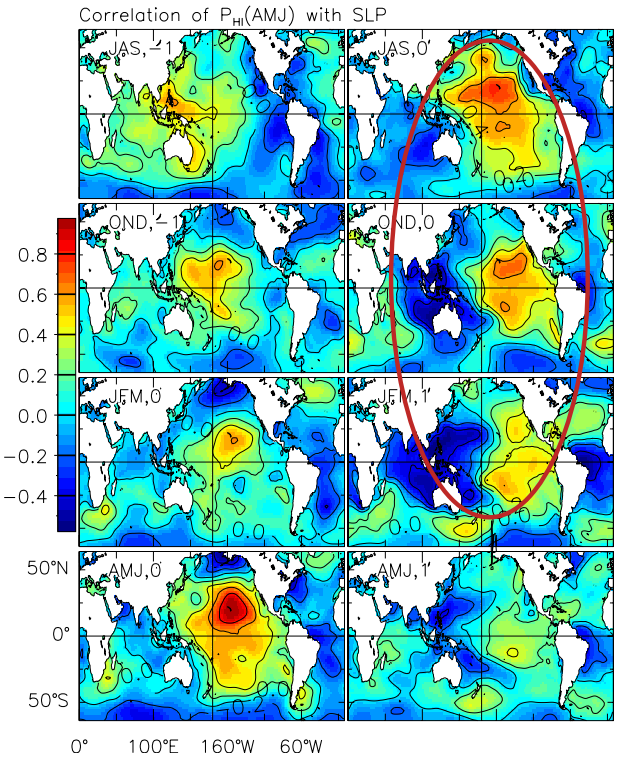

Figure 1.4. Correlations of Hawaii spring (April–June) sea level pressure (SLP) with the average worldwide SLP from the year before to the year after: (left column from the top) with the preceding summer (July–September), with preceding fall (October–December), winter (January–March) of the same year, and contemporaneous; (right column from the top) with fall of the same year through spring of following year (April–June). Data is from the NCAR/NCEP reanalysis. Note that the contemporaneous correlation (April–June, 0) shows a dipole with a negative pole over the Alaskan gyre, reminiscent of the North Pacific Oscillation. This NPO type patters develops in the subsequent winter in response to the sea level pressure signature of the El Niño–Southern Oscillation, as predicted by the so called foot printing mechanism.

Decadal variations in Kuroshio Extension strength and position. The dynamical framework for understanding the decadal variations in the Kuroshio Extension (KE) has traditionally been based on Rossby waves in a background state without flow and with potential vorticity given by the planetary vorticity. This framework captures the timescale but not the spatial structure of the decadal variations. The reason for this lack could be the existence of potential vorticity gradients associated with strong jets in the KE. IPRC scientists revisited the problem using the thin jet model framework to explain decadal variations that occurred in a simulation of the KE with the eddy-resolving Ocean GCM for the Earth Simulator (OFES). In OFES, the meridional shift in the KE starts east of the Dateline and propagates westward along the meridionally tilted mean jet axis. Under proper scaling, the thin-jet theory can account for these westward propagations of the meridional jet shifts. In fact, forcing the thin-jet model with latitude fluctuations in the jet at the Dateline produces meridional shifts of the jet in the upstream KE similar to the shifts noted in OFES (Figure 1.5). [Y. N. Sasaki and N. Schneider (IPRC), and E.A. Ralph (University of Guam]

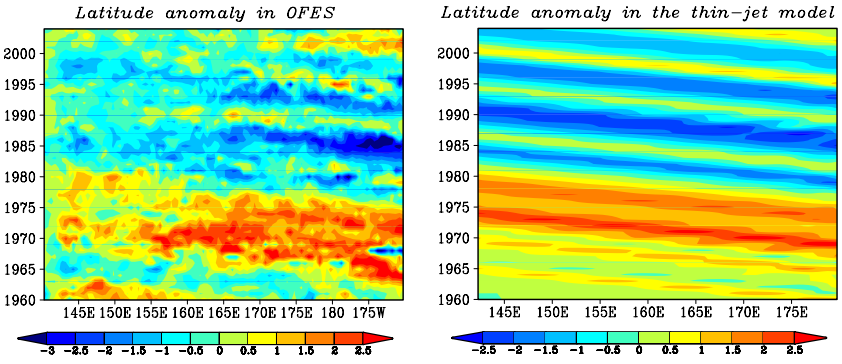

Figure 1.5. Annual mean latitude anomalies of the Kuroshio Extension jet in OFES (left) and the thin-jet model (right). The unit is degree of latitude.

Kuroshio Extension northern recirculation gyre. Over the past several years, many profiling floats have been deployed in the western North Pacific Ocean as part of the Kuroshio Extension System Study (KESS) and the International Argo program. Using the drift information from these floats at their parking depths, KESS examined the regional mean circulation at 1500 m depth (Figure 1.6). The float-inferred mean flow field confirmed several mid-depth circulation features noted in previous observations: for example, the existence of the deep, meandering Kuroshio Extension (KE) jet, its northeastward branching upstream of the Shatsky Rise, and the intense recirculation south of the KE jet.

The float measurements also revealed new circulation features at 1500 m depth. In particular, a well-defined recirculation gyre exists *north* of the KE jet: it extends from east of the Japan Trench at 145°E to west of the Shatsky Rise at 156°E and is confined in the north by the subarctic boundary along 40°N. Although in the past, westward recirculating flows have been observed north of the KE jet, the float results presented in this study provide the first observational picture of the spatial pattern of the mean northern recirculation gyre. It will be interesting in future analyses of the profiling float data to clarify the time-varying nature of the northern recirculation gyre.

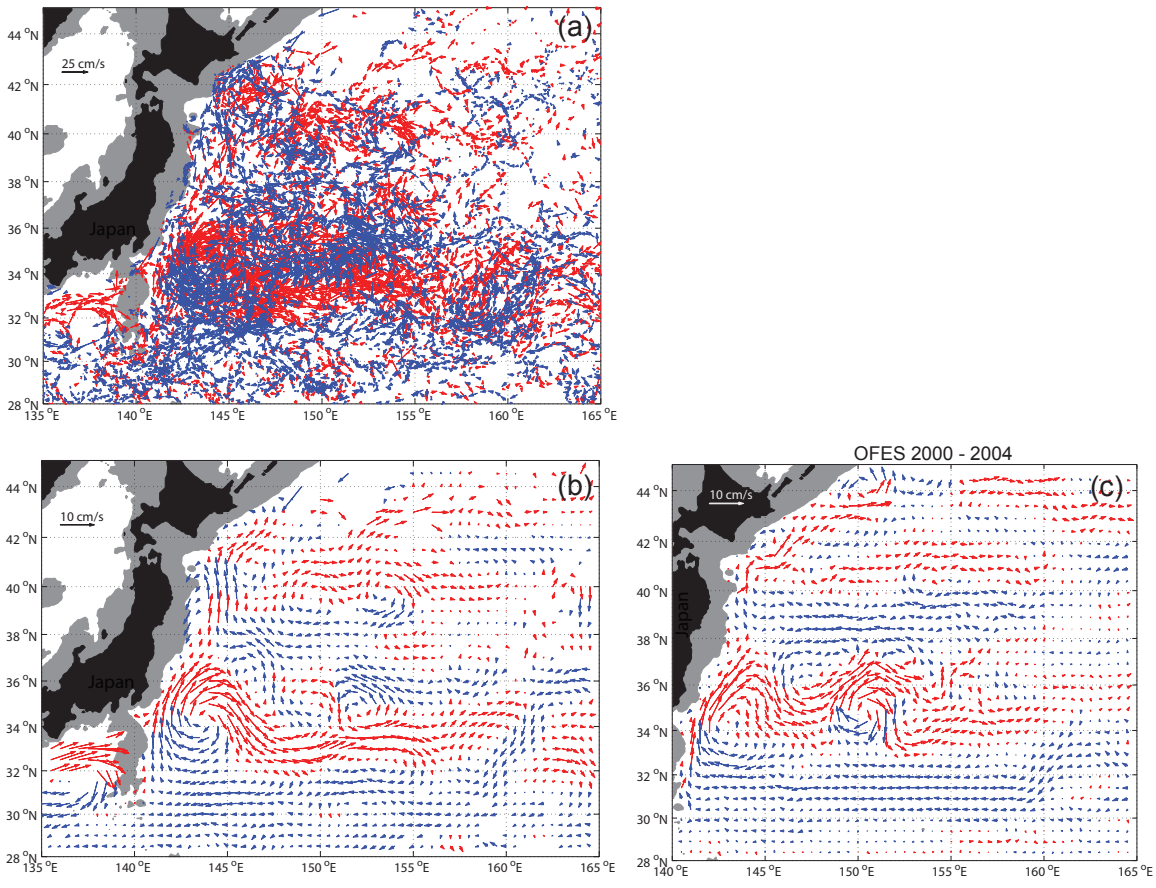

Figure 1.6. Velocity vectors calculated from Argo floats and OFES. Vectors with an eastward (westward) component are plotted in red (blue) in all panels. (a) Velocity at the 1500 m depth estimated from the 8813 available pairs of ascending–descending Argo float positions. Floats with the parking depth at 1000 and 2000 m have their velocity values adjusted according to local, climatological geostrophic shears. (b) Time-mean velocity field at the 1500 m depth objectively mapped from the available velocity vectors shown in top panel. (c) Mean velocity field at the 1500 m depth averaged over 2000–2004 from the OFES hindcast run. Velocity vectors are sub-sampled from the original 0.1° x 0.1° model grid.

The deep-reaching, eastward-flowing subarctic boundary and northeastward-flowing Subarctic Front are other new mid-depth circulation features revealed by the float measurements. Both of these currents have heretofore been regarded as "shallow" circulations in the western subarctic gyre of the North Pacific Ocean. Moreover, a continuous northward flow is found to exist offshore of the southward flowing Oyashio; this northward flow overrides the eastern flank of the Japan Trench and delineates the western end of the northern recirculation gyre.

The northern recirculation gyre has a maximum volume transport at 26.4 Sv across 159°E, and its presence persists on interannual and longer time scales (Figure 1.6 bottom left panel). The mean velocity field averaged from 1950–2004 (not shown), is very similar to that shown in Figure 1.6 (top panel). The gyre is well simulated in the eddy-resolving Ocean GCM for the Earth Simulator (OFES) hindcast. An examination of the time-mean x-momentum balance from the OFES hindcast-run output reveals that horizontal convergence of Reynolds stresses accelerates both the eastward-flowing KE jet and the *westward* mean flow north of the meandering jet. The fact that this gyre is eddy-driven is further confirmed by examining the turbulent Sverdrup balance, in which convergent eddy potential vorticity fluxes are found to induce the cyclonic recirculation across the background potential vorticity gradient field.

JAMSTEC colleagues participated in KESS by conducting Argo float observations and delivering and analyzing the eddy-resolving OFES hindcast-run output (Figure 1.6, bottom right panel). The KESS project has been one of the heaviest users of OFES output on the APDRC servers. [Qiu, B. and S. Chen (U. Hawaii); P. Hacker (IPRC); N.G. Hogg and R. Jayne (WHOI), and H. Sasaki (JAMSTEC), 2008: The Kuroshio Extension northern recirculation gyre: Profiling float measurements and forcing mechanism. *J. Phys. Oceanogr*., **38**, 1764–1779].

The subtropical countercurrents in the South Indian Ocean. Subtropical countercurrents (STCCs) are shallow eastward flows in the equatorward half of the subtropical gyres, where Sverdrup theory predicts a westward flow (hence the "countercurrent" tag). The STCCs in the South Indian Ocean (SIO) are particularly conspicuous, and unlike those in the other oceans, extend up to the eastern boundary (the west coast of Australia). IPRC scientists investigated whether this feature is due to the unusually steep surface density gradient of the eastern SIO. Calculating the geostrophic flow from Argo climatology (Figure 1.7, left panel), they found that these STCCs are accompanied by a westward-flowing, subsurface flow. Argo climatology also suggests that the southern-most STCC, known as the South Indian Countercurrent, is stronger and extends deeper than the other STCCs. These characteristics are shared by a solution of the global, eddy-resolving Ocean GCM for the Earth Simulator (OFES; Figure 1.7, right panel).

To understand the dynamics of these STCCs, IPRC scientists, in discussion with colleagues at PMEL, developed an idealized 2½-layer model of the SIO. When the subsurface layer is forced to outcrop at a prescribed latitude (a so-called ventilated-thermocline model), the analytical and numerical solutions produce a surface STCC and an associated westward subsurface flow. The model STCC is driven by subduction at the outcropping, and its path is determined by an interplay between the Sverdrup circulation and the propagation of baroclinic Rossby waves emanating from the outcropping. An ocean GCM with a very similar configuration of the ocean basin and forcings is being developed to explore the effects of continuous stratification and thermodynamics on the STCC. [R. Furue, J. McCreary, and J. Potemra (IPRC)]

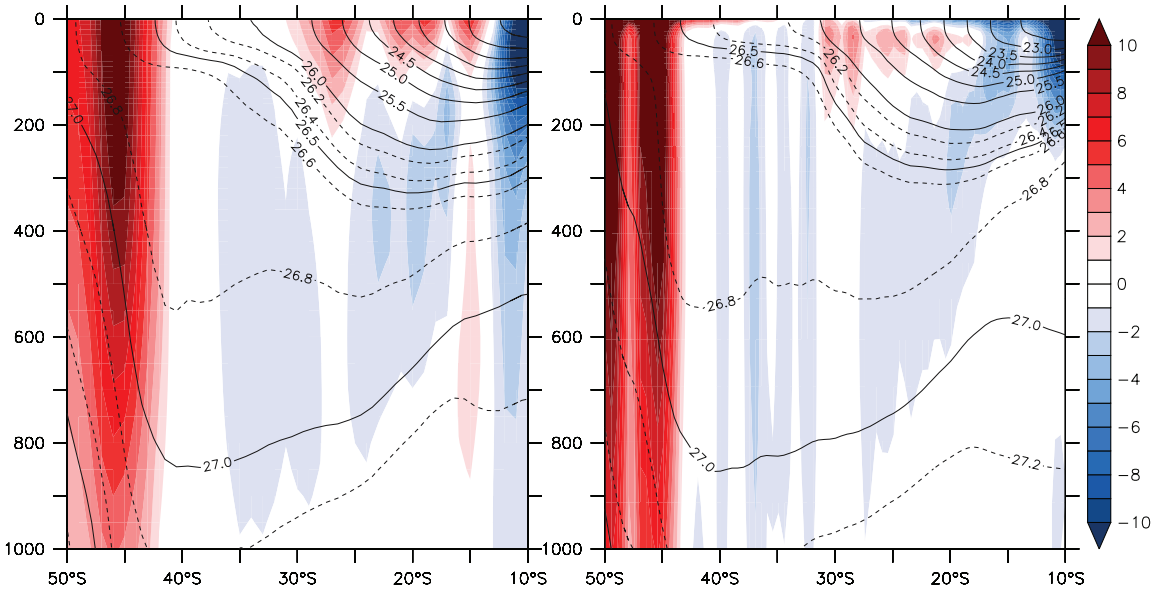

Figure 1.7. Meridional sections at 100°E of zonal velocity (cm/s; color) and potential density (contours) from a geostrophic calculation referenced to 2000 m based on Argo climatology (left) and from a 20-year average of the OFES NCEP run (right).

Westward propagation of the barrier layer in 2006–07 during the simultaneous El Niño and Indian Ocean Dipole events. The tropical southwest Indian Ocean (SIO) impacts climate because the thermocline shoaling in response to basin-scale Ekman pumping gives such subsurface anomalies as downwelling Rossby waves the opportunity to readily affect the sea surface temperature (SST). The 2006–07 co-occurrence of an El Niño and an Indian Ocean Dipole event, accompanied by anomalous easterly winds, resulted in a strong downwelling Rossby wave, which traveled westward across the tropical SIO, raising SST and increasing rainfall in its path.

Though interannual Rossby waves are routinely monitored with satellite altimeters and SST measurements, their vertical structure as they move across the Indian Ocean has not been observed systematically. Using Argo float data, IPRC scientists analyzed the subsurface path of this 2006–2007 Rossby wave. The wave displaced the thermocline vertically, resulting in warm subsurface water migrating westward in the Indian Ocean along 10°S from September 2006 to January 2007.

In the Indo-Pacific warm pool, the isothermal layer is often much deeper than the mixed layer because freshwater input after heavy rainfall form a barrier layer (BL) below the mixed layer. The Argo observations (Figure 1.8a; shaded) reveal that during July 2006–April 2007, the downwelling Rossby wave was accompanied by an abnormally thick BL propagating westward (Figure 1.8a, contour). The downwelling Rossby wave pushed the thermocline down, nearly eliminating the seasonal shoaling during the second half of 2006 (Figure 1.8b). As a result, the isothermal layer depth increased from 35 m in October 2005 to 70 m a year later, with a thick BL during the second half of 2006. Thus, as the Rossby wave warms the surface along its westward path, the increased rainfall provides a surface freshwater source for the BL that also moves westward. The slow Rossby wave propagation sustains the BL for several months. By shielding the surface from the influence of colder thermocline water, the BL itself may contribute to the surface warming, an overlooked process conceivably important for the thermocline feedback. [J. S.Chowdary and S.-P. Xie (IPRC); C. Gnanaseelan

(Indian Institute of Tropical Meteorology), 2009: Westward propagation of barrier layer formation in the 2006–07 Rossby wave event over the tropical southwest Indian Ocean, *Geophys. Res. Lett.*, **36**, L04607, doi:10.1029/2008GL036642.]

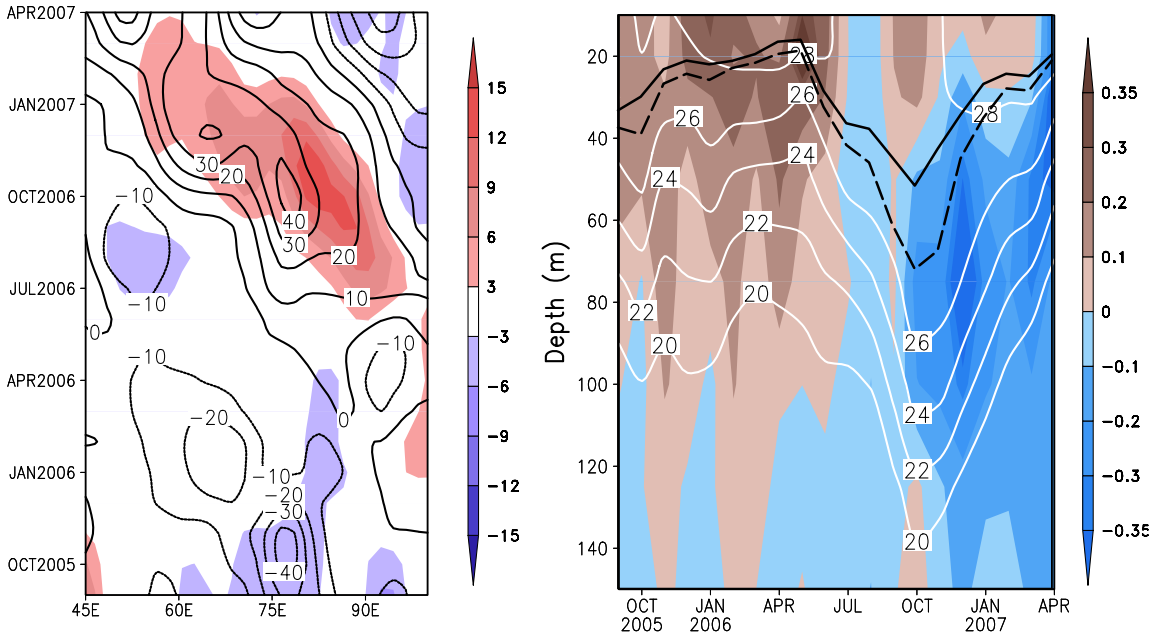

Figure 1.8. (left panel) Time-longitude sections of barrier-layer thickness (shaded in m) and 20°C isotherm depth (d20; contours in m) anomalies at 10°S; (right panel) time-depth sections of mean temperature (white contours in °C) and salinity anomaly (shaded in psu) averaged over the region 75°E–90°E and 10°S–5°S. The thick solid black line shows mixed-layer depth and the dashed line isothermal-layer depth.

Charting the pattern of mesoscale eddies in the Gulf of Aden. IPRC scientists are studying the role of mesoscale eddies in the Gulf of Aden (GoA) and its potential impact on the biogeochemical cycle in the Arabian Sea. They hypothesize that these eddies are essential for carrying the high-in-oxygen, deep Red Sea Water into the Arabian Sea. Quality observations are critical to the validation of numerical models with which sensitivity experiments are carried out to isolate the underlying dynamics. To obtain such data for model validation, the scientists have taken advantage of satellite observations, in this case the AVISO data set, to resolve the westward-propagating mesoscale eddies in the GoA (left and middle panels of Fig. 1.9). This work thus far has resulted in a significant revision of a former composite of in situ observations of these eddies during winter (see right panels of Fig. 1.9), the peak period of water exchange between the Red Sea and the GoA. The original composite was derived from in situ data collected during a 30-day period, with inadequate temporal resolution to resolve the swiftly moving eddies, resulting in a cyclonic-cyclonic-anticyclonic eddy sequence (right panels of Fig. 1.9). The satellite data, which has much better spatial and temporal resolutions, shows alternating anticyclonic-cyclonic eddies. This revision of the composite provides much-needed guidance for numerical modeling of the area, a necessary first step toward understanding the dynamics and impact of these vigorous eddies.

The team is currently working on determining the separate impacts of the Red Sea Water, local winds, and remote winds in the GoA, the Arabian Sea, and the Indian Ocean on generating and modify-

ing these eddies. [J. McCreary, K. Richards, Z. Yu, and R. Furue (IPRC); R. Hood (U. Maryland), T. Jensen (now at NRL), A. Ishida (JAMSTEC), X. Cheng (SCSIO)].

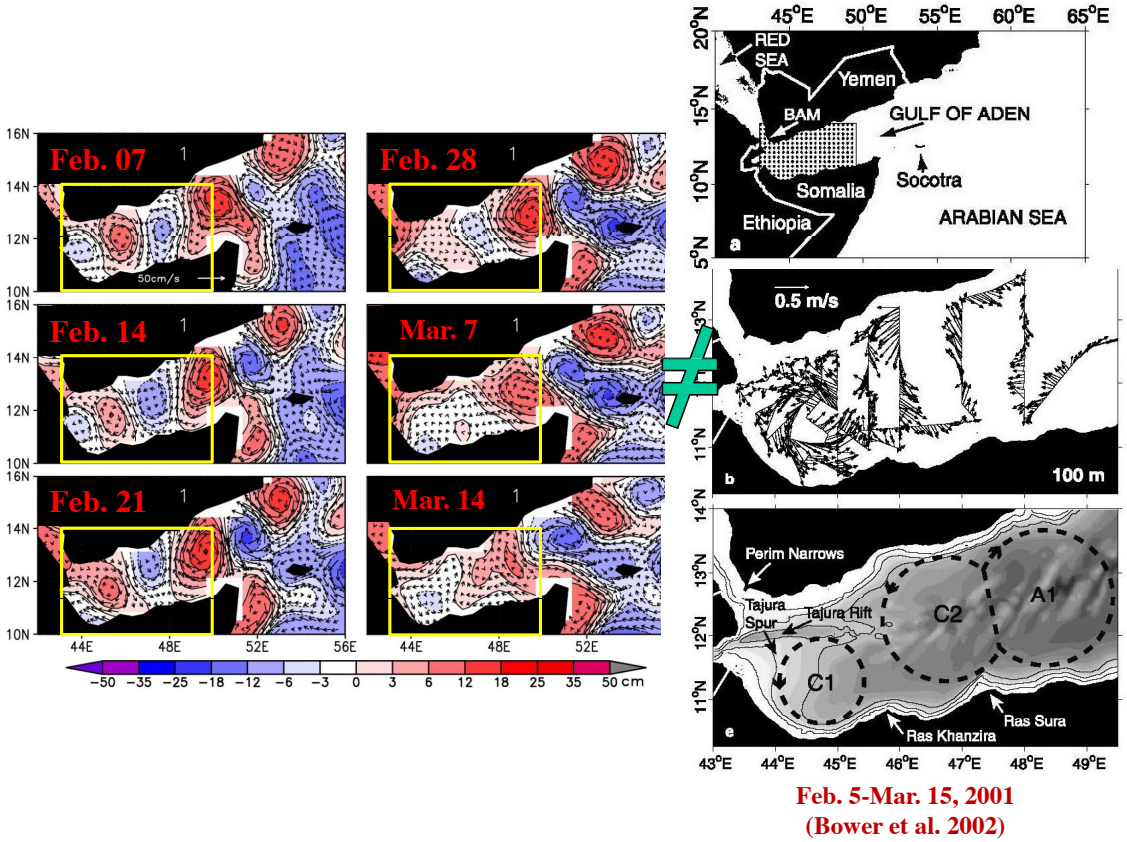

Figure 1.9. Left and middle panels: geostrophic flows (arrows) superimposed on sea-level anomaly of AVISO data. Right: reproduction of Figures 1a, b, and e of Bower et al. (2002) — (a) Map showing location of the Gulf of Aden as well as study region during February 2001 REDSOX cruise (stippled area); (b) Fifteen-minute average velocity vectors at 100 m from shipboard ADCP; (e) Schematic diagram of three large eddies observed during February 2001, cyclones C1and C2, and anticyclone A1. Bathymetry is shaded in 200-m intervals, and contoured at 100, 500 and 1000 m.

Chapter 2: REGIONAL AND SMALL-SCALE CLIMATE PROCESSES AND PHENOMENA

Atmospheric Processes

Cloud properties over the eastern Pacific. By effectively reflecting incoming solar radiation, marine stratocumulus clouds have a major impact on Earth's radiation budget and thus on climate. One of the largest and most persistent stratocumulus decks is found off the coast of South America in the eastern Pacific. Tight coupling between atmosphere, ocean, and land surfaces makes it difficult for numerical climate models to capture these subtropical stratocumulus decks. The IPRC Regional Atmospheric Model (iRAM) has been applied to the eastern Pacific and successfully simulates, for instance, the observed vertical structure of marine boundary layer clouds off South America.

Now iRAM has been improved with incorporation of a detailed double-moment cloud microphysics scheme. An extensive comparison with aircraft, ship, and satellite measurements shows that the new model system is able to reproduce well such average cloud properties as liquid water content, cloud droplet number concentration, cloud cover, and cloud radiative forcing as well as the diurnal cycle of cloud liquid water. Figure 2.1 compares the liquid water path in the extended iRAM with satellite observations from the Special Sensor Microwave Imager (SSM/I). The extended version improves significantly upon the single-moment cloud scheme originally implemented in iRAM for such important parameters as effective cloud droplet radius and shortwave cloud forcing.

A first application of the new model system was to assess the indirect aerosol effect of anthropogenic emissions of particles and precursor gases on clouds over the eastern Pacific by comparing simulations with preindustrial aerosol fields and corresponding present-day fields. This sensitivity experiment shows that the average cloud droplet number concentration over the ocean has increased, particularly along the Pacific Coast of North and South America and over the Gulf of Mexico. With only a small increase in cloud liquid water content, the additional anthropogenic cloud condensation nuclei result in increased cloud reflectivity and cloud forcing (producing a net cooling effect).

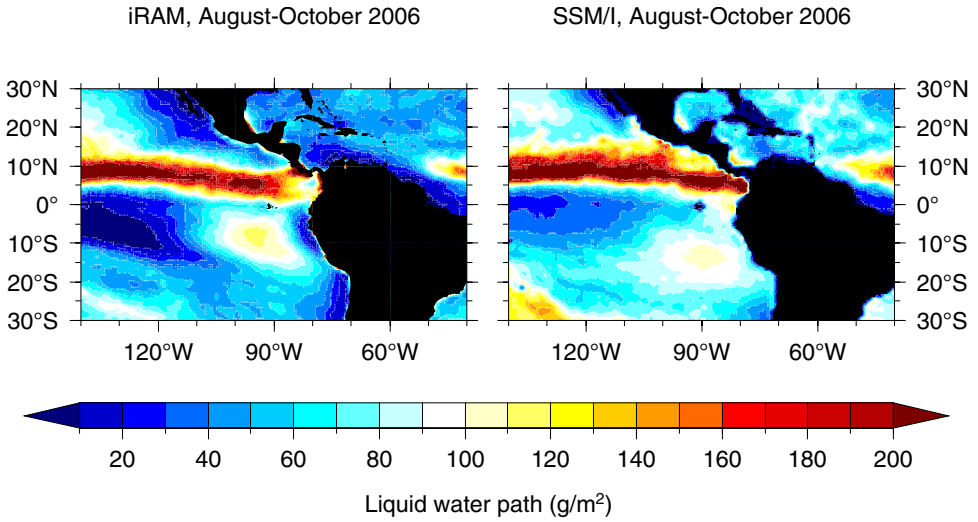

Figure 2.1. August–October 2006 average of the vertically integrated cloud liquid water content in g/m^2. Left: iRAM simulation, right: Special Sensor Microwave Imager (SSM/I) satellite observations (O'Dell et al., 2008). From Lauer et al. (2009).

The new iRAM version is now being used to assess potential changes in cloud properties and cloud radiative forcing in response to global warming. Specifically, IPRC scientists are studying the impact of rising sea surface and atmospheric temperatures and changes in the vertical humidity profiles on marine clouds by applying a downscaling technique known as the Pseudo-Global-Warming (PGW) method. The global warming signal calculated by IPCC AR4 models is added to present-day lateral boundary conditions, which are obtained from the National Centers for Environmental Prediction (NCEP) final analysis (FNL), from daily mean satellite SST observations provided by the Advanced Very High Resolution Radiometer (AVHRR), and from the NOAA Advanced Microwave Scanning Radiometer (AMSR). Results from these simulations are then compared to corresponding present-day scenarios to study the cloud feedback in response to global warming. First results suggest that the cloud feedback in the eastern Pacific could be larger than predicted by the current IPCC models. The positive cloud feedback calculated by iRAM as a response to global warming tends to further increase temperatures because the average amount of sunlight reflected back into space decreases with diminishing cloud cover. Figure 2.2 shows changes in cloud cover between present-day and the end of the 21st century calculated by iRAM for a global warming signal obtained from the IPCC SRES A1B scenario. [A. Lauer, Y. Wang, and K. Hamilton (IPRC); V. Phillips, C. McNaughton, and A. Clarke (U. of Hawai‘i); and R. Bennartz (U. of Washington)]

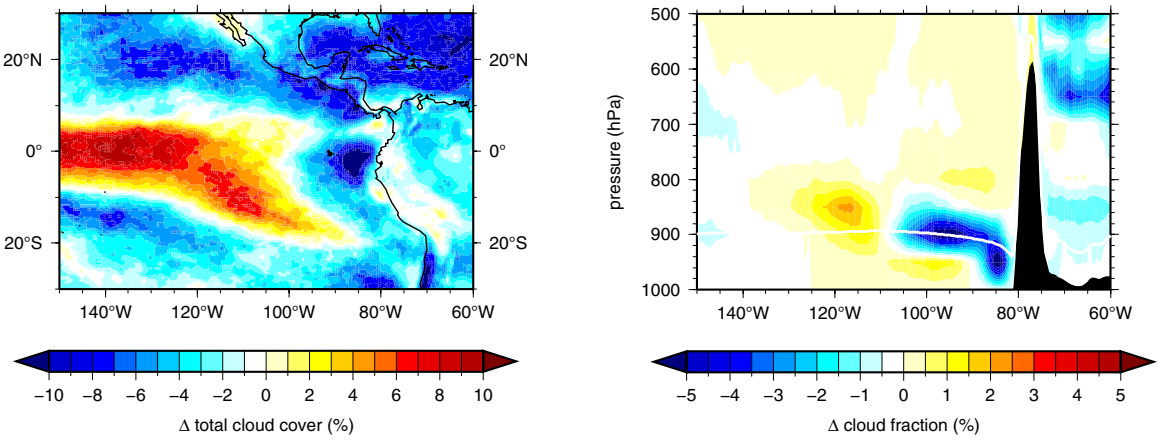

Figure 2.2. Changes in climatological annual-mean total cloud cover over the eastern Pacific due to global warming. Left: Geographical distribution, right: Zonal cross section (5°S to 10°S average).

Effects of Tibetan Plateau spring-snow albedo and soil-moisture on East Asian Summer Monsoon Rainfall. Observational and numerical modeling studies suggest that variations in the Tibetan Plateau spring snow-amount impact East Asian summer monsoon (EASM) rainfall. This impact is mostly attributable to the snow albedo and the hydrological effects related to snowmelt. Information on snow conditions in springtime could thus help to improve seasonal prediction of EASM rainfall, but the individual contributions of albedo and hydrology have not yet been evaluated quantitatively. Using the IPRC Regional Atmospheric Model (iRAM), the present study assessed the relative importance of these two effects on EASM rainfall.

The model was initialized with springtime snow conditions existing on the Tibetan Plateau in 2005 because rainfall in East Asia was unusual that year: in May–June, southern China received unusually heavy rain, but the Yangtze River Basin was unusually dry; and in July–August, the Huai River Basin

further north was unusually wet. Three ensemble simulations were conducted. The *Control* simulations included both albedo and hydrological effects of snow. The *No Albedo* simulations excluded the surface albedo effect on the radiation budget. The *No Snowmelt Water* simulations excluded the addition of snowmelt to groundwater. A comparison of these simulations indicated that the snow albedo significantly affected rainfall throughout the four-month simulation, its effect on rainfall over the Yangtze River Basin being about three times the hydrological effect in May–June; from July to August, the albedo effect weakened and the hydrological effect strengthened (Figure 2.3). [K. Souma and Y. Wang (IPRC)]

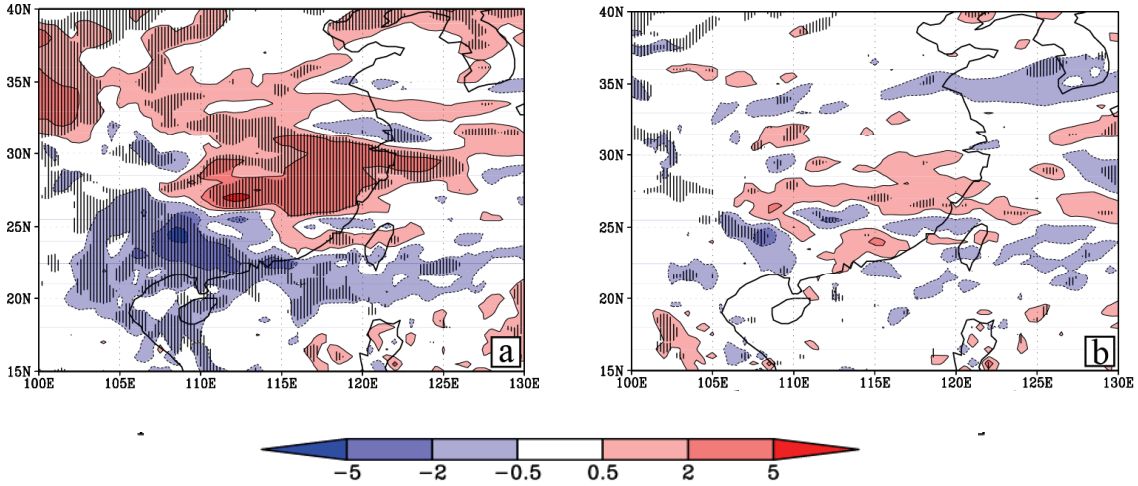

Figure 2.3. The difference in daily mean rainfall (mm/d) in May–August over eastern Asia: (a) between No Albedo and Control; (b) between No Snowmelt and Control. Hatching indicates areas where a t-test shows that the two ensemble simulations are significantly different at the 95% level.

Surface topographic stress in high resolution atmospheric GCMs. The momentum exchange between the atmosphere and the solid earth due to the pressure gradients across topographic features - the so-called "mountain drag" - plays an important role in the general circulation of the atmosphere. Mountain drag in the zonal direction significantly affects the angular momentum balance of the atmosphere. The drag associated with fairly large horizontal scale orography can be computed from global observed gridded analyses.

The evidence suggests that significant mountain drag comes from small horizontal scales (say 10 to 500 km). The contribution to the drag from smaller-scale topographic features, however, can only be computed for individual small regions in which dense surface observations (e.g., from special field campaigns) are available. This is a problem for typical climate models for which the horizontal grid spacing may be ~100 to 300 km. The situation is illustrated schematically in Figure 2.4, which shows a section of topography in blue and the corresponding coarse model representation in red. Standard practice has been to assume a significant mountain drag associated with unresolved subgrid-scale topography and to parameterize the momentum transfer to the atmosphere, generally referred to as a "gravity wave drag" (GWD) parameterization.

The parameterizations have many uncertainties, however, and are typically adjusted somewhat arbitrarily so that climate models simulate reasonable large-scale atmospheric flow. The availability of

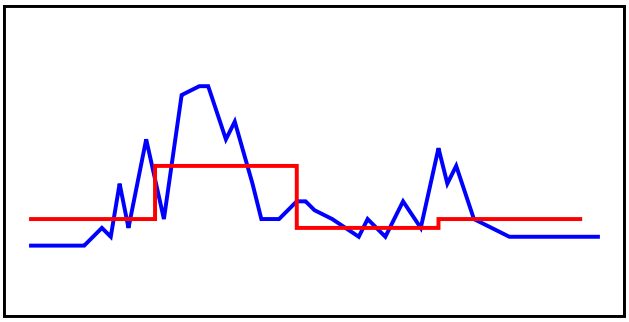

Figure 2.4. A schematic representation of an east-west cross-section of the real topography (blue) and the topography that would be used in a coarse horizontal resolution atmospheric model (red).

ultrafine resolution, comprehensive global atmospheric simulation models opens a new approach to determining the scale-dependence of mountain drag and to testing current parameterizations. In the present study, control results from high resolution versions of the Nonhydrostatic ICosahedral Atmospheric Model (NICAM) and the Atmospheric GCM for the Earth Simulator (AFES) were analyzed to determine how the drag is partitioned between large and small scales. Figure 2.5 shows boreal winter results obtained with T1279 resolution AFES (about 10 km horizontal grid spacing) and L11 resolution NICAM (about 3.5 km horizontal grid spacing). The total zonally-averaged drag computed for each of the models using the full resolution is shown in the lower panel. The drag was also calculated using the model data after the topography and atmospheric pressure were smoothed to roughly 300 km horizontal resolution. The difference (shown in the top panel) is then interpreted as the "unresolved" component that would have to be parameterized in a coarse resolution model. The latitude dependence of the "unresolved" drag also differs from that predicted by at least some GWD parameterizations now in use. [K. Hamilton (IPRC), W. Ohfuchi (JAMSTEC), M. Satoh (U. Tokyo and JAMSTEC)]

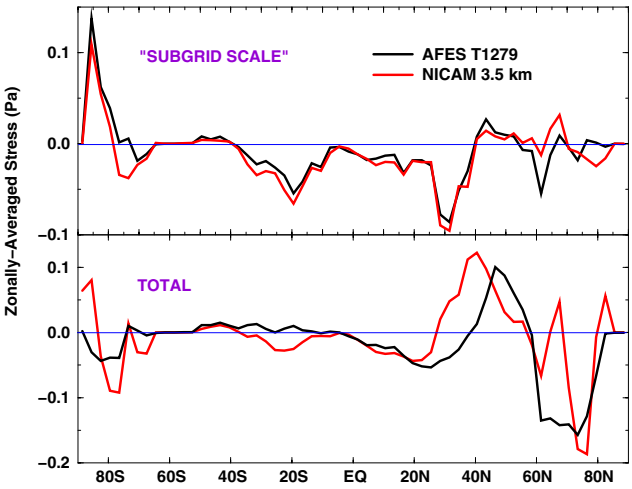

Figure 2.5. The total zonally averaged surface stress due to mountain drag as simulated in two ultra-fine resolution atmospheric GCMs. The top panel shows the component of the drag that would not be resolved in a 300 km horizontal scale data set. The bottom panel shows the total drag in the models. Results are averaged for several days during boreal winter control simulations.

The large-scale circulation impacts the lifecycle of a tropical storm. Last year's report described the successful simulation of the lifecycle of the observed tropical storm Isobel by the global cloud-system-resolving model, NICAM. The large-scale aspects that affected Isobel's lifecycle in the simulation have now been analyzed. Isobel's lifecycle was closely related to the concurrent evolution of the Madden-Julian Oscillation (MJO). The westerly wind bursts (WWB) accompanying the MJO pre-conditioned the large-scale environment for the birth of Isobel by interacting with the easterly trade winds to produce large-scale cyclonic shear over the Timor Sea. This disturbance then triggered a series of cyclonic

eddies. As the eddies moved southward away from the equator, the vertical shear between the low-level WWB and the upper-level easterlies during the initial stage of the storm decreased significantly, allowing the storm to intensify. But as the MJO center and the WWBs moved eastward, the ensuing zonal wind divergence stretched Isobel's inner core zonally. This evolution increased the vertical shear, suppressed inner core convection, and hence weakened the storm.

As with some observed tropical cyclones, Isobel showed resilience to the sheared environment, weakening temporarily but not dissipating. With the development of an anticyclonic circulation in the upper troposphere, northwesterlies appeared in the upper troposphere above Isobel. This not only weakened the vertical shear but also changed the vertical-shear direction from easterly to northerly, and produced intense outer spiral rainbands on the downshear side of the vertical shear vector. The outer rainbands spiraled cyclonically inward and replaced the original broken eyewall. These changes were accompanied by a re-intensification of the storm. Again this reformation and development of an intense mesoscale vortex and strong convection downshear of the original storm center has been noted in observed tropical cyclones. Isobel finally decayed when it made landfall in northwest Australia.

This analysis shows how the global cloud-system-resolving model NICAM allows diagnosis of the effects of the large-scale circulation and the role of vertical shear on the birth, growth, and decay of tropical cyclones (Figure 2.6). [H. Fudeyasu and Y. Wang (IPRC); Masaki Satoh (CCSR and JAMSTEC); T. Nasuno and H. Miura (JAMSTEC); W. Yanase (CCSR)]

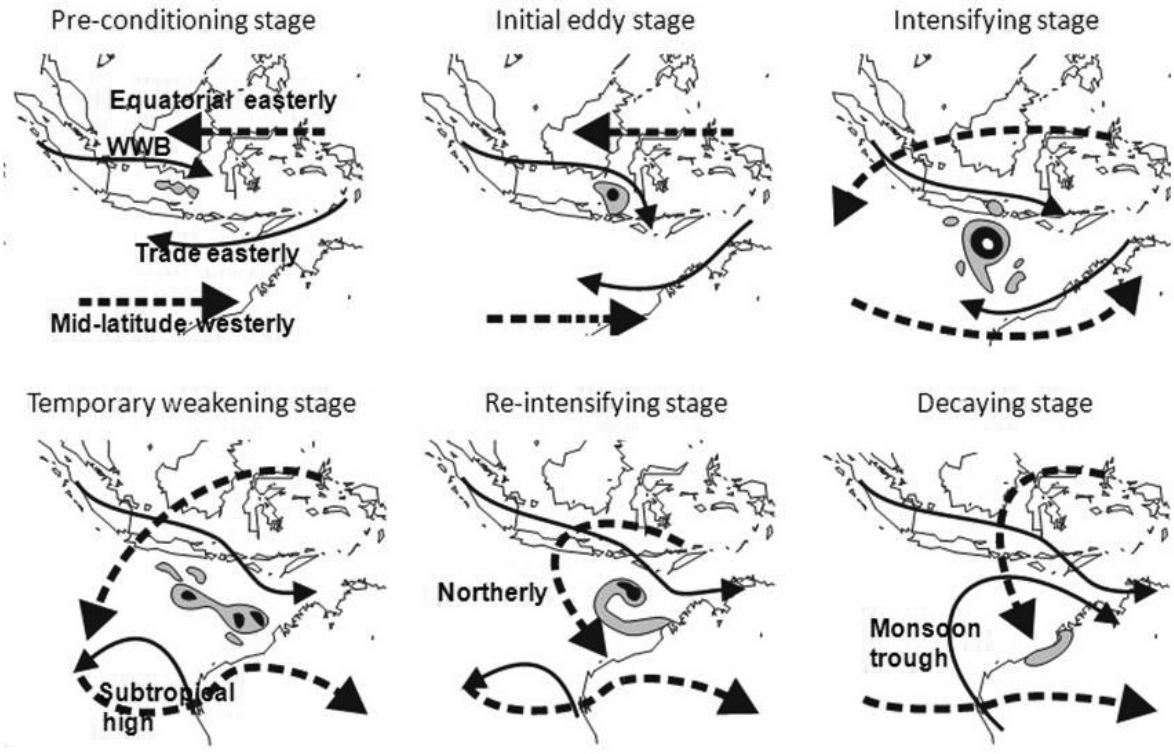

Figure 2.6. Schematic of the large-scale circulation that affected Isobel's evolution. Solid arrows are for lower-level flow while broken arrows for upper-level flow. Shaded areas show the convective regions in Isobel. The areas with intense rainfall associated with Isobel are filled, while those with weak precipitation are lightly shaded.

From concentric eyewall to annular hurricane: A numerical study with the cloud-resolving WRF Model. In over half of strong hurricanes, a secondary eyewall forms outside the first one, and eventually replaces the initial eyewall. Recent observation revealed that concentric eyewalls may lead to the formation of intense annular hurricanes (AH), which have big eyes and thick eyewalls that resist destruction. Prediction of the formation of a concentric eyewall and its evolution is thus important for forecasting the intensity of a hurricane. Using the next generation, cloud-system-resolving Weather Research and Forecasting (WRF) model, the transformation from a concentric eyewall replacement to an AH was, for the first time, successfully simulated under a resting environment (Figure 2.7). The simulated hurricane went through three distinct stages: formation of a secondary eyewall, eyewall replacement, and formation of an AH. The simulated eyewall succession and accompanying intensity change are qualitatively consistent with observations. The transition from concentric eyewalls to the AH took less than 24 hours, suggesting that concentric-eyewall-replacement is an efficient route to AH formation. Bottom-up mixing of strong potential vorticity in the concentric eyewalls is the main mechanism in AH formation. Results show that the WRF model can be useful in predicting the formation of concentric eyewall-cycles and annular hurricanes, and the associated intensity changes. [X. Zhou (U. of Hawaii) and B. Wang (IPRC), 2009: From concentric eyewall to annular hurricane: A numerical study with the cloud-resolved WRF model. *Geophy. Res. Let.*, **36**, L03802, doi:10.1029/2008GL036854]

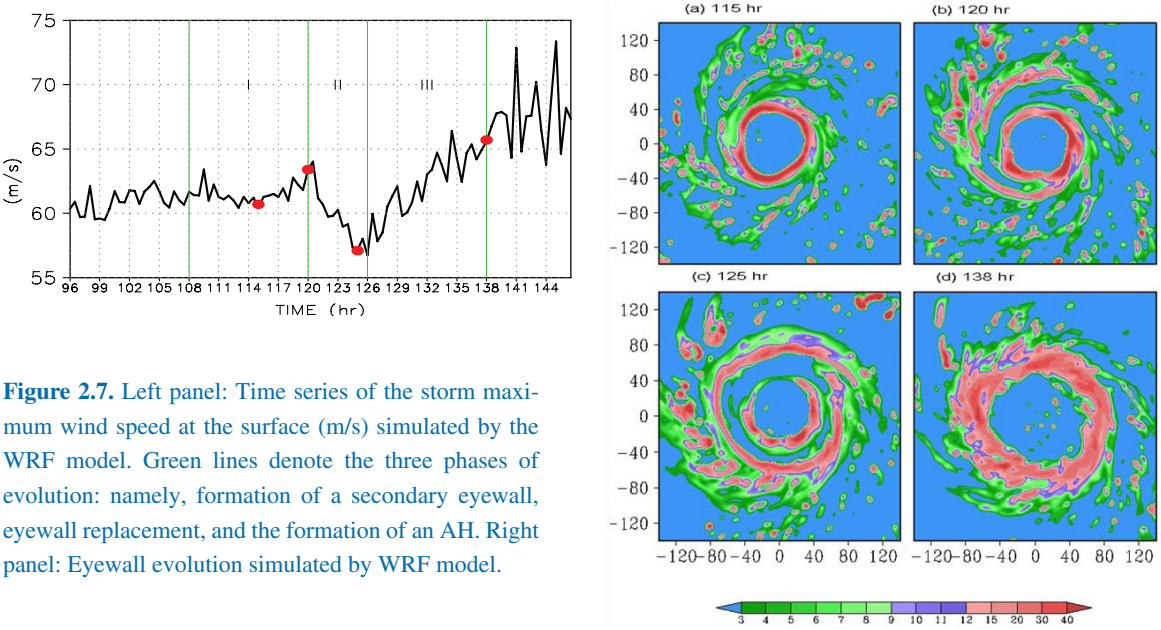

Figure 2.7. Left panel: Time series of the storm maximum wind speed at the surface (m/s) simulated by the WRF model. Green lines denote the three phases of evolution: namely, formation of a secondary eyewall, eyewall replacement, and the formation of an AH. Right panel: Eyewall evolution simulated by WRF model.

A numerical study of Typhoon Songda's remote effect on rainfall in Japan. When Typhoon Songda approached Japan southeast of Okinawa in September 2004, southern regions of central Japan that lay more than 1,200 km from the typhoon center experienced extremely heavy rainfall. Using the Advanced Weather Research and Forecast (WRF) model, IPRC scientists investigated whether the heavy rainfall could be attributed to the remote effects of Typhoon Songda. The National Centers for Environmental Prediction (NCEP) global final analysis provided the initial and lateral boundary conditions for the WRF model. In the *Control* simulation a bogus vortex was inserted into the final analysis, which produced initial model-typhoon-winds of similar intensity to those observed. In the *No-Typhoon* simulation, the vortex was removed by a smoothing algorithm so that there was no typhoon at initialization. In both experiments, the model was initialized at 1800 UTC on September 2 and integrated for 96 hours, the period during which Songda was a super typhoon.

The Control experiment captured reasonably well the evolution of the storm with regard to both geographic distribution and rainfall patterns, including the distant heavy precipitation in Honshu; in the No-typhoon experiment, there was little rainfall in southern Honshu (Figure 2.8). Further comparison and analysis of the two experiments revealed that Songda's winds transported much moisture northward, resulting in the heavy remote rainfall. [Y. Wang, Y. Wang, and H. Fudeyasu (IPRC): A numerical study of the effect of Typhoon Songda (2004) on remote heavy rainfall in Japan, *Mon. Weath. Rev.*, in press]

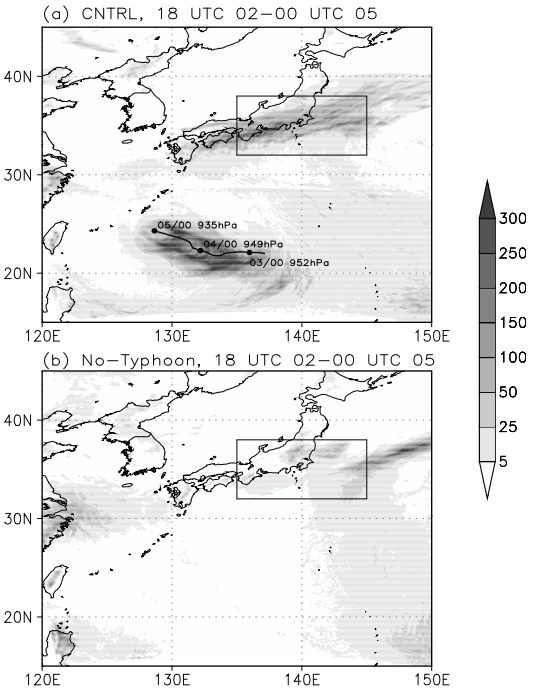

Figure 2.8. Total precipitation (mm) between 18 UTC 2 September and 00 UTC 5 September 2004 in (a) the Control and (b) the No-Typhoon experiment. The typhoon track during this time period together with the minimum central sea level pressure from the control experiment is also shown in (a).

Response of tropical cyclone potential intensity to a global warming scenario in the IPCC AR4 coupled GCMs. An analysis of the potential intensity (PI) of tropical cyclones (TCs) and control parameters were calculated for Coupled Model Intercomparison Project/CMIP3 integrations during the first 70 years of a transient run forced by 1% CO_2 increase per year. The linear trend over the period was used to project a 70-year change in relevant model parameters. Results for a 15-model ensemble mean climate projection showed that the thermodynamic potential intensity (THPI) increases on average by 1.0%~3.1% over the different ocean basins. The increase is attributed mostly to changes in the surface enthalpy transfer (thermodynamic disequilibrium between the ocean and atmosphere) in the transient response to increasing CO_2 concentrations. The projected increase in THPI is consistent with that found in other recent studies.

The effects of the evolving large-scale dynamical variables on the projected PI were determined using the empirical formulation of Zeng et al. (2007, 2008), which takes into account the effects of vertical shear and translational speed based on a statistical analysis of present-day observations. Inclusion of the dynamical efficiency calculations in the formulation led to larger increases in PI in some basins and to smaller increases in other basins compared to results obtained for just the THPI. The largest effect for including dynamical efficiency was found in the main tropical-cyclone development region of the North Atlantic, where the projected PI change was reduced by 50%. Projections from individual model results vary greatly (Figure 2.9), and some models project an increase in PI of 10% in the eastern Pacific and South Indian Ocean. [J. Yu, Y. Wang, and K. Hamilton (IPRC)]

A study focusing on the PI projections for the North Indian Ocean has been published. [J. Yu and Y. Wang, 2009: Response of tropical cyclone potential intensity over the north Indian Ocean to global warming, *GRL*, **36**, L03709, doi:10.1029/2008GL036742]

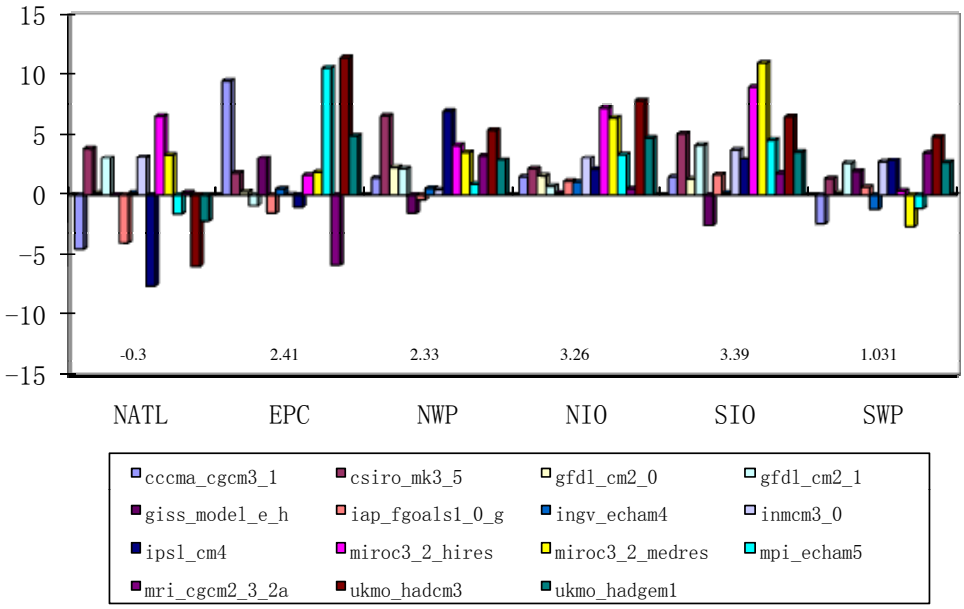

Figure 2.9. Percentage change in the PI, modified by including empirical dynamical efficiency, for six individual ocean basins in response to a transient doubling of CO_2 concentration in 15 state-of-the art coupled GCMs. The different color bars correspond to the different CGCMs as given in the legends. The percentage change for each region averaged across all models is also given.

Ocean Processes

Origin and pathway of Equatorial 13°C Water in the Pacific. Analogous to the subtropical cells (STCs), which are thought to be involved in the dynamics of the El Niño–Southern Oscillation (ENSO), the circulation of the Equatorial 13°C Water is part of a meridional overturning cell, but extends deeper down in the ocean and to higher latitudes than the STCs. Variations in this lower thermocline cell are likely to be related to variations in the eastern equatorial Pacific surface temperature, where mixed layers are typically very shallow. This suggests that variations in the Equatorial 13°C Water may play a role in the evolution of the eastern Pacific "cold tongue" and thus in ENSO.

IPRC scientists and their colleagues at other institutions explored the origin and pathways of this 13°C Water by using a simulated passive tracer and its adjoint that were based on circulation estimates of a global general circulation model. The results confirmed earlier hypotheses on the origin of the 13°C Water, suggesting that some of this water mass is formed northeast of New Zealand. Water subducted there in winter spreads in the mid and low latitudes of the South Pacific and moves into the equatorial region mostly via the western boundary current.

Of interest is that 47% of the total volume of the 13°C Water comes from depths above the σ_θ=25.8 kg/m^3 surface. Some of the water transformation occurs near New Guinea and Philippine coasts. Convergence of warm water and mixing associated with the intense western boundary current could bring

about the transformation as others have suggested. The warm water originates from the eastern subtropical gyre, making the eastern subtropical mode water a major source of the 13°C Water.

The amount of the 13°C Water coming from the Southern Hemisphere is larger than that from the Northern Hemisphere (Figure 2.10). With a significant contribution from the deep waters, the Southern Hemisphere origin becomes increasingly important with time, and its relative importance to the Northern Hemisphere origin is close to double at the end of the integration. The dominance of South Pacific origin is probably related to the Indonesian throughflow as some have suggested.

The study further suggests that more than 90% of the 13°C Water enters the equatorial region mostly through the low-latitude western boundary currents in their respective hemispheres and only a little through the corresponding pathways in the interior ocean. Most of the 13°C Water that forms in the subtropics is trapped and recirculates in the subtropical gyre, with only a small portion reaching the equatorial region through the low-latitude western boundary current after having been mixed substantially. This means that the 13°C Water originates from the subtropics but water formed in the subtropics does not necessarily move to the equatorial region. The subtropical gyre seems to act as a water capacitor, storing variations in the subtropics and conveying their impact to the equatorial region, a topic of future studies. [T. Qu and S. Gao (IPRC); I. Fukumori (JPL); R.A. Fine (U. of Miami); and E.J. Lindstrom (NASA): Origin and Pathway of Equatorial 13°C Water in the Pacific identified by a simulated passive tracer and its adjoint, *JPO*, in press.]

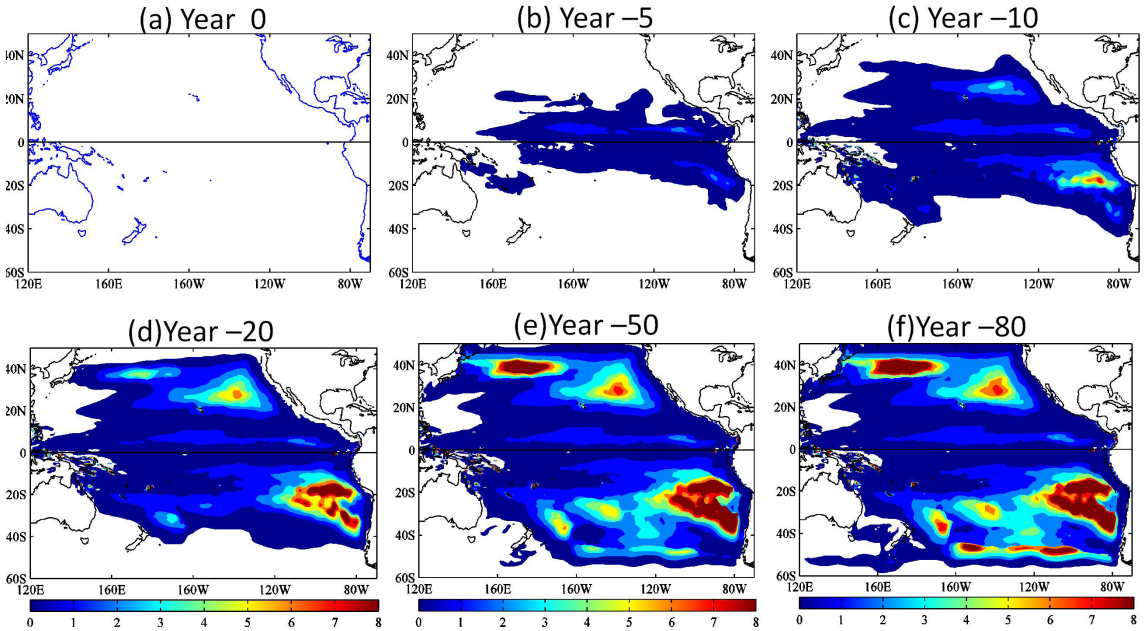

Figure 2.10. Adjoint tracer (ATU/m^2) tracked into the winter mixed layer at year (a) 0, (b) –5(c), –10, (d) –20, (e) –50, and (f) –80. The tracer was originally released in the density range of 0.1 kg/m^3 above and below its vertical gradient minimum in the region 8°S–8°N and 130W°–90°W.

Semiannual variation in the western tropical Pacific Ocean. The North Equatorial Current (NEC) bifurcates into the northward-flowing Kuroshio and the southward-flowing Mindanao Current (MC), which in turn feeds the North Equatorial Countercurrent (NECC), forming a highly variable current system in the western tropical Pacific. Linked to a cold, cyclonic circulation, the Mindanao Dome, the conditions in this

current system are closely related to the Asian monsoon and the El Niño–Southern Oscillation. Scientists at the IPRC and their colleagues elsewhere analyzed this current system last year by using altimeter data and results from the high resolution Ocean GCM for the Earth Simulator (OFES). This work has now revealed the existence of a semiannual variation in the western tropical Pacific that can be explained by a combination of local Ekman pumping and westward propagation of Rossby waves originating in the central tropical Pacific along a band that lies within the Intertropical Convergence Zones of the Northern and Southern Hemispheres. Moored acoustic Doppler current profile measurements and results from OFES both show that, once these Rossby waves approach the western tropical Pacific, they, together with the local Ekman pumping associated with the monsoon, affect the sea surface height downstream, altering the alongshore pressure gradient that drives the MC (Figure 2.11). Since the semiannual variation in the MC is as large as the annual variation, these waves must be responsible for much of the variation in this current. Long-term sustained observations, as well as continued modeling efforts for the region, are warranted, given the large variation and its possible climatic significance. [T. Qu (IPRC); J. Gan (U. Science and Technology); A. Ishida and Y. Kashino (JAMSTEC); and T. Tozuka (U. Tokyo): Semiannual variation in the western tropical Pacific Ocean, *Geophys. Res. Lett.*, **35**, L16602, doi:10.1029/2008GL035058, 2008.]

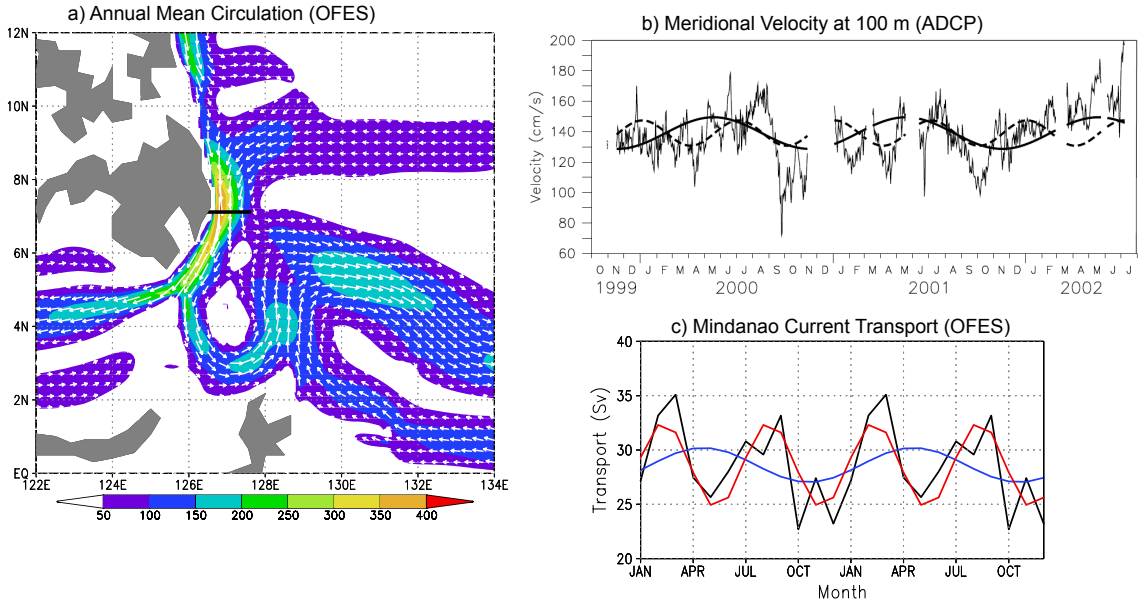

Figure 2.11. (a) Transport (0–1000 m) per horizontal unit (m^2/s) in the western tropical Pacific from OFES, (b) time series of daily averaged velocity (cm/s) toward 197° true north at 100 m depth at 6°50'N, 126°43'E from ADCP measurements, superimposed with its mean annual and semiannual cycles during October 1999– July 2002, and (c) seasonal variation of southward Mindanao Current transport (Sv) superimposed with its annual (blue) and semiannual (red) components across 7°N from OFES. The asterisk in (a) indicates the location of ADCP measurements used for (b) and the solid line, the location of transaction used for (c).

Small vertical scale velocity features in the equatorial thermocline. Using the JAMSTEC RV *Mirai* and the regular cruises to service the TRITON moorings in the western equatorial Pacific, IPRC scientists have collaborated with JAMSTEC in deploying a high-frequency (600kHz) Acoustic Doppler Current Profiler (ADCP) to get higher vertical resolution measurements of ocean currents than available from ADCP mounted on ship hulls or on moorings. Because the high-frequency ADCP has limited range, the device is attached to a conductivity-temperature-depth (CTD) sensor frame and lowered through the water column. One of the meridional sections taken with the instrument is shown in Figure 2.12.

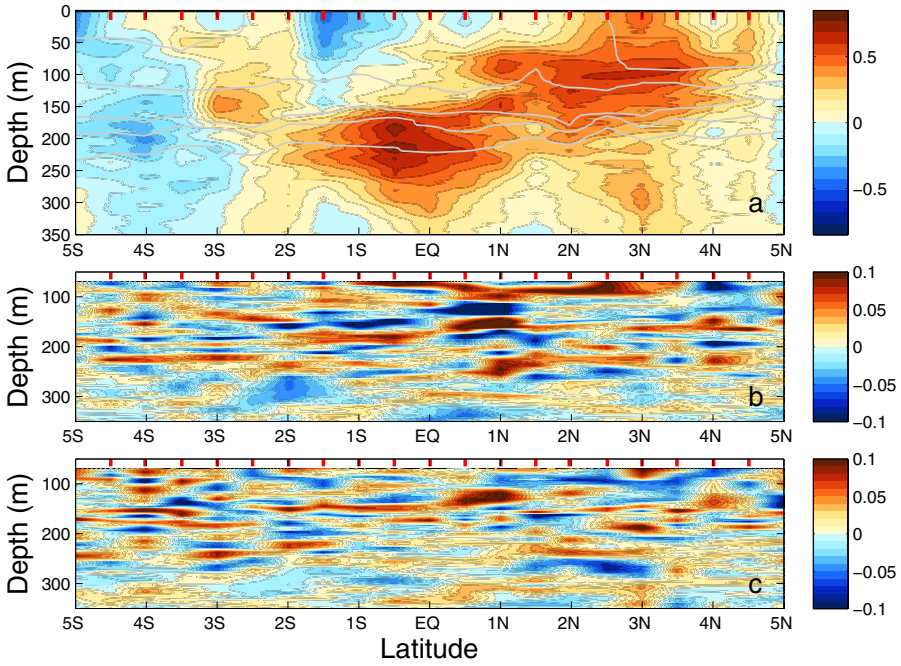

Figure 2.12. (a) The eastward (zonal) component of velocity measured along 156°E in July 2008. Red colors indicate eastward flow, blue westward (contour interval: 0.085 m/s). Gray lines show contours of potential density (contour interval: 1 kg/m^3). (b) Eastward component of velocity, u_a after a high-pass filter has been applied in the vertical. Data are plotted on constant density surfaces at the mean depth of each surface (contour interval: 0.01 m/s; color saturates at ± 0.1 m/s). (c) Same as (b) but for the northward component of velocity, v_a. The red lines at the top of each panel indicate the location of individual stations.

The general distribution of the zonal component of velocity (Figure 2.12a) is typical for this longitude (although the strength and position of individual currents can vary markedly, even on relatively short time scales). The prominent eastward flowing currents are the Equatorial Undercurrent (EUC), centered just south of the equator at 220 m depth, and the North Equatorial Countercurrent (NECC), centered around 3°N and 100 m depth. A somewhat weaker South Equatorial Countercurrent (SECC) is centered around 3°S and 150 m depth.

Numerous small vertical scale features are superimposed on the major currents. These features have such strength that the core of the EUC is split into multiple maxima. Because of their small vertical scale, they are masked in measurements using conventional, lower resolution, instrumentation.

To focus on the small scales, a high-pass filter was applied to the data in the vertical, and the remaining eastward and northward components of velocity, respectively, are plotted on constant potential density surfaces at the mean depth of the individual surfaces (Figure 2.12b and c). Numerous small vertical scale features are present across the width of the section. A number of these features stretch over more than one sampling location, with some extending over 100 km.

Probable causes for the small vertical scale structures include instabilities of equatorial currents (inertial and parametric subharmonic instabilities) and wind generated near-inertial oscillations. Associated modeling studies are being conducted to establish the controls and impact of the features.

The vertical shear associated with these small vertical scale velocity features is large enough to lower the local Richardson number, indicating shear-induced mixing. These features probably contribute

significantly to both vertical and lateral mixing in the equatorial thermocline, and their presence needs to be taken into account in mixing parameterizations in ocean models. Such a parameterization scheme should include a functional dependence on the stability of the equatorial current system and wind variability. Both of these factors depend on the state of the ocean-atmosphere system, which raises the possibility of potential feedbacks between ENSO and small-scale mixing. [K. J. Richards and A. Natarov (IPRC); E. Firing (U. Hawai‘i); and Y. Kashino (JAMSTEC)]

Satellite images reveal two regimes for ocean eddies west of the Hawaiian Islands. Ocean eddies with a scale of 100 km or more greatly impact ocean dynamics and marine life. Weekly satellite sea surface height (SSH) anomaly data over a 15-year period were thus analyzed to determine the mesoscale eddy characteristics in the lee of the island of Hawaii, the largest island in the Hawaiian Island chain. The lee eddy variability can be separated into two geographical regions: in the immediate lee southwest of Hawaii (Region-E), eddy signals have a predominant 60-day period, whereas in the region along 19°N west of ~160°W (Region-W), the eddy variability is dominated by 100-day signals. By applying the simple Ekman pumping model forced by the weekly QuikSCAT wind data, the observed 60-day eddy signals are seen to originate in the southwest corner of Hawaii and are induced by the local 60-day wind stress curl variability associated with the blocking of the trade wind by the islands of Maui and Hawaii. The fact that the 60-day signals are confined to the lee of the island of Hawaii implies that these wind-induced eddies have a relatively short life span and that they are independent of the 100-day signals that extend further westward. Since the large-amplitude, 60-day SSH anomalies take 1~2 weeks to fully develop, the real-time observed wind stress data could be used to predict the anomalies. [S. Yoshida and P. Hacker (IPRC), B. Qiu (U. Hawai‘i)]

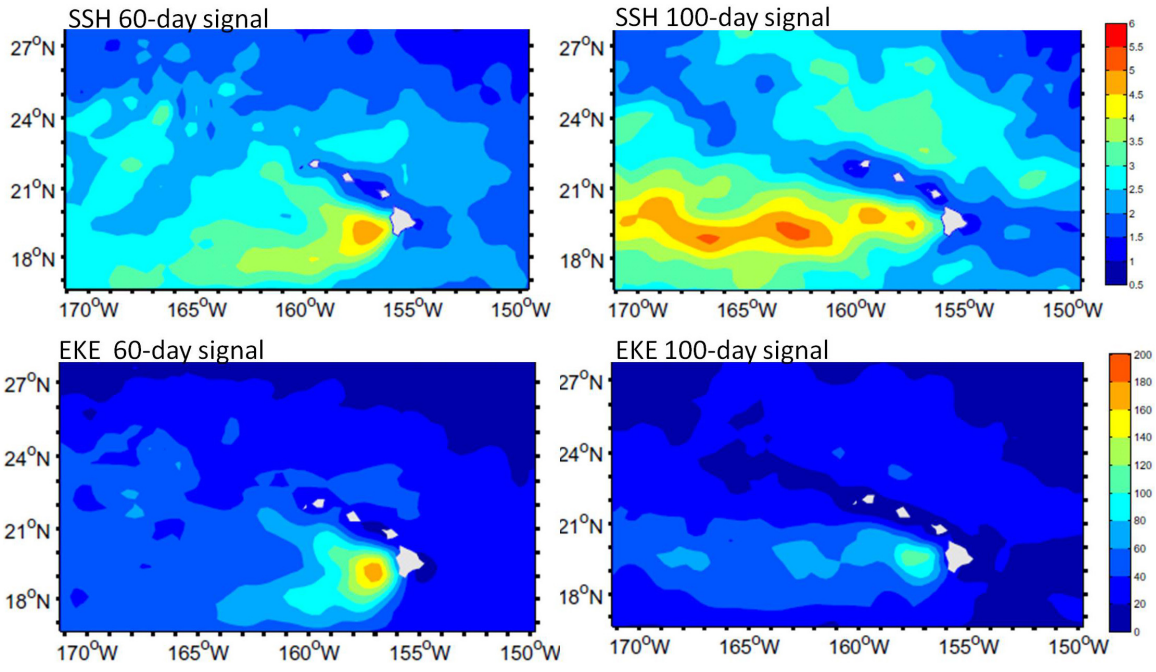

Figure 2.13. Horizontal maps of the root mean square of sea surface height (SSH) anomaly (top; in cm) and eddy kinetic energy (bottom; in cm/s^2). SSH anomaly is bandpassed at 60-days (left) and 100-days (right).

Chapter 3: MONSOON

Monsoon Annual Cycle and Intraseasonal Oscillation

Objective definition of the Indian summer monsoon onset. Every year the Indian Meteorological Department (IMD) makes an official, but subjective, prediction of the onset of the Indian summer monsoon (ISM) and rainy season. Analyzing records from 1948 to 2007, IPRC scientists showed that the onset of the sustained 850 hPa zonal wind averaged over the southern Arabian Sea (SAS; 5°N–15°N, 40°E-80°E) is in excellent agreement with the abrupt start of the rainy season, and it agrees in 90% of the years with the official onset date of the IMD (Figure 3.1). Given the objectiveness of the SAS low-level westerlies and their representation of the large-scale circulation, the onset of these sustained zonal winds is proposed as the ISM onset definition. It provides an objective metric for verification of numerical model simulations, prediction of the ISM onset, and predictability studies of the interannual variations of the ISM onset. [B. Wang and Q. Ding (IPRC); and P.V. Joseph (Cochin University): Objective definition of the Indian summer monsoon onset. *J. Climate*, in press. IPRC-561]

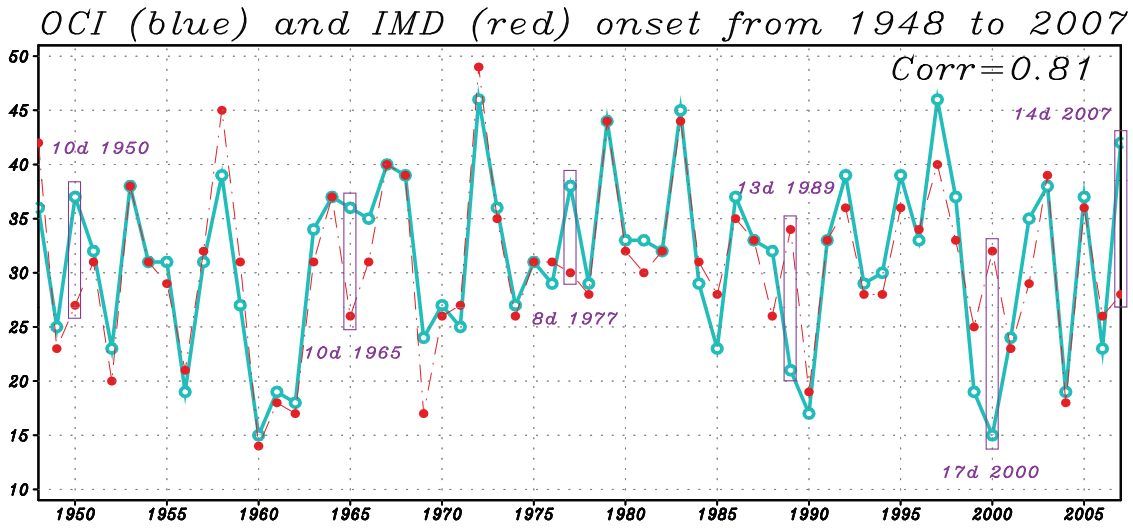

Figure 3.1. Time series of onset dates (days after May 1) defined by IMD (red dot) and Ocean Circulation Index (OCI) (blue circle) for the 60-year period from 1948 to 2007. The years with large discrepancies are enclosed with boxes.

Worldwide study of quasi-biweekly oscillations. To improve understanding of tropical and subtropical weather systems, the evolution of the quasi-biweekly oscillation (QBW) with periods 12–20 day was investigated by tracking these periods globally and deriving an extended empirical orthogonal function (EEOF) analysis of their occurrence. Based on their propagation characteristics and association with extratropical disturbances, the QBW modes were classified as either westward- or eastward-propagating. The westward mode is found in Asia–Pacific and Central America during boreal summer; it originates in the tropics and dissipates in the subtropics and can be understood in terms of equatorial Rossby waves in the monsoon mean flow and convective coupling. The eastward-propagating mode, on the other hand, connects with upstream extratropical Rossby wave trains and propagates both eastward and equatorward. Barotropic Rossby wave trains are essential to its initiation, development, and propagation in the subtropics. Results suggest that both tropical and extratropical atmospheric dynamics contribute to the behavior of the QBW systems worldwide. This global conceptual picture of the QBW helps to

understand both day-to-day tropical weather variability and the longer-term weather variability arising from the Madden-Julian Oscillation. [K. Kikuchi and B. Wang (IPRC), 2009: Global Perspective of the Quasi-Biweekly Oscillation, *J. Climate*, **22**, 1340–1359. IPRC-550]

Moisture structure of the Quasi-biweekly Mode in the western Pacific. To describe the structure of the summer quasi-biweekly mode (QBM) over the western Pacific, IPRC scientists analyzed the 2000–2004 Atmospheric Infrared Sounder (AIRS) humidity profiles, Tropical Rainfall Measuring Mission (TRMM) Global Precipitation Index (GPI), Quick Scatterometer (QSCAT) satellite-observed surface winds, and SST from the Advanced Microwave Scanning Radiometer (AMSR_E). The 10-to-20-day oscillation originates in the Philippine Sea and propagates northwestward to southern China. The AIRS data reveal that the boundary-layer moisture preconditions the atmosphere for QBM propagation and leads the mid-troposphere moisture during the entire QBM cycle. The anomalous high SST is in-phase with the boundary-layer moistening and may strengthen the disturbance by moistening the boundary layer, destabilizing the troposphere, and leading the QBM in its northwestward path in the western North Pacific. In the ECMWF/TOGA analysis, however, the boundary-layer (BL) moisture anomalies do not lead the mid-troposphere moisture. [T. Li (Nanjing University of Information Science & Technology), X. Fu (IPRC), and W. Lu (Nanjing University), 2009: Moisture Structure of the Quasi-biweekly Mode Revealed by AIRS in Western Pacific, *Advances in Atmospheric Sciences*, **26**, 513–522]

MJO characteristics in the global high-resolution NICAM simulations. The detailed MJO characteristics in two 30-day integrations of the global cloud-system-resolving Nonhydrostatic ICosahedral Atmospheric Model (NICAM) were analyzed with the Multivariate MJO index of Wheeler and Hendon. Results show that the MJO has a realistic evolution in amplitude pattern, geographical locations, eastward propagation, and baroclinic and westward-tilted structures. In the central Indian Ocean, convection develops in anomalous low-level easterly winds and grows to its characteristic strength where the low-level easterly and westerly anomalies meet. In contrast, over the western Pacific, the convection grows with anomalous low-level westerly winds (Figure 3.2). Moisture fluctuations, leading convection in its eastward propagation, tilt clearly to the west with height. The frictional moisture convergence mechanism

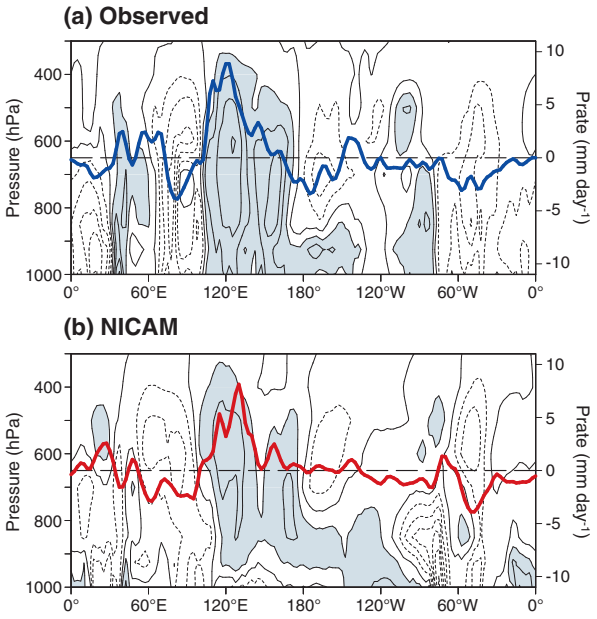

Figure 3.2. Specific humidity anomalies (contour interval is 0.5 g/kg; shaded areas are equal to or greater than zero). Thick blue and red lines represent precipitation rate anomalies (mm/day) in (a) TRMM and (b) NICAM, respectively. Values are averaged between 15°S and 15°N.

operates to maintain the MJO. Such success can be attributed to the explicit representation of the interactions between convection and large-scale circulations. Compared to observations, however, the simulated event grows faster in phases 2 and 3, and peaks with 30% higher amplitude. The fast-growth phases are induced by the fast-growing low-level convergence in the Indian Ocean and the strongly biased ITCZ in the West Pacific during model spinup. [P. Liu, B. Wang, H. Fudeyasu, T. Li, X. Fu, and H. Annamalai (IPRC); M. Satoh, T. Nasuno, H. Miura, H. Taniguchi (JAMSTEC), H. Masunaga (Nagoya University): An MJO Simulated by the NICAM at 14 km and 7 km Resolutions. *Mon. Wea. Rev*, in press.]

Planetary scale-selectioin of the Madden-Julian Oscillation. To examine the reason for the planetary scale of the Madden-Julian Oscillation (MJO), numerical experiments were conducted with a 2.5-layer and 2-level model. The evolution of initial perturbations of equatorial Kelvin waves, ranging from zonal wavenumbers 1 to 15, was analyzed. With a frictional boundary layer, a short wavelength under linear heating is the most unstable mode, but with nonlinear heating, the zonal wavenumber 1 grows fastest. This outcome differs significantly from that in a model without a boundary layer, in which neither linear nor nonlinear heating leads to long waves. The simulations point out that the combined effect of nonlinear heating and a frictional boundary layer is crucial to the planetary scale of the MJO. Under nonlinear heating, a dry Kelvin wave and a wet Kelvin-Rossby wave couplet have different phase speeds. A fast dry Kelvin wave, triggered by a convective branch, may "catch up" and suppress a convective branch traveling ahead of it at the phase speed of the wet Kelvin-Rossby wave couplet *if the distance between the two neighboring convective branches is smaller than a critical distance* (about 16,000 km) (Figure 3.3). The interference between the dry Kelvin wave and the wet Kelvin-Rossby wave couplet eventually dissipates and "filters out" shorter wavelength perturbations, resulting in a long wave. The boundary layer is important in destabilizing the MJO through frictional moisture convergences and in retaining the in-phase zonal-wind-pressure structure. [T. Li, and C. Zhou (University of Hawai'i): Planetary scale selection of the Madden-Julian Oscillation. *J. Atmos. Sci.*, IPRC-606.]

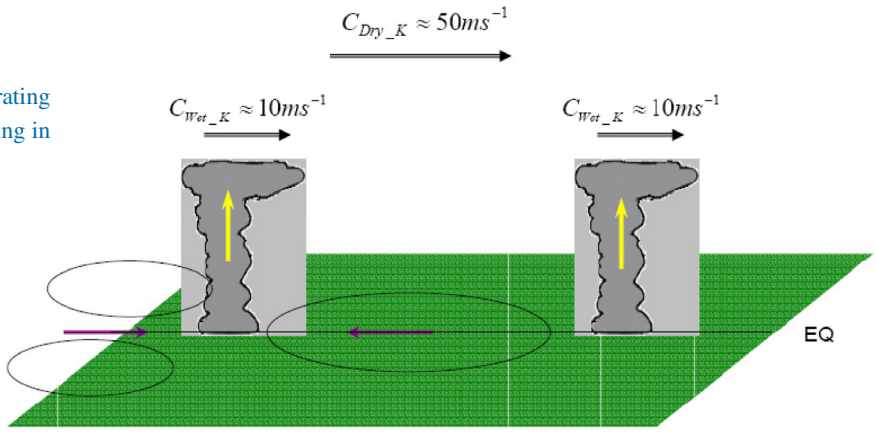

Figure 3.3. Schematic illustrating the role of the nonlinear heating in the MJO.

Stratiform rainfall sustains the Madden-Julian Oscillation in GCM experiments. The impact of stratiform (large-scale) rainfall on the development and maintenance of the Madden-Julian Oscillation (MJO) was examined in a suite of sensitivity experiments with the ECHAM-4 atmospheric general circulation model (GCM) and its ocean-coupled version run in a weather-forecast mode and in three, 20-year, free integrations. The detrainment rate ratio of deep to shallow convection, which supplies water to stratiform clouds, was systematically varied, resulting in significant changes in the amount of stratiform rainfall. Both the forecast experiments and the extended free integrations indicate that the model must produce a

significant proportion (≥ 30%) of stratiform rainfall to sustain a robust MJO. Too little stratiform rainfall results in drizzle-like regimes with neither an eastward- nor a northward-propagating MJO. The reason is that the latent heat released in stratiform rainfall significantly warms the upper troposphere. The heating together with anomalously higher temperatures produces eddies that provide potential energy to sustain the MJO and to allow the heating from precipitation to interact with the large-scale, low-frequency circulation, a critical aspect to the development and maintenance of the MJO. This finding implies that a realistic representation of stratiform rainfall and its connection to the convective component in GCMs should improve simulation of the MJO. [Fu, X., and B. Wang (IPRC): Critical roles of the stratiform rainfall in sustaining the Madden-Julian Oscillation: GCM Experiments. *J. Climate*, in press. IPRC-602]

Monsoon Interannual and Decadal Variability

The rainfall–SST relationship in the western North Pacific depends on phases of El Niño. An analysis of the summer rainfall-SST relationship over the western North Pacific (WNP) from 1979 to 2005 shows an overall weak negative correlation and significant interannual variation (Figure 3.4) that is related to phases of El Niño. During El Niño developing (decaying) summers, the rainfall-SST correlation is significantly positive (negative). The *positive* correlation is attributed to an interplay between the anomalous Walker circulation and cross-equatorial flows associated with an enhanced WNP summer monsoon. The former leads to less than normal rainfall in the western Pacific, and the latter to lower than normal SST due to enhanced surface latent heat fluxes. The *negative* correlation is attributed to the maintenance of an anomalous Philippine Sea anticyclone that lasts from the El Niño peak in winter to the subsequent summer. The anomalous anticyclone suppresses the local rainfall, and the sea surface warms because of increased solar radiation (less clouds) and reduced surface latent heat flux (weak monsoon westerlies). In the remaining summers, the rainfall-SST correlation is insignificant. The overall weak negative rainfall-SST correlation is attributable to the significant negative correlation during El Niño decaying summers. [B. Wu and T. Zhou (Chinese Academy of Sciences); and T. Li (IPRC): Contrast of rainfall-SST relationships in the western North Pacific between the ENSO developing and decaying summers. *J. Climate*, in press. IPRC-600.]

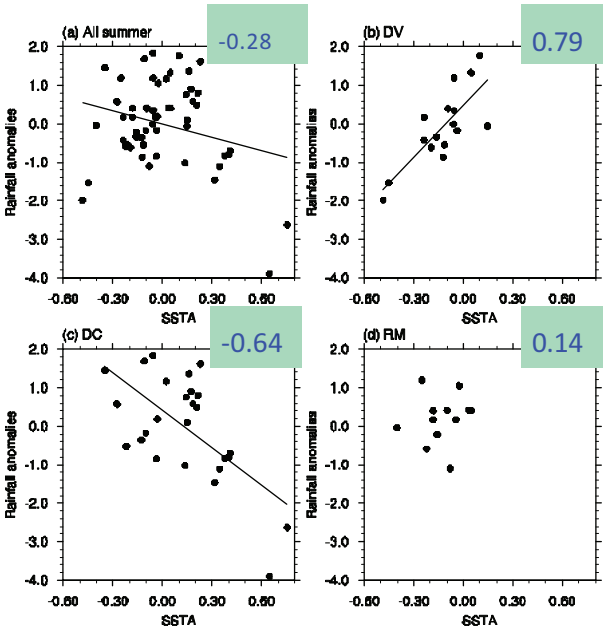

Figure 3.4. Scatter plots of the area-averaged (2.5°N–15°N, 120°E–140°E) precipitation and SST anomalies for (a) all summers from 1979 to 2005, (b) El Niño developing summers, (c) El Niño decaying summers, and (d) remaining summers. The area-averaged rainfall–SST correlation coefficients are written at the top right corner of each panel.

The impact of conditions in the tropical Indian Ocean and Indonesian Seas on El Niño. Earlier observational studies suggest that the tropical Indian Ocean SST impacts the amplitude of a developing El Niño. Now diagnostics of model-composited ocean-atmosphere variables in 20th century integrations of the GFDL_CM2.1 coupled model show that El Niño events that co-occur with the Indian Ocean Dipole-Zonal mode (IODZM) tend to be stronger than those without IODZM events. Maps across the Indian Ocean and western Pacific of differences in the composites (El Niño with IODZM minus El Niño without IODZM) reveal that during May-June in the year of both a developing El Niño and an IODZM, equatorial westerly winds increase abruptly over the western Pacific leading to a deeper thermocline and warmer SST than normal in the equatorial eastern Pacific. The stronger westerly winds coincide with the time when the mean-state conditions in the equatorial Pacific favor instability growth. Solutions with the model not only confirm the earlier results, but they also suggest that when an El Niño develops with an IODZM, the abrupt stronger westerly winds over the equatorial western Pacific are largely due to cold SST anomalies in Indonesian Seas. An examination of observed conditions during 2006, when both an El Niño and an IODZM occurred, confirm this finding. Additional sensitivity experiments with a high-resolution ocean model indicated that the cold SST anomalies over the Indonesian Seas during IODZM years are due to southwesterly wind anomalies, which increase surface heat loss and evaporation, and subsurface upwelling. The implication is that to understand and accurately predict the intensity of El Niño, coupled models need to represent regional air-sea interactions over the equatorial Indo-Pacific warm pool realistically. [H. Annamalai, S. Kida, and J. Hafner (IPRC)]

Interactions between the Indian summer monsoon and the intraseasonal oscillation. Observations show that Indian summer (June–September) monsoon rainfall is negatively correlated with intraseasonal oscillation (ISO) intensity as measured by the standard deviation of filtered outgoing longwave radiation (Figure 3.5). A strong Indian monsoon, as measured by the all-India rainfall index (the average of the June–September rainfall measured by rain gauges across India), is thought to decrease convection over the equatorial eastern Indian Ocean, suppressing the eastward and northward propagating ISO and weakening the intraseasonal activity over the monsoon region. The ISO may feed back to the Indian summer mean monsoon through nonlinear eddy momentum transport. ISO intensity, moreover, tends to differ during summers when El Niño is developing or decaying. [Qi, Y., R. Zhang, T. Li, and M. Wen, 2008: Interactions between the summer mean monsoon and the intraseasonal oscillation in the Indian monsoon region. *Geophys. Res. Lett.*, **35**, L17704, doi:10.1029/2008GL034517. IPRC-577.]

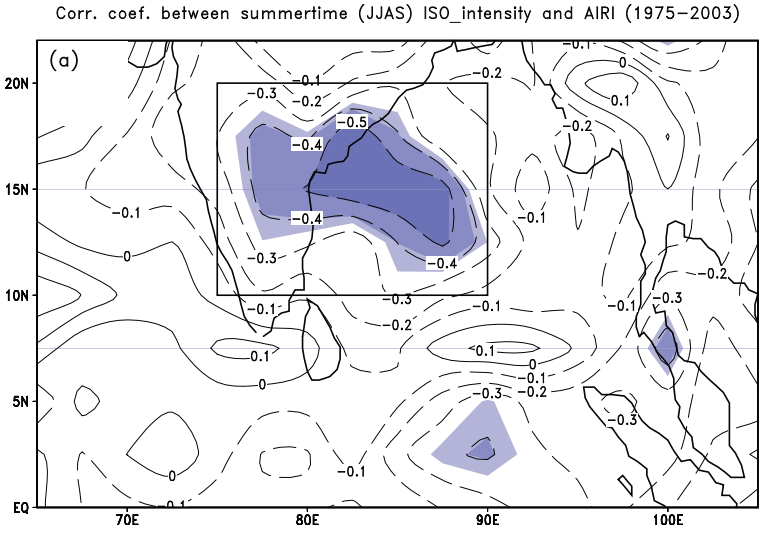

Figure 3.5. Correlation coefficients between the summer time (June–September) ISO intensity and all-India rainfall index for the period 1975–2003. Shaded areas exceed the 95% significance level.

Decadal change in intraseasonal variability over the western North Pacific. The average periodicity of the intraseasonal variability (ISV) in convective rainfall over the South China Sea (SCS) has decreased significantly from around 64 days during 1979–1993 to around 42 days during 1994– 2007. Analysis of the mean temporal-spatial evolution of the ISV and convection over the SCS reveals several differences between the two time-periods. (1) During 1979–1993, the northward propagating convection from the maritime continent merges with the westward propagating convection along 20°N–25°N from the central North Pacific. (2) During 1994–2007, OLR has a tilted band structure and vorticity anomalies are seen in the west-northwest to east-southeast direction and are connected to the equatorial eastward propagating Madden-Julian Oscillation (MJO). (3) During 1979–1993 (1994–2007), the convection anomalies between the northern Indian Ocean and the western North Pacific are in (out of) phase. (4) During 1994–2007, the convection anomalies over the Bay of Bengal are closely correlated with those over the SCS as part of an elongated spatial structure. This change in circulation pattern suggests that the merged convection from the two regions during 1979–1993 prolonged and increased convection over the SCS, resulting in a weak relationship with the eastward propagating MJO. [Y. Kajikawa (IPRC), T. Yasunari (Nagoya University), and Bin Wang (IPRC): Decadal change in intreaseasonal variability of the South China Sea, *Geophys. Res. Lett.*, in press. IPRC-598]

The 2008 record-breaking extreme cold period in China. During February 2008, a series of severe, cold winter storms occurred over large regions of southern and central China. In contrast to usual cold surges that last less than 10 days, this cold period persisted for over a month. Diagnosis of observations and numerical experiments showed that the cold period was associated with a prolonged Siberian High and persistent northerly winds over Southeast Asia. The onset of the anomalous conditions concurred

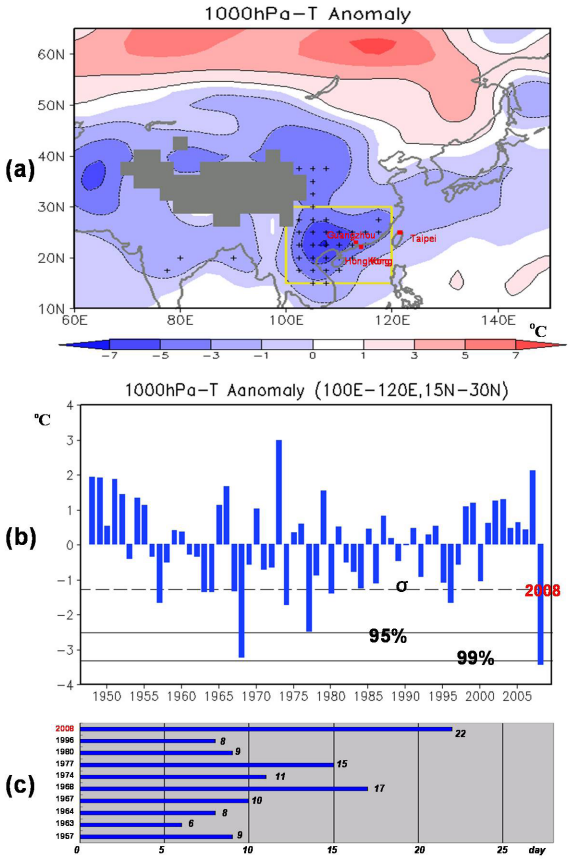

Figure 3.6. (a) Distribution of surface temperature anomalies over Eurasia in February 2008. The areas marked by "+" indicate temperatures significantly lower than average at the 95% confidence level. (b) Interannual variation of average (box in panel a) February 1000 hPa temperature anomalies from 1949–2008. The horizontal lines denote the threshold of the 95% and 99% confidence level respectively. (c) number of consecutive days surface mean-temperature below –1 standard deviation in February.

with a phase-change in the intraseasonal oscillation (ISO) over Sumatra. During a normal rainy ISO event, convection continues its eastward journey; in this case, convection stayed over Sumatra the entire February 2008. Anomaly atmospheric GCM experiments suggest that the ISO heating over the Maritime Continent sustained the anomalous northerly winds and that it was blocked from moving eastward by circulation and SST anomalies associated with a La Niña event, which by early February had progressed westward into the western Pacific. La Niña not only blocked the ISO, but increased heating over the Maritime Continent through the anomalous Walker circulation. Thus the prolonged heating due to the stationary ISO and La Nina sustained the northerly winds and cold spell into southern China. [C.-C. Hong (Taipei Municipal University of Education) and T. Li (IPRC): The Extreme Cold Anomaly over Southeast Asia in February 2008: Roles of ISO and ENSO. *J. Climate*, in press. IPRC-580.]

Monsoon Predictability

Advances in seasonal prediction: Assessment of the APCC/CliPAS 14-model ensemble seasonal hindcasts (1980–2004). The skill of multi-model ensemble (MME) deterministic and probabilistic seasonal prediction was assessed in 25-year (1980–2004) hindcasts performed with 14 climate model systems (7 one-tier and 7 two-tier systems) that participate in the Climate Prediction and its Application to Society (CliPAS) project, sponsored by the Asia-Pacific Economic Cooperation Climate Center (APCC). Furthermore, MME forecasts using 7 DEMETER models were evaluated for the period 1981–2001.

The temporal correlation coefficient between the deterministic CliPAS one-tier MME forecast at a six-month lead (initiated May 1) and the Niño 3.4 SST index is 0.77, which is significantly higher than the corresponding averaged skill of 7 individual coupled models (0.63). The MME consisting of 14 coupled models from DEMETER and CliPAS results in an even higher correlation (0.87). The MME also predicts well the amplitude of Niño 3.4 SST index. The accuracy of the CliPAS MME forecasts increases with the number of models.

Equatorial sea surface temperature (SST) anomalies are a source of atmospheric climate variability worldwide. The one-month lead MME hindcast can predict with high fidelity the spatial-temporal structures of the first two leading empirical orthogonal modes of the equatorial SST anomalies in both boreal summer (June–August) and winter (December–February), accounting for about 80% to 90% of the total SST variance. The six-month-lead CLIPAS MME hindcasts of equatorial eastern Indian Ocean SST have a temporal correlation of about 0.68. However, the correlation of three-month-lead hindcasts of the Indian Ocean Dipole (IOD) index drops below 0.40 in May and November because of the prediction barriers in July and January (Figure 3.7).

The forecasts for 2 m air-temperature are better in El Niño than in La Niña years. The forecasts of precipitation and circulation are better in ENSO-decaying than in ENSO-developing summers. There is virtually no skill in ENSO-neutral years.

In the one-tier climate models, more skill in long-lead seasonal forecasts will require improved representation of low frequency coupled dynamics that are basic to realistic simulation of amplitude, spatial patterns, and temporal evolution of the ENSO cycle. Forecasting monsoon precipitation remains a challenge: the local seasonal rainfall predictions over land during summer have little skill, especially over tropical Africa. Little is known about the impact of land-surface initialization on seasonal and monthly forecasts in a multi-model framework. [B. Wang (IPRC) and 27 co-authors, 2009: Advance and Prospectus of Seasonal Prediction, 2008: Assessment of the APCC/CliPAS 14-Model Ensemble Retrospective Seasonal Prediction (1980–2004), *Clim. Dyn.*, **33**, 93–117. IPRC-548]

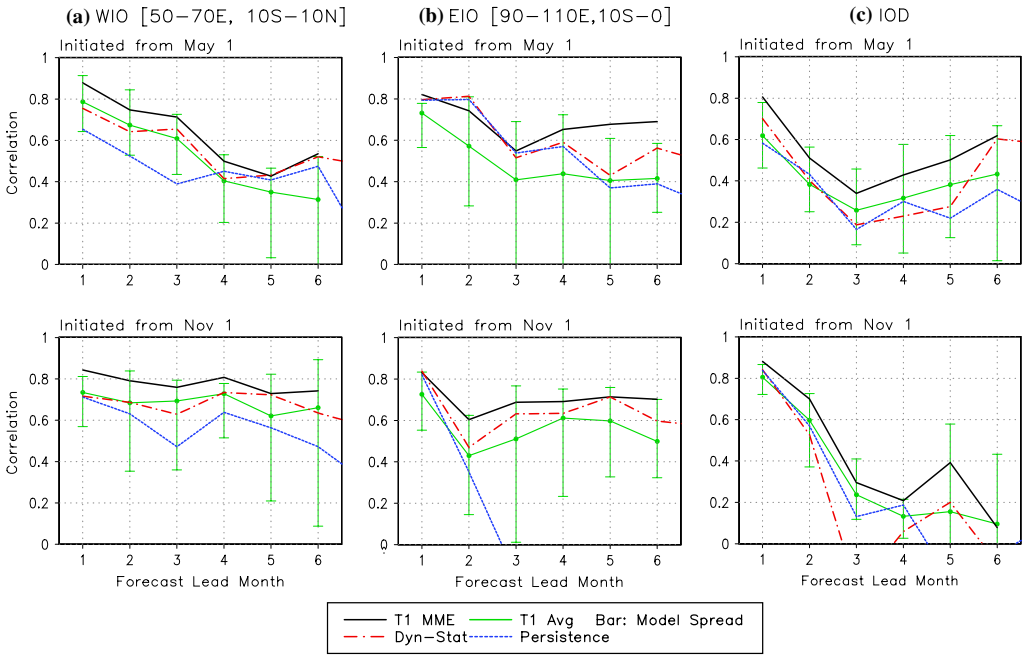

Figure 3.7. For the period 1981–2001, the temporal correlations between SST anomaly observations and "forecasts" from MME with 7 CliPAS coupled models as a function of lead time and initiation month for: (a) the West Indian Ocean (WIO, 50°E –70°E, 10°S–10°N); (b) the East Indian Ocean (EIO, 90°E –110°E, 10°S–0) SSTA; and (c) the Indian Ocean Dipole (IOD) index, which is difference between WIO and EIO SST anomalies. The green lines indicate the averaged skill of the individual models and the bars show the range of the best and worst coupled model skills. For comparison, the skills of the persistence forecast (blue) and the Seoul National University dynamic-statistical model forecast (red) are also shown.

Seasonal climate prediction skill depends upon coupled model mean state and annual cycle. The precipitation hindcasts at one-month lead made by thirteen state-of-the-art coupled climate models and their multi-model ensemble (MME) were analyzed from 1981 to 2001. The evaluation of the precipitation was based on a new metric that consists of the annual mean precipitation as well as summer–winter and spring–fall precipitation modes.

The one-month lead *seasonal* prediction of the 13-model ensemble is comparable to ERA-40 and NCEP-2 reanalyses and is much better than the individual model ensemble predictions. The individual coupled model's seasonal rainfall prediction skill is positively correlated with the individual model's prediction skill of the annual mean and annual cycle rainfall. Correcting the inherent model bias in the mean state is thus critical for improving long-lead seasonal prediction.

Most individual coupled models reproduce realistically the long-term annual mean precipitation and the summer–winter precipitation mode, but they have difficulty in capturing the spring–fall mode, especially over the Indian Ocean and Western North Pacific, where the seasonal SST measures are significantly biased. The coupled models replicate the monsoon-rain domains well except in subtropical East Asia and the tropical western North Pacific. The models also capture the gross features of the seasonal march of the rainy season, including onset and withdrawal of the Asian–Australian monsoon over four major sub-domain. Considerable biases, however, exist in both the amplitude and phase of the annual cycle and the summer precipitation amount, with interannual variability seriously underestimated. [J. -Y. Lee (IPRC) and 13 collaborators]

Predicting extreme phases of the Indian summer monsoon over northern India. Extreme active or break phases in the Indian summer monsoon (ISM) often bring about devastating floods or severe droughts. IPRC scientists found that these extreme phases over northern India are preceded by certain circulation conditions in both the tropics and extratropics. A strengthening of the upper tropospheric Central Asian High together with arrival of enhanced tropical convection from the equatorial Indian Ocean and the South China Sea precedes the likelihood of a heavy rainy period in northern India. Conversely, an anomalous low over Central Asia together with arrival of suppressed convection from the equatorial Indian Ocean and the South China Sea precedes severe droughts. Therefore, the normalized 200 hPa geopotential height over Central Asia and the outgoing longwave radiation over southern India can be used to predict extreme active and break phases in the northern ISM about five days in advance (Figure 3.8). These atmospheric conditions result into an extreme event with a 40% probability, in contrast to the climatological probability of less than 4%. [Q. Ding (U. of Hawai'i) and B. Wang (IPRC), 2009: Predicting extreme phases of the India Summer Monsoon. *J. Climate*, **22**, 346–643. IPRC-536.]

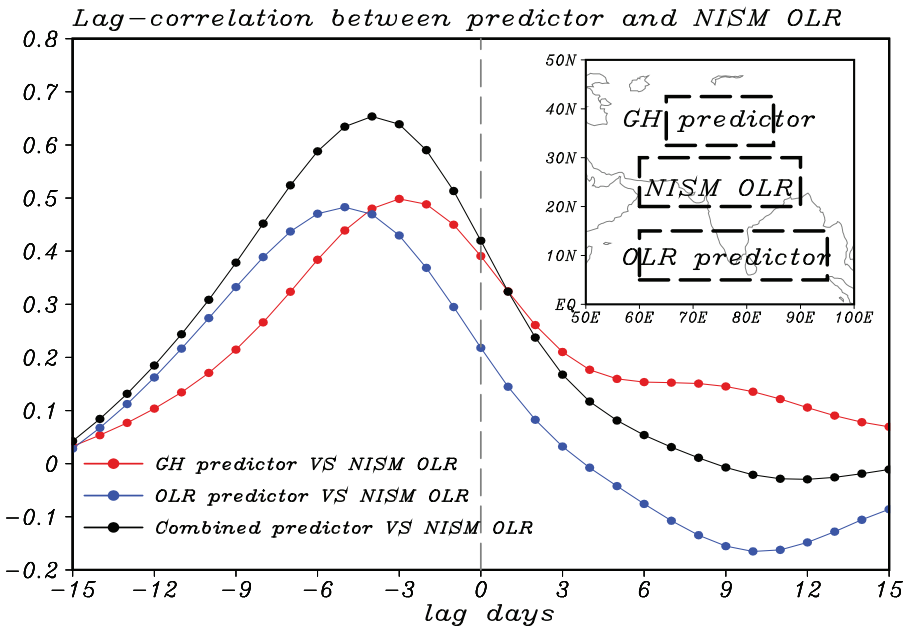

Figure 3.8. Lead-lag correlation coefficients between three predictors of the north India Summer Monsoon: outgoing longwave radiation (OLR), geopotential height (GH) and OLR, and combined GH-OLR. The negative lag days represent the number of days before the onset of an extreme event. The domains of GH and OLR predictors are shown in the embedded map.

Impacts of initial conditions on monsoon intraseasonal forecasts. Using the University of Hawai'i Hybrid Coupled Model, IPRC researchers carried out a suite of experiments to examine the sensitivity of intraseasonal monsoon-rainfall forecasts to initial conditions. They found that during May–September 2004, the NCEP reanalysis convection amplitude associated with intraseasonal monsoon rainfall variation is smaller by a factor of two or three than that observed. When the NCEP reanalysis is used as initial conditions, the monsoon intraseasonal forecast skill of 850 hPa zonal winds and rainfall extends only about a week over the global tropics (30°S–30°N) and Southeast Asia (10°N–30°N, 60°E–120°E). Prediction skill increases steadily with increased convection amplitude in the initial conditions. When the amplitude reaches a level similar to observations, forecast skill extends to 25 days for 850-hPa zonal winds and 15 days for rainfall over both the global tropics and Southeast Asia. Inclusion of high-frequency weather variations in initial

conditions generally extends rainfall predictability about another 5 days. [X. Fu, B. Wang, P. Liu, and J.-Y. Lee (IPRC): Q. Bao (Chinese Academy of Sciences), 2009: Impacts of initial conditions on monsoon intraseasonal forecasting. *Geophys. Res. Lett.*, **36**, L08801; doi:10.1029/2009GL037166. IPRC-603]

Genesis of tropical cyclone Nargis in satellite observations. The formation of Tropical Cyclone (TC) Nargis, which battered Myanmar with deadly consequences on May 2, 2008, was investigated in satellite observations. Nargis became organized as a storm as the result of an abnormally strong disturbance associated with the Madden-Julian oscillation (MJO) in the eastern Indian Ocean. The cyclonic disturbance began to emerge from a Rossby-wave-induced vortex when the MJO reached the Maritime Continent. The northeastward movement of MJO convection facilitated the growth of the disturbance, which became a tropical storm with a central warm-core structure on April 26. The evolution to a tropical cyclone on April 28 was characterized by a radial contraction of the disturbance, which was followed by rapid intensification. This sequence is proposed as a new scenario for understanding how major TCs can develop in the northern Indian Ocean. [K. Kikuchi, B. Wang, and H. Fudeyasu (IPRC), 2009: Genesis of Tropical Cyclone Nargis revealed by multiple satellite observations. *Geophys. Res. Lett.*, **36**, L06811, doi:10.1029/2009GL037296. IPRC-585.]

Monsoon Changes under a Warming Climate

A more arid climate for northern China. Climate changes in northern China, the regions of semiarid steppe and the Gobi Desert, were investigated by applying the Köppen climate classification to Chinese station measurements and to global gridded-datasets compiled from 1951 to 2000. The use of the Köppen scheme enables the detection of climate changes over a longer time-scale than is possible with satellite remote sensing. Comparing the periods 1951–1970 and 1981–2000, the analysis showed a robust climatic shift toward warmer and dryer conditions and conspicuous changes in the already arid climate of northern China. Specifically, the Köppen climate classification showed that from 1951 to 2000 the semiarid (BS) and desert (BW) regions had expanded greatly at the periphery of the existing arid zones (Figure 3.9). The BS area increased by 108×10^3 km^2 and the BW by 39×103 km^2 from 1980

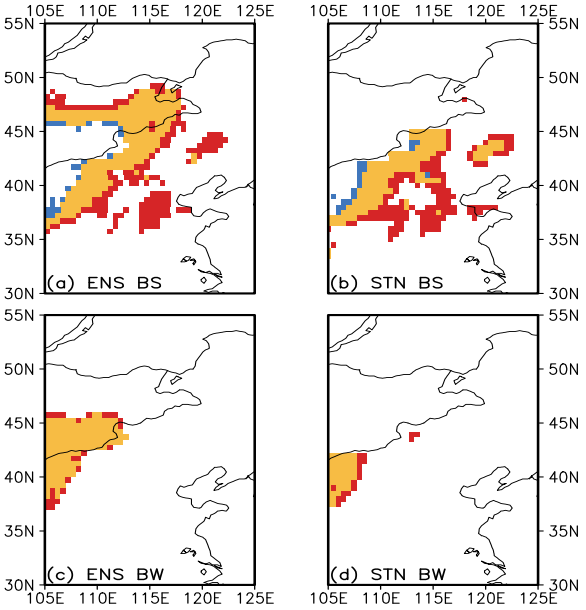

Figure 3.9. Changes in semiarid (top) and desert (bottom) regions between the periods 1951–1970 and 1981–2000. The results are obtained from the ensemble average of the global grid data sets (left) and the Chinese station measurements (right). Yellow indicates the climate type recognized in both periods, and blue (red) denotes the regions identified only in the first (last) period.

to 2000. The growth of BS region for this period is statistically significant at the 99% confidence level in all the data sets examined; for the BW region, only half of the data sets were significant at the 90% confidence level, suggesting that the areal change in BW type is marginally significant. [Kim, H.-J., B. Wang (IPRC), and Q. Ding (U. of Hawai'i), and I.-U. Chung (Kangnung National University), 2008: Changes in arid climate over North China detected by the Köppen Climate Classification, *J. Meteor. Soc. Japan*, **86**, 981–990. IPRC-551.]

Chapter 4: PALEOCLIMATE

North African Humid Periods. Two major studies were conducted on the North African Humid Periods (AHP) over the last 130,000 years: the first study focused on the latest humid period; the second, on the orbital pacing of humid periods.

Study 1. Paleoclimate proxy data consistently show that around 14–12 ka before present (B.P.), grass and low shrubs began to extend northward into the Sahel/Sahara until the early Holocene. This greening was accompanied by significant changes in the region's hydrology. The few studies that have investigated the onset of this latest AHP have difficulty pinpointing its trigger and driver, because the onset occurred during a time when glacial ice-sheets shrank rapidly, atmospheric CO_2 concentrations increased, and Northern Hemispheric climate was punctuated by abrupt climate transitions. This last AHP – according to paleoproxies, archaeological data and climate modeling studies – ended abruptly around 6–4 ka B.P. Although it is generally believed that a declining summer insolation triggered a rapid reduction in the precipitation and vegetation, a final consensus on what produced this transition is missing.

IPRC scientists therefore conducted a series of transient climate simulations with the fully coupled atmosphere–ocean–sea-ice–vegetation model LOVECLIM, spanning the time from the last glacial maximum 21,000 years ago to the pre-industrial age. These simulations used various combinations of prescribed ice-sheet evolution, CO_2 concentrations, and orbital forcing to estimate the importance of the individual forcing factors. The onset of the last AHP was found to be in response to an increase in both the local summer insolation and melting ice-sheets in the Northern Hemisphere. The albedo contrast between vegetation and desert provided a strong positive feedback that accelerated the formation of the AHP. Increased atmospheric CO_2 had only a minor effect, serving as a vegetation fertilizer. These model results suggest the onset of the AHP was only possible after a major reduction of the Northern Hemispheric ice sheets. An "insolation threshold" for AHP onset and termination, as some have suggested, was not found in the LOVECLIM simulations. [Timm, O., A. Timmermann, and L. Menviel (IPRC); Köhler (AWI)]

Study 2. A few exceptionally long records from ocean sediments off the northwest African coast provide compelling evidence that North Africa has alternated between dry and wet climate states during the last five million years. This long-term climate variability is a key argument in faunal evolution theories and in theories of hominid evolution. The marine and lacustrine Pliocene-Pleistocene proxies of past AHPs have supported the notion that summer insolation with a precession period of 19,000–23,000 years drives meridional shifts of the rainbelt and vegetation zones of North Africa.

These data further document that around 3 million years ago the North African summer monsoon started to vary on the dominant timescale of glacial cycles ~ 41,000 years. Around one million years ago this periodicity shifted to a new dominant glacial cycle periodicity of ~100,000 years. This finding supports the idea that the Northern Hemispheric ice sheets have a direct effect on the waxing and waning of vegetation over North Africa.

To see whether the variations in vegetation over Northern Africa can be explained as a response to high-latitude climate and ice sheet changes in the Northern Hemisphere, a transient simulation with the LOVECLIM model over the entire glacial-interglacial cycle from 130,000 years B.P. to present day was conducted. In contrast to comparable previous modeling studies, the IPRC transient simulation used the ice-sheet evolution from the state-of-the-art, 3-dimensional JAMSTEC ice sheet model (IcIES). This

more realistic forcing allowed for the first time the study of the combined effects of the ice sheet and CO_2 forcing during an entire glacial-interglacial cycle. The ice sheet thickness and the resulting land topography were prescribed to the LOVECLIM atmosphere using accelerated forcing. The results (Figure 4.1) confirm the paleoclimatic proxy interpretation that the Northern Hemispheric ice-sheets have a strong influence on climate over North Africa. During times with large ice sheets and overall cooler climate, the increase in insolation due to the precession cycles produces smaller increases in precipitation and vegetation over the Sahara (80,000–20,000 B.P.) than during the last AHP, when the ice sheets were retreating.

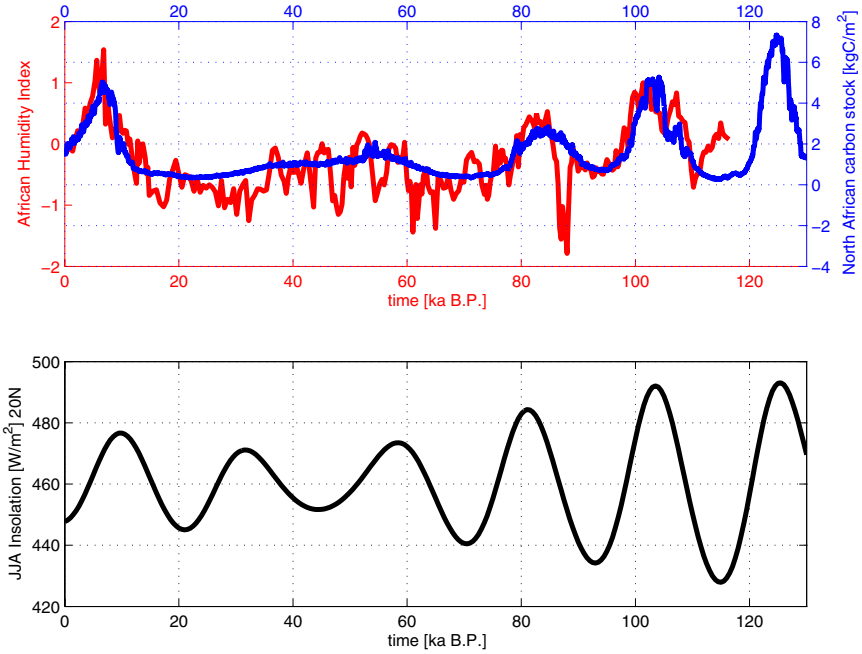

Figure 4.1. (top) Time series of the African Humidity Index (from Tjallingii et al., 2008) (red) and North African carbon stock simulated by LOVECLIM (blue) forced with the time-evolution of ice sheet height and CO_2; (bottom) summer insolation over North Africa (black).

In the simulation, the signature of the 100,000-year signal is much weaker for the Indian/Southeast Asian monsoon than for North Africa. Do existing paleoclimatic proxy records from these other monsoon regions show a minimal 100,000-year ice-sheet signal? What is their response to the precessional cycle? This question was addressed with Independent Component Analysis (ICA), which decomposes a set of observed mixed signals with a non-Gaussian distribution into statistically independent signals. The idea behind the ICA is that monsoon proxies from different sites contain a different mix of precession and 100,000-year ice-sheet signals in their different monsoon responses to the forcing.

The ICA supports the model results: the 100,000-year signal dominates the African monsoon proxies, whereas the precession signal dominates the Asian and South American monsoon proxies. Thus, both model simulation and proxies show the importance of the remote forcing from the Northern Hemispheric ice sheets for the North African monsoon. Further sensitivity model runs and analysis of the ocean's impact on ice-sheet variations will help to understand how the ice-sheets influence the far-away tropical-subtropical rainfall. [O. Timm and A. Timmermann (IPRC); P. Köhler (AWI); A. Abe-Ouchi (CCSR, U. Tokyo and JAMSTEC), F. Saito and T. Segawa (JAMSTEC)]

A "Unified ENSO Proxy" to study past variability of the El Niño-Southern Oscillation. El Niño events are associated with floods, droughts, and other weather disturbances around the world. The strength of these events is measured by anomalously high sea surface temperature (SST) in the tropical eastern Pacific. The determination of the extent to which SST in this region has varied in the past will allow better forecast of what we may expect in the future with regard to the climate impacts of El Niño.

Numerous reconstructions of El Niño-Southern Oscillation (ENSO) variance based on various current and paleo-proxy data sources exist as well as various methods of arriving at a variability index. Individual proxies correlate reasonably well with observations of ENSO variations during the instrumental period, but they vary greatly amongst each other, particularly across different time periods. For example, the standard deviation between the normalized proxies at each time step is almost as large as the standard deviation of each index. To overcome this barrier to reconstructing ENSO variability, IPRC scientists have developed a 'Unified ENSO Proxy' (UEP) by extracting the joint co-variation of 10 frequently used ENSO proxies.

This UEP (Figure 4.2, top panel) is being validated by comparing it to the following: (1) observations during the instrumental period; (2) historic documented chronologies of ENSO; (3) other proxies of ENSO variability not part of the UEP proxy; and (4) evidence obtained through model experiments. The UEP has already shown considerable skill in cross-validation with independent instrumental data.

The UEP suggests that from the 1660 (Little Ice Age) onward, a trend has taken place toward greater ENSO variance, i.e., greater variance in sea surface temperature anomalies. The UEP will now be used to investigate the variations and to seek possible causes. Past studies have found a statistical connection between explosive tropical volcanic eruptions and ENSO, whereby El Niño events tend to be more probable in the years immediately after an explosive eruption (e.g., Adams et al. 2003). IPRC scientists have now used the UEP to study ENSO variability 3 years before, during, and after 13 major such volcanic eruptions that occurred from 1650 to 1977. Early results point to a significantly increased probability of an El Niño event in the year of an explosive eruption (Figure 4.2, bottom panel) and an increased probability of a La Niña event 3 years after an eruption. [S. McGregor and A. Timmermann]

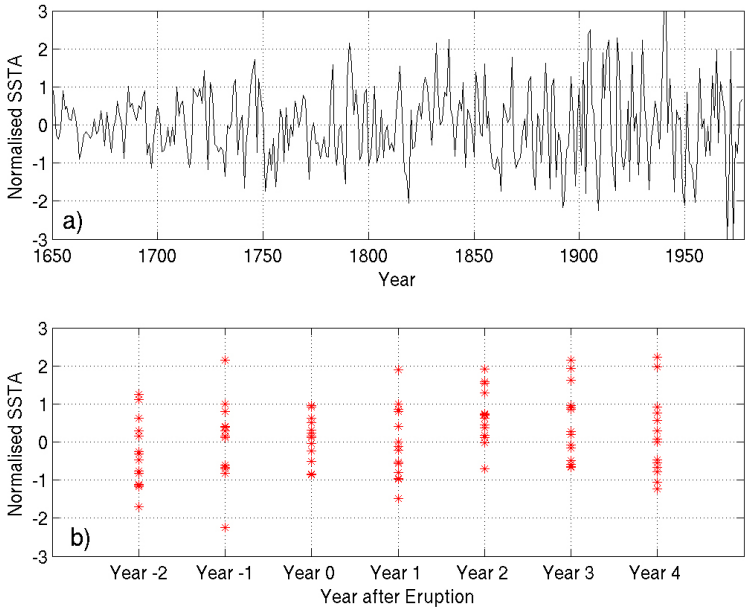

Figure 4.2. (top) The unified ENSO proxy (UEP) for the period 1650–1978; (bottom) composites of the UEP around years in which explosive volcanic eruptions occurred (as obtained from the volcanic forcing index of Gao et al (2008).

Global climate response to an abrupt meltdown of the West Antarctic Ice Sheet. To assess the possible climate impact of a rapid partial meltdown of the West Antarctic Ice Sheet, an idealized experiment was conducted with LOVECLIM, an earth system model of intermediate complexity. A meltwater pulse equivalent to a 6-m sea-level rise over 200 years was added in the Southern Ocean (158°E–60°W, 80°S–70°S). This addition of freshwater decreases surface density and increases stratification of the Southern Ocean, inhibiting Bottom Water formation. The Antarctic Circumpolar Circulation transport is sharply reduced due to a weaker meridional density gradient. Figure 4.3 left panel shows SST anomalies and wind stress anomalies 100 years into the experiment. The Southern Hemisphere upper ocean has cooled by up to 6°C due to the greater stratification and the sea-ice margin stretches further equatorward. The Southern Hemispheric westerlies have intensified, leading to greater equatorward Ekman transport. The Northern Hemisphere warms slightly while the Southern Hemisphere cools, indicating a weak seesaw effect. The reduction in atmospheric CO_2 (not shown) is relatively small (about –6 ppmv).

A key finding is that due to the reduction of Antarctic Bottom Water Formation, subsurface temperatures in the Ross Sea (at depths of 500–1500m) increase by several degrees Celsius (Figure 4.3 right panel). Since the West Antarctic ice sheet is a marine-based ice sheet (large areas are below sea level), this temperature increase could potentially lead to increased melting and accelerated retreat of the grounding line. The resulting freshwater forcing would further weaken the deep convection near Ross Sea and lead to a subsurface ocean warming. This newly identified positive feedback between ocean and ice sheet may accelerate ice-loss over West Antarctica and thereby accelerate of global sea level rise. [A. Timmermann and L. Menviel (IPRC)]

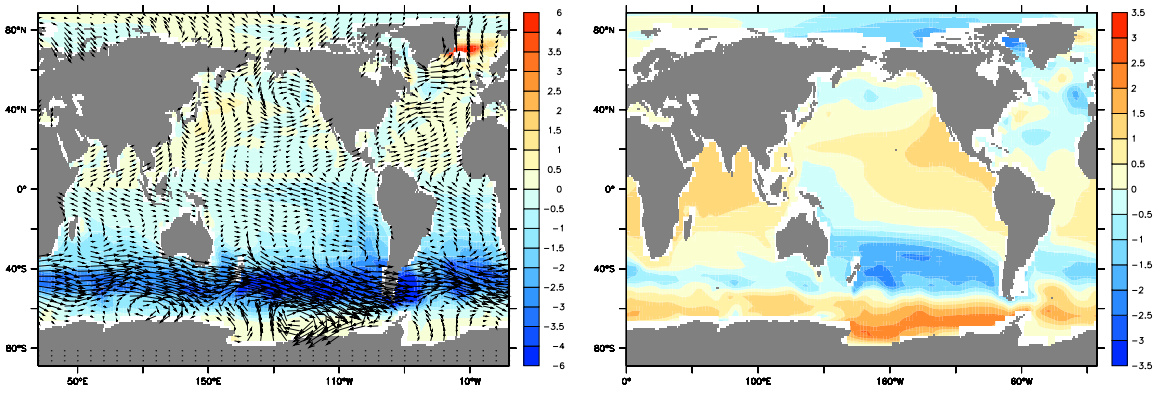

Figure 4.3. (left) SST anomalies (ºC, shaded) and wind stress anomalies (Pa, vectors) and (right) simulated subsurface temperature anomaly (ºC) (averaged between 500–1000 m depth) in response to a Southern Hemispheric meltwater pulse.

Chapter 5: ASIA-PACIFIC DATA-RESEARCH CENTER (APDRC)

The APDRC goals are to advance NOAA's mission and meet regional data and product needs for ocean, climate, and ecosystem information; to support the Global Earth Observation System of Systems (GEOSS) and the NOAA Integrated Data and Environmental Applications (IDEA) Center; and to provide an infrastructure for Global Ocean Data Assimilation Experiment (GODAE) activities. The vision of the APDRC is to link data management and preparation to research within a single center, and to provide a unified source for climate data and products that can be accessed by local researchers and collaborators, the climate research community, and the public.

The APDRC is organized around three main activities:

1) Providing integrated data server and management systems for climate data and products;
2) Developing and serving new climate-related products for research and applications users; and
3) Conducting climate research in support of the IPRC and NOAA research goals.

The first activity involves the acquisition, formatting, organization and storage of local data (data management; DM), along with the development, implementation and maintenance of a suite of data-serving software (data-server system; DSS) that allows direct binary and web-based access to the data sets, which may be held either locally or at remote sites. The DSS/DM component provides the necessary infrastructure for research at IPRC and for users outside the IPRC.

Data Server System

To provide access to climate-related data and data products, the APDRC maintains web-based and binary access servers. These data server systems (DSS) continue to evolve and grow. The APDRC now maintains three different types of OPeNDAP servers: THREDDS, GDS and DAPPER. This allows the APDRC to provide access to a wide variety of data for many different client-end software programs. The OPeNDAP servers work together so users can access data in different formats from different servers, without knowing the underlying mechanism (see Figure 5.1). Figure 5.2a shows the number of bytes transferred from the ADPRC through OPeNDAP. In the early years, users tended to transfer complete data sets via OPeNDAP: users seem to have become more familiar with the technology, and they tend now to access only subsets, reducing the number of bytes transferred and increasing efficiency.

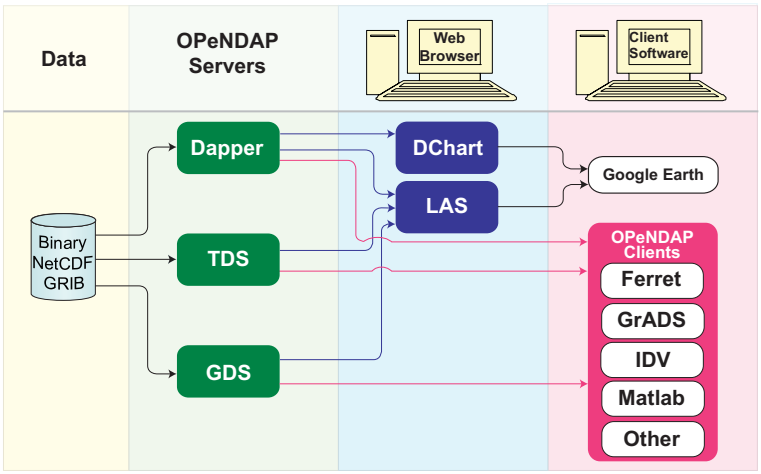

Figure 5.1. A schematic showing the connections between the various software servers maintained by the APDRC. Unlike most data centers, the APDRC effectively integrates different servers (Dapper, THREDDS and GrADS DOS Servers), which provide binary access to data and which are also accessible by such web-based browsing tools as DChart and the Live Access Server (LAS). The new versions of DChart and LAS allow direct output to Google Earth applications.

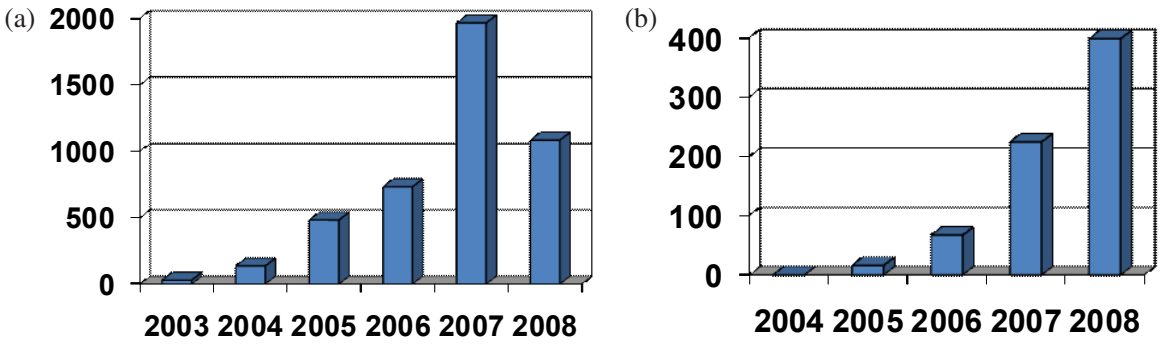

Figure 5.2. Shown are the number of bytes transferred from the ADPRC through (a) OPeNDAP and (b) LAS. Since the bytes transferred in (b) are plots rather than raw binary data, the volume is less than OPeNDAP, even with similar data requests.

The APDRC also runs two types of web-based data browsing tools: a Live Access Server (LAS) and DChart. These servers have been developed to serve all types of data, while maintaining their separate functions. Figure 5.2b shows the data access through LAS. These servers are now also capable of accessing or displaying through Google Earth. A user can, for example, use DChart in conjunction with Google Earth to make plots or to access data.

Given certain access restrictions to data, the APDRC has set up the data servers to run in various configurations. The APDRC is now running authenticated services for OFES (Ocean GCM for the Earth Simulator) output, U.S. Navy model output, and a variety of regional, research-only model output.

The APDRC is one of few data centers that provide such a wide range of services with seamless integration, and its staff has successfully implemented such systems elsewhere. This past year, APDRC staff has helped to install and configure similar servers at the University of Tokyo, JAMSTEC, the South China Sea Institute, and the Ocean University of China.

The APDRC has begun to address the needs of non-scientific users and access to data, including the Global Climate Observing System (PI-GCOS), the Global Ocean Observing System (PI-GOOS), and the Hydrological Cycle Observing System (Pacific HYCOS). It plans to work with the US component of the Integrated Ocean Observing System (IOOS), the Pacific (PacIOOS) and the Hawaii regional efforts (HIOOS).

Data Management

The APDRC maintains about 20 Terabytes (TB) of on-line data for use by IPRC scientists and the broader community. These data sets include in situ and remote (satellite) observations, as well as output from ocean, atmosphere and coupled climate models. The main data holdings are from the OFES hindcast experiments. This past year, the APDRC archived and configured for the servers an additional 10 TB of OFES output, mainly from the climatologically forced run at full global resolution and 3-day interval. Other data sets acquired this past year were the GODAE High Resolution Sea Surface Temperature (GHRSST) data set, and updates to SODA, NCEP, SeaWIFS, QuikSCAT, and others.

The APDRC has also provided data management services for locally generated data sets and model output. Now available on the APDRC servers are different runs of the LOVECLIM and SIM2bl models, which have been conducted by the paleoclimate modeling group. The APDRC also archives and serves

output of the near-operational model runs of the flow around the Hawaiian Islands. These are examples of how the APDRC data management and data server systems both assist IPRC scientists and provide a mechanism for disseminating IPRC results to the broader community.

Applied Research: Product Development and Distribution

In 2006 the APDRC released its first velocity estimates for the global ocean determined from the Argo float trajectories in the technical report and database "Velocity data assessed from trajectories of Argo floats at parking level and at the sea surface." The database was updated and re-released in 2007. Since May 2008, the APDRC has been releasing monthly updated versions of this database as part of the CLIVAR/GSP Velocity Panel of the CLIVAR/ Global Synthesis and Observations Panel. The Argo database and project site are found at http://apdrc.soest.hawaii.edu/projects/argo/index.html.

Data processing techniques have been developed to calculate in near real-time global Argo in situ and gridded datasets of temperature, salinity, absolute dynamic height and geostrophic velocities, and mixed and barrier layer depths. Global Argo products available on APDRC servers include surface and deep velocities from float trajectories, profile data interpolated on standard depth levels and isopycnals, and mixed-layer, isothermal-layer, and barrier-layer depths; and statistics, climatologies, and monthly and annual averages. Map products, which include data coverage information, are available as both gridded/interpolated products and spatially bin-averaged products (see Figure 5.3).

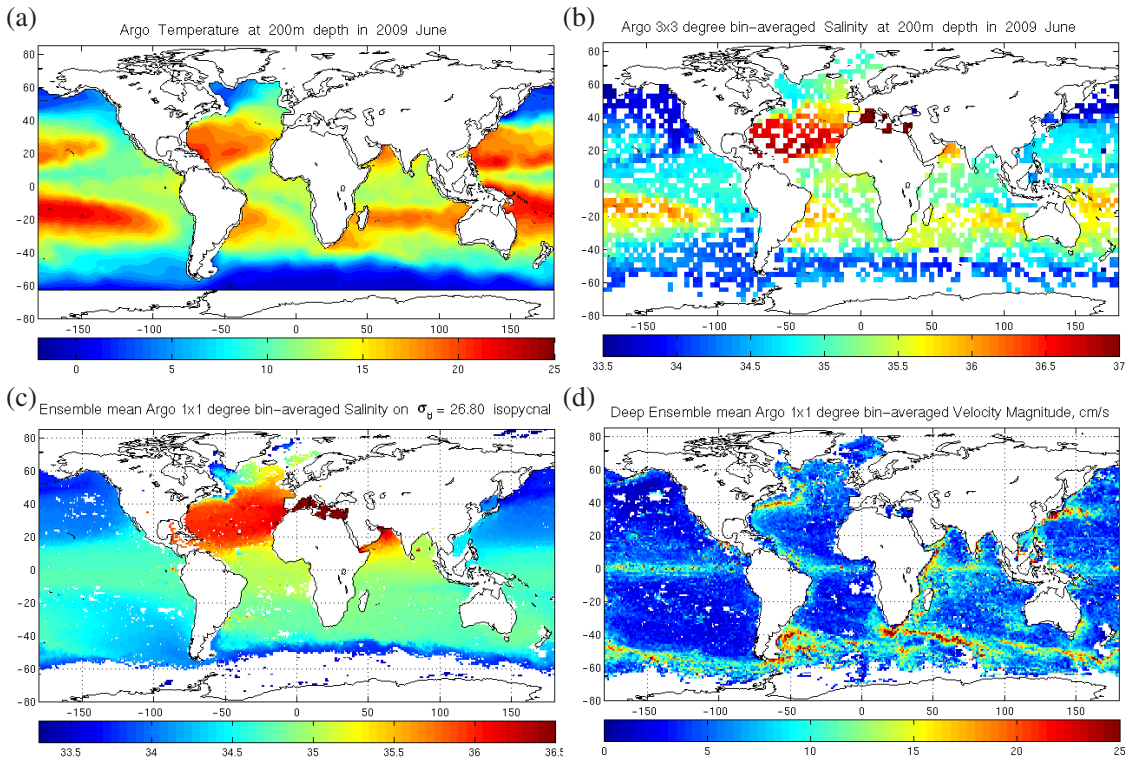

Figure 5.3. Example plots that can be made from the APDRC Argo products: (a) temperature at 200 m depth in June 2009; (b) 3° × 3° bin-averaged salinity at 200 m depth in June 2009; (c) ensemble mean 1° × 1° bin-averaged salinity on $\sigma_\theta = 26.80$ isopycnal; (d) deep ensemble mean 1° × 1° bin-averaged velocity in cm/s.

Also available as monthly updates are the following synthesized products:

- Mean surface dynamic topography computed form drifter, wind, and altimetry data;
- Instantaneous surface dynamic topography computed from mean dynamic ocean topography and Aviso sea level anomalies;
- Absolute topography at depth computed from Argo T/S profiles referenced to the instantaneous surface topography;
- Absolute geostrophic velocities at Argo float parking depths.

Regional ocean prediction system for Hawaii. The APDRC is running a regional ocean prediction system for Hawaii in nearly real-time based on the Hybrid Coordinate Ocean Model (HYCOM). The HYCOM Consortium's global prediction system provides initial and lateral boundary conditions for the regional system; the regional system, in turn, improves global model solutions in the local region through increased horizontal resolution and use of high-resolution surface forcing from a regional atmospheric forecast system.

The regional model domain encompasses the 8 main Hawaiian Islands (166°W –150°W; 16°N–26°N). The horizontal resolution is 0.04°; vertical resolution is the same as that of the global HYCOM: 32 layers, with the upper 28 active in the Hawaii region. High-resolution bathymetry (1/60° GEBCO) in the interior of the regional domain defines geographic features, including the islands' coastlines.

An opportunity to test the regional model skill presented itself by the presence of the cyclonic eddy Opal during February–March 2005 in the lee of the island of Hawaii. This eddy's physical, biological and biogeochemical processes had been studied during a field campaign in March 10–28, 2005. The IPRC regional ocean prediction system was run for the January–April 2005 period using output from a global HYCOM simulation for the initial and lateral boundary conditions, heat and freshwater fluxes at 0.5° resolution from the Navy Operational Global Atmospheric Prediction System, and QuikSCAT winds at 0.25° resolution.

The observed lifecycle of Opal evolved as follows: in late February in 2005, the MODIS and GOES satellite observations first registered the cool sea surface temperature (SST) due to oceanic upwelling in Opal's center; March 11–20, ship-based ADCP data showed Opal moving southward from 20°N to 19°N; satellite SST imagery suggested that Opal then propagated westward and dissipated in April.

The regional model shows a cyclonic eddy centered at 156.5°W and 20°N beginning to spin up in early February. By early March, it reached its maximum strength in the lee of the island of Hawaii as shown in Figure 5.4. From March 4 to 11, the eddy moved southward at an accelerated rate, and then continued its journey southward, merging with a cyclonic eddy from the east at 17.5°N and dissipating after moving westward. During the mature phase, sea surface height (SSH) at the eddy center was about 30 cm lower than the high SSH associated with an anticyclonic eddy (Figure 5.4a) to the south. Isotherms were lifted some 60 m at the eddy center relative to its edge (Figure 5.4b). The maximum tangential current reached near 50 cm/s (Figure 5.4c), and high positive relative vorticity indicated a coherent feature (Figure 5.4d). The simulated eddy, thus, resembles the observed Opal in origin, time of appearance, strength and initial southward propagation. It differs in its duration in the island lee and its westward propagation pathway, beginning its southward journey about a week earlier and traveling westward at a more southerly latitude.

Previous studies have suggested that cyclonic eddies result from the local wind shear: the tall islands Hawaii and Maui interrupt the steady trades, creating weak winds downstream of the island of Hawaii

and a strong wind jet between the islands (Figure 5.5a). In the model, the cyclonic eddy spun up at a location and during a time that the wind stress curl distribution (Figure 5.5b) was strongly positive. That is, the eddy was a direct response to positive vorticity input from the atmosphere (Figure 5.5c).

To summarize, the regional ocean model's ability to capture Opal was as much due to the high-resolution ocean model as to the use of the QuikSCAT winds, which reflect the local wind features. The propagation characteristics after eddy formation are much more difficult to capture and will be a subject of future investigations. [Y. Jia]

For the latest results from the regional prediction system, see http://apdrc.soest.hawaii.edu/datadoc/hycom_hawaii_0.04.htm.

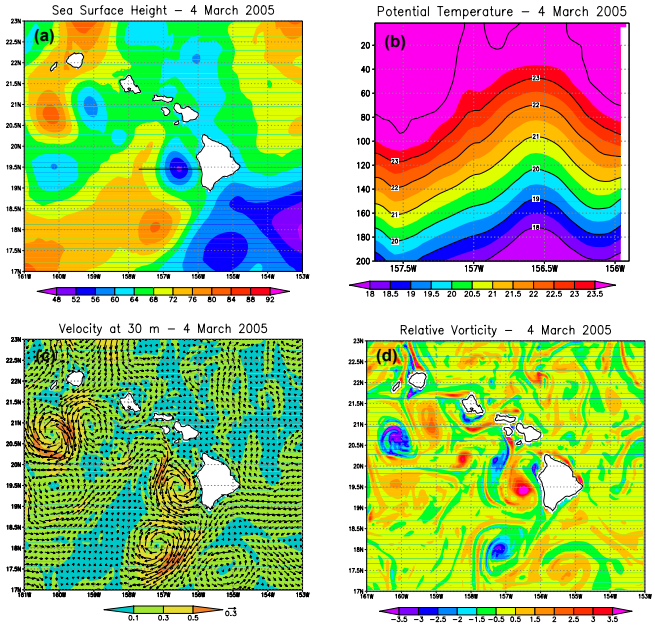

Figure 5.4. Regional model variables on March 4, 2005: (a) sea surface height (cm); (b) potential temperature (°C) in the upper 200 m along 19.45°N as indicated by the black line in (a); (c) velocity (m/ s) at a depth of 30 m; and (d) relative vorticity ($\times 10^{-5}$/s).

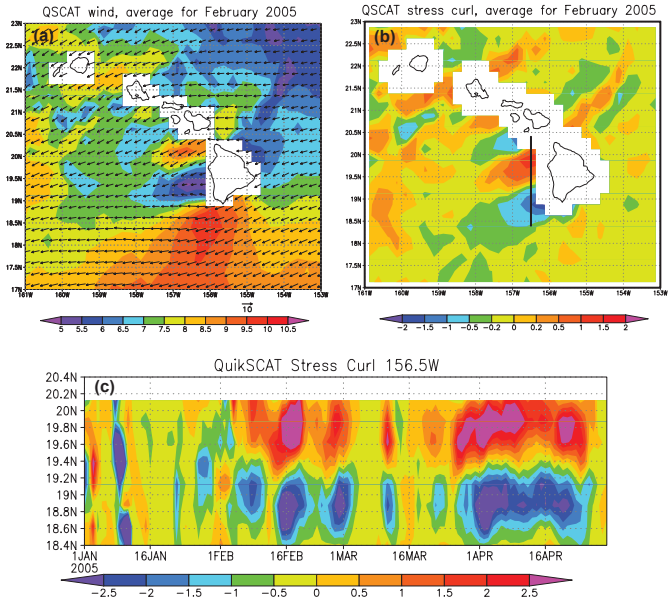

Figure 5.5. QuikSCAT: (a) wind vector and speed in color (m/s) averaged for February 2005; (b) wind stress curl ($\times 10^{-6}$ Pa/m) averaged for February 2005; and (c) wind stress curl ($\times 10^{-6}$ Pa/m) along 156.5°W as indicated by the black line in (b) for January–May 2005.

PUBLICATIONS

Published Papers

Aiki, H., and K.J. Richards, 2008: Energetics of the global ocean: The role of layer-thickness form drag. *J. Phys. Oceanogr.*, **38**, 1845–1869. IPRC-504.

Boer, G. J., and K. Hamilton, 2008: QBO influence on extratropical predictive skill. *Clim. Dyn.*, **31**, 987-1000. IPRC–506.

Cahyarini, S.Y., M. Pfeiffer, O. Timm, W.-C. Dullo, D.G. Schönberg, 2008: Reconstructing seawater δ18O from paired coral δ18O and Sr/Ca ratios: Methods, error analysis and problems, with examples from Tahiti (French Polynesia) and Timor (Indonesia). *Geochimica et Cosmochimica Acta*, **72** (12), 2841–2853. IPRC-520.

Calil, P.H.R., K.J. Richards, Y. Jia, and R.R. Bidigare, 2008: Eddy activity in the lee of the Hawaiian Islands. *Deep-Sea Research II*, **55**, 1179–1194. IPRC-462.

Chhak, K. C., E. Di Lorenzo, N. Schneider, and P. Cummins 2009: Forcing of low-frequency ocean variability in the Northeast Pacific. *J. Climate*, **22** (5), 1255–1276. IPRC-539.

Chowdary, J.S., C. Gnanaseelan, and S.-P. Xie, 2009: Westward propagation of barrier layer formation in the 2006-07, Rossby wave event over the tropical Southwest Indian Ocean, *Geophys. Res. Lett.*, **36**, L04607, doi:10.1029/2008GL036642. IPRC-582.

de Szoeke, S.P., and S.-P. Xie, 2008: The tropical eastern Pacific seasonal cycle: Assessment of errors and mechanisms in IPCC AR4 coupled ocean-atmosphere general circulation models. *J. Climate*, **21**, 2573–2590. IPRC-480.

Ding, Q., and B. Wang, 2009: Predicting extreme phases of the India Summer Monsoon. *J. Climate*, **22** (2), 346–363. IPRC-536.

Du, Y., S.-P. Xie, 2008: Role of atmospheric adjustments in the tropical Indian Ocean warming during the 20th century in climate models. *Geophys. Res. Lett.*, **35**, L08712, doi:10.1029/2008GL033631. IPRC-517.

Du, Y., T. Qu, and G. Meyers, 2008: Interannual variability of sea surface temperature off Java and Sumatra in a global GCM. *J. Climate*, **21**, 2451–2465, IPRC-487.

Fu, X., B. Wang, B. Qing, P. Liu, and B. Yang, 2008: Experimental dynamical forecast of an MJO event observed during TOGA-COARE Period. *Atmospheric and Oceanic Science Letters*, **1**, 24–28. IPRC-538.

Fu, X., B. Yang, Q. Bao, and B. Wang, 2008: Sea surface temperature feedback extends the predictability of tropical intraseasonal oscillation. *Mon. Wea. Rev.*, **136**, 577–597. IPRC-482.

Fudeyasu, H., Y. Wang, M. Satoh, T. Nasuno, H. Miura, and W. Yanase, 2008: Global cloud-System-resolving model NICAM successfully simulated the lifecycles of two real tropical cyclones. *Geophys. Res. Lett.*, **35**, L22808, doi:10.1029/2008GL036003. IPRC-557.

Ge, X., T. Li, Y. Wang, and M. S. Peng, 2008: Tropical cyclone energy dispersion in a three-dimensional primitive equation model: Upper-tropospheric influence. *J. Atmos. Sci.*, **65** (7), 2272–2289. IPRC-489.

Geller, M., T. Zhou, and K. Hamilton, 2008: Morphology of tropical upwelling in the lower stratosphere. *J. Atmos. Sci.*, **65**, 2360–2374. IPRC-476.

Haertel, P. T., L. Van Roekel and T. G. Jensen, 2009: Constructing an idealized model of the North Atlantic Ocean using Slippery Sacks. *Ocean Modelling*, **27** (3-4), 143–159. IPRC-563.

Hamilton, K., S.C. Ryan, and W. Ohfuchi, 2008: Topographic effects on the solar semidiurnal surface tide simulated in a very fine resolution general circulation model. *JGR-Atmos.*, **113**, doi:10.1029/2008JD010115. IPRC-518.

Hamilton, K., Y.O. Takahashi, and W. Ohfuchi, 2008: The mesoscale spectrum of atmospheric motions investigated in a very fine resolution global general circulation model. *JGR.-Atmos.*, **113**, D18110, doi:10.1029/2008JD009785. IPRC-521.

Hong, C.-C., T. Li, and J.-J. Luo, 2008: Asymmetry of the Indian Ocean Dipole. Part II: Model Diagnosis, *J. Climate*, **21** (18), 4849–4858 IPRC-500.

Hong, C.-C., T. Li, LinHo, and J.-S. Kug, 2008: Asymmetry of the Indian Ocean dipole. Part I: Observational analysis. *J. Climate*, **21** (18), 4834–4848. IPRC-499.

Jochum, M., and J. T. Potemra, 2008: Sensitivity of tropical rainfall to Banda Sea diffusivity in the Community Climate System Model. *J. Climate*, **21**, 6445–6454. IPRC-528.

Kikuchi, K., and B. Wang, 2008: Diurnal precipitation regimes in the global tropics. *J. Climate*, **21**(11), 2680–2696. IPRC-491.

Kikuchi, K., B. Wang, and H. Fudeyasu, 2009: Genesis of Tropical Cyclone Nargis revealed by multiple satellite observations. *Geophys. Res. Lett.*, **36**, L06811, doi:10.1029/2009GL037296. IPRC-585.

Kim, H.-J., B. Wang, and Q. Ding, 2008: The global monsoon variability simulated by CMIP3 coupled climate models. *J. Climate*, **21**, 5271–5294 IPRC-542.

Kobashi, F., S.-P. Xie, N. Iwasaka, and T. Sakamoto, 2008: Deep atmospheric response to the North Pacific oceanic subtropical front in spring. *J. Climate*, **21**, 5960–5975. IPRC-524.

Li, L.-J., Y. Wang, B. Wang, and T.-J. Zhou, 2008: Sensitivity of the Grid-point Atmospheric Model of IAP LASG (GAMIL1.1.0) climate simulations to cloud droplet effective radius and liquid water path. *Adv. in Atmos. Sc.*, **25**, 529–540. IPRC-565.

Li, T., F. Tam, X. Fu, T. Zhou, W. Zhu, 2008: Causes of the intraseasonal SST variability in the tropical Indian Ocean. *Atmos. & Oceanic Sc. Lett.*, **1**, 18–23. IPRC-537.

Lin, A., and T. Li, 2008: Energy spectrum characteristics of boreal summer intraseasonal oscillations: climatology and variations during the ENSO developing and decaying phases. *J. Climate*, **21**. 6304–6320. IPRC-529.

Liu, J., B. Wang, and J. Yang, 2008: Forced and internal modes of variability of the East Asian summer monsoon. *Climate of the Past*, **4**, 225–233. IPRC-587.

Maximenko, N.A., O. V. Melnichenko, P. P. Niiler, and H. Sasaki, 2008: Stationary mesoscale jet-like features in the ocean. *Geophys. Res. Lett.*, **35**, L08603, doi:10.1029/2008GL033267. IPRC-516.

Maximenko, N.A., P. P. Niiler, and O. V. Melnichenko, 2008: Global mean dynamic ocean topography reveals new coherent features of surface circulation. *Proceedings of the 2007 International Conference* "Fluxes and Structures in Fluid," pp. 146–155. Moscow, Russia, IPRC-488.

Menviel, L., A. Timmermann, A. Mouchet, and O. Timm, 2008: Meridional reorganizations of marine and terrestrial productivity during Heinrich events. *Paleoceanography*, **23**, PA1203, doi:10.1029/2007PA001445. IPRC-484.

Menviel, L., A. Timmermann, A. Mouchet, and O. Timm, 2008: Climate and marine carbon cycle response to changes in the strength of the Southern Hemispheric westerlies. *Paleoceanography*, **23**, PA4201, doi:10.1029/2008PA001604. IPRC-526.

Nakamura, H., T. Sampe, A. Goto, W. Ohfuchi, and S-P Xie, 2008: On the importance of midlatitude oceanic frontal zones for the mean state and dominant variability in the tropospheric circulation. *Geophys. Res. Lett.*, **35**, L15709, doi:10.1029/2008GL034010. IPRC-531.

Nakano, H., H. Tsujino, and R. Furue, 2008: The Kuroshio Current System as a jet and twin "relative" recirculation gyres embedded in the Sverdrup circulation. *Dyn. Atmos.-Oceans*, **45**, 135–164. IPRC-597.

Natarov, A., and K. J Richards, 2009: Three-dimensional instabilities of oscillatory equatorial zonal shear flows. *J. Fluid Mech.*, **623**, 59–74. IPRC-574.

Peng, J., M. S. Peng, and T. Li, 2008: Dependence of vortex axisymmetrization on the characteristics of the asymmetry. *Quart. J. Royal Met. Soc.*, **134**,1253–1268. IPRC- 530.

Qi, Y., R. Zhang, T. Li, and M. Wen, 2008: Interactions between the summer mean monsoon and the intraseasonal oscillation in the Indian monsoon region. *Geophys. Res. Lett.*, **35**, L17704, doi:10.1029/2008GL034517. IPRC-577.

Qu, T., J. Gan, A. Ishida, Y. Kashino, and T. Tozuka, 2008: Semiannual variation in the western tropical Pacific Ocean. *Geophys. Res. Lett.*, **35**, L16602, doi:10.1029/2008GL035058. IPRC-532.

Qu, T., T. Song, and T. Yamagata, 2009: An introduction to the South China Sea throughflow: Its dynamics, variability, and application for climate. *Dyn. Atmos. & Oceans*, **47**, 3–14. IPRC-525.

Richter, I., and S.-P. Xie, 2008: On the origin of equatorial Atlantic biases in coupled general circulation models. *Climate Dynamics*, **31** (5), 587–598. IPRC-498.

Richter, I., and S.-P. Xie, 2008: Muted precipitation increase in global warming simulations: A surface evaporation perspective. *J. Geophys. Res.-Atmos.*,**113**, D24118, doi:10.1029/2008JD010561. IPRC-559.

Sasaki, Y. N., S. Minobe, N. Schneider, T. Kagimoto, M. Nonaka and H. Sasaki, 2008: Decadal sea level variability in the South Pacific in a global eddy-resolving ocean model hindcast. *J. Phys. Oceanogr.*, **38**, 1731–1747. IPRC-508.

Schott F. A., S.-P. Xie, and J. P. McCreary Jr., 2009: Indian Ocean circulation and climate variability. *Rev. Geophys.*, **47**, RG1002, doi:10.1029/2007RG000245. IPRC-522.

Shi, X.-Y., Y. Wang, and X.-D. Xu, 2008: Effect of mesoscale topography over the Tibetan Plateau on summer precipitation in China: A regional model study. *Geophys. Res. Lett.*, **35**, L19707. doi:10.1029/2008GL034740. IPRC-570.

Small, R.J., S.P. deSzoeke, S.-P. Xie, L. O'Neill, H. Seo, Q. Song, P. Cornillon, M. Spall, and S. Minobe, 2008. Air-sea interaction over ocean fronts and eddies. *Dyn. Atmos. and Oceans*, **45**, (3-4), 274–319. IPRC-535.

Solomon, A., S.-I. Shin, M. A. Alexander, J. P. McCreary, 2008: The relative importance of tropical variability forced from the North Pacific through ocean pathways. *Clim. Dyn.*, **31** (2-3), 315–331. IPRC-496.

Sperber, K.R., and H. Annamalai, 2008: Coupled model simulations of boreal summer intraseasonal (30–50 day) variability, Part I: Systematic errors and caution on use of metrics. *Clim. Dyn.*, **31**, 345-372. IPRC-519.

Timm, O., A. Timmermann, A. Abe-Ouchi, F. Saito, and T. Segawa, 2008: On the definition of seasons in paleoclimate simulations with orbital forcing, *Paleoceanography*, **23**, PA2221, doi:10.1029/2007PA001461. IPRC-513.

Tozuka, T., T. Qu, Y. Masumoto, and T. Yamagata, 2009: Impacts of the South China Sea throughflow on seasonal and interannual variations of the Indonesian throughflow. *Dyn. Atmos.- Oceans*, **47**, 73–85, IPRC-549.

Ueda, H., M. Ohba, and S.-P. Xie, 2009: Important factors for the development of the Asian-Northwest Pacific summer monsoon. *J. Climate*, **22** (3), 649–669. IPRC-540.

Wang, B., 2008: Thrusts and prospects on understanding and predicting Asian monsoon climate. *Acta Meteorogica Sinica*. **22** (4), 383–403. IPRC-591.

Wang, B., and H. Yang, 2008: Hydrological issues in lateral boundary conditions for regional climate modeling: simulation of East Asian summer monsoon in 1998, *Clim. Dyn.*, **31** (4), 477–490, doi: 10.1007/s00382-008-0385-7. IPRC-512.

Wang, B., and Q. Ding, 2008: Global monsoon: Dominant modes of annual variations in the tropics. *Dynamics of Atmos. and Ocean*, **44** (3-4), 165-183, doi:10.1016/j.dynatmoce.2007.05.002. IPRC-502.

Wang, B., J. Yang, T. Zhou, and B. Wang, 2008: Interdecadal changes in the major modes of Asian-Australian monsoon variability: Strengthening relationship with ENSO since the late 1970s. *J. Climate*, **21** (8), 1771–1789. IPRC-481.

Wang, B., and 27 collaborators, 2008: Advance and prospectus of seasonal prediction: Assessment of the APCC/CliPAS-14 model ensemble retrospective seasonal prediction (1980-2004)., *Clim. Dyn.*, **33**, 93–117. IPRC-548.

Wang, B., J.-Y. Lee, I.-S. Kang, J. Shukla, J.-S Kug, A. Kumar, J. Schemm, J.-J. Luo, T. Yamagata, C.-K. Park, 2008: How accurately do coupled climate models predict the leading modes of the Asian-Australian monsoon interannual variability? *Clim. Dyn.*, **30** (6), 605–619. IPRC-478.

Wang, B., Q. Bao, B. Hoskins, G. Wu and Y. Liu, 2008: Tibetan Plateau warming and precipitation changes in East Asia. *Geophys. Res. Lett.*, **35**, L14702, doi:10.1029/2008GL034330. IPRC-534.

Wang, B., Z. Wu, J. Li, J. Liu, C.-P. Chang, Y. Ding, and G.-X. Wu, 2008: How to measure the strength of the East Asian summer monsoon, *J. Climate*, **21**, 4449–4463. IPRC-511.

Wang, Y., 2008: Rapid filamentation zone in a numerically simulated tropical cyclone. *J. Atmos. Sci.*, **65** (4), 1158–1181. IPRC-479.

Wang, Y., 2008: Structure and formation of an annular hurricane simulated in a fully compressible, nonhydrostatic model - TCM4. *J. Atmos. Sci.*, **65** (5), 1505–1527. IPRC-474.

Wu, C.-C., H.-J. Cheng, Y. Wang, and K.-H. Chou, 2009: A numerical investigation of the eyewall evolution of a landfalling typhoon. *Mon. Wea. Rev.*, **137** (1), 21–40. IPRC-571.

Wu, L., and B. Wang, 2008: What has changed the proportion of intense hurricanes in the last 30 years? *J. Climate*, **21**, 1432-1439. IPRC-594.

Wu, L., B. Wang, and S. A. Braun, 2008: Implications of tropical cyclone power dissipation index (PDI). *International J. Climatology*, **28**: 727–731. DOI: 10.1002/joc.1573. IPRC-593.

Wu, L., C. Li, C. Yang, and S.-P. Xie, 2008: Global teleconnections in response to a shutdown of the Atlantic meridional overturning circulation. *J. Climate*, **21** (12), 3002–3019. IPRC-492.

Xie, B.-G., Q.-H. Zhang, and Y. Wang, 2008: Trends in hail in China during 1960-2005. *Geophys. Res. Lett.*, **35**, L13801. IPRC-564.

Xie, S.-P., K. Hu, J. Hafner, H. Tokinaga, Y. Du, G. Huang, and T. Sampe, 2009: Indian Ocean capacitor effect on Indo-western Pacific climate during the summer following El Nino. *J. Climate*, **22** (3), 730–747. IPRC-541.

Xie, S.-P., Y. Okumura, T. Miyama, and A. Timmermann, 2008: Influences of Atlantic climate change on the tropical Pacific via the Central American Isthmus. *J. Climate*, **21** (15), 3914–3928. IPRC-503.

Xu, H., S.-P. Xie, Y. Wang, W. Zhuang, and D. Wang, 2008: Orographic effects on South China Sea summer climate. *Meteor. Atmos. Phys.*,**100**, 275–289. IPRC-527.

Xu, X.-D., X.-Y. Shi, Y. Wang, S.-Q. Peng, and X.-H. Shi, 2008: Data analysis and numerical simulation of moisture source and transport associated with summer monsoon precipitation in the Yangtze River Valley over China. *Meteor. Atmos. Phys.*, **100**, 217–231. IPRC-569.

Yang, B., X. Fu, and B. Wang, 2008: Atmosphere-ocean conditions jointly guide convection of the boreal summer intraseasonal oscillation: Satellite observations. *J. Geophys. Res.-Atmos.*, **113**, D11105, doi:10.1029/2007JD009276. IPRC-510.

Yang, J., B. Wang, and B. Wang, 2008: Anticorrelated intensity change of the quasi biweekly and 30–50-day oscillations over the South China Sea. *Geophys. Res. Lett.*, **35**, L16702, doi:10.1029/2008GL034449. IPRC-592.

Yang Y., J. Ma, and S.-P. Xie, 2008: Observations of the trade wind wakes of Kauai and Oahu. *Geophys. Res. Lett.*, **35**, L04807, doi:10.1029/2007GL031742. IPRC-497.

Yang, Y., S.-P. Xie, and J. Hafner, 2008: Cloud patterns lee of Hawaii Island: A synthesis of satellite observations and numerical simulation. *J. Geophys. Res.-Atmos.*, **113**, D15126, doi:10.1029/2008JD009889. IPRC-523.

Yang, Y., S.-P. Xie, and J. Hafner, 2008: The thermal wake of Kauai Island: Satellite observations and numerical simulations. *J. Climate*, **21**, 4568–4586, IPRC-509.

Yang, Y., Y.-L. Chen, 2008: Effects of terrain heights and sizes on island-scale circulations and rainfall for the island of Hawaii during HaRP. *Mon. Wea. Rev.*, **136**, 120–146, doi: 10.1175/2007MWR1984.1. IPRC-457.

Yu, J. and Y. Wang, 2009: Response of Tropical Cyclone Potential Intensity over the North Indian Ocean to Global Warming. *Geophys. Res. Lett.*, **36**, L03709, doi:10.1029/2008GL036742. IPRC-533.

Zeng, Z., L.-S. Chen, and Y. Wang, 2008: An observational study of environmental dynamical control of tropical cyclone intensity in the Atlantic. *Mon. Wea. Rev.*, **136**, 3307-3322. IPRC-566.

Zhang, C.-X., Q.-H. Zhang, and Y. Wang, 2008: Climatology of hail in China: 1961-2005. *J. Appl. Meteor. Climatol.*, **47** (3), 795–804. IPRC-473.

Zhang, C.-X., Q.-H. Zhang, Y. Wang, and X.-D. Liang, 2008: Climatology of warm season cold vortices in East Asia: 1979-2005. *Meteor. Atmos. Phys.*, **100**, 291–301. IPRC-568.

Zhang, S., and B. Wang, 2008: Global summer monsoon rainy season, Revised. *Int. J. Climatol.*, **28** (12), 1563–1578, doi: 10.1002/joc.1659. IPRC-595.

Zhang, Y., and T. Li, 2008: Influence of the sea surface temperature in the Indian Ocean on the in-phase transition between the South Asian and North Australian summer monsoons. *Terr. Atmos. Ocean. Sci.*,**19**, 321–329. IPRC-515.

Zhao, H., D.-L. Tang, and Y. Wang, 2008: Comparison of phytoplankton blooms triggered by two typhoons with different intensities and translation speeds in the South China Sea. *Marine Ecol. Progr. Series*, **365**, 57–65. IPRC -567.

Zhu, C., B. Wang, and W. Qian, 2008: Why do dust storms decrease in northern China concurrently with the recent global warming? *Geophys. Res. Lett.*, **35**, L18702, doi:10.1029/2008GL034886 IPRC-546.

Zhu, W., and K. Hamilton, 2008: Empirical estimates of global climate sensitivity: An assessment of strategies using a coupled GCM. *Advances in Atmospheric Sciences*, **25**, 339–347. IPRC-514.

Zinke, J., M. Pfeiffer, O. Timm, W.-Chr. Dullo, D. Kroon, and B.A. Thomassin, 2008: Mayotte coral reveals hydrological changes in the western Indian Ocean between 1881 and 1994. *Geophys. Res. Lett.*, **35**, L23707, doi:10.1029/2008GL035634. IPRC-552.

In Press

Ceballos, L.I., E. Di Lorenzo, C. D. Hoyos, N. Schneider, B. Taguchi: North Pacific Gyre Oscillation synchronizes climate fluctuations in the eastern and western boundary systems. *J. Climate*, IPRC-590.

Du, Y. S.-P. Xie, G. Huang, and K. Hu: Role of air-sea interaction in the long persistence of El Niño-induced North Indian Ocean warming. *J. Climate*, IPRC-558.

Friedrich, T., and A. Oschlies: Neuralnetwork-based estimates of North Atlantic surface pCO2 from satellite data - A methodological study. *J. Geophys. Res.-Oceans*, IPRC-581.

Fu, X., and B. Wang: Critical roles of the stratiform rainfall in sustaining the Madden-Julian Oscillation: GCM Experiments. *J. Climate*, IPRC-602.

Fu, X., B. Wang, Q. Bao, P. Liu, and J.-Y. Lee: Impacts of initial conditions on monsoon intraseasonal forecasting. *Geophys. Res. Lett.*, IPRC-603.

Furue, R., J. P. McCreary, and Z. Yu: Dynamics of the northern Tsuchiya Jet. *J. Phys. Oceanogr.*, IPRC-586.

Hong, C.-C., and T. Li: The Extreme Cold Anomaly over Southeast Asia in February 2008: Roles of ISO and ENSO. *J. Climate*, IPRC-580.

Kajikawa, Y., T. Yasunari, and B. Wang: Decadal change in intraseasonal variability over the South China Sea. *Geophys. Res. Lett.*, IPRC-598.

Kashino Y., N. Espana, F. Syamsudin, K.J. Richards, T. Jensen, P. Dutrieux and A. Ishida: Observations of the North Equatorial Current, Mindanao Current, and the Kuroshio Current system during the 2006/7 El Nino and 2007/08 La Nina. *J. Oceanogr.*, IPRC-562
.

Kikuchi, K., and B. Wang: Global perspective of the Quasi-Biweekly Oscillation. *J. Climate*, IPRC-550.

Kim, H.-Ji., B. Wang, Q. Ding, and I-U. Chung: Changes in arid climate over North China detected by the Köppen Climate Classification. *J. Meteor. Soc. Japan*. IPRC-551.

T. Li, X. Fu, and W. Lu: Moisture Structure of the Quasi-biweekly Mode Revealed by AIRS in Western Pacific. *Advances in Atmospheric Sciences*.

Liu, P. , Y. Kajikawa, B. Wang, A. Kitoh, T. Yasunari, T. Li, H. Annamalai, X. Fu, K. Kikuchi, R. Mizuta, K. Rajendran, D. E. Waliser, D. Kim: Tropical Intraseasonal Variability in the MRI-20km60L AGCM. *J. Climate*, IPRC-556.

Lu, B., L. Pandolfo, and K. Hamilton: Nonlinear representation of the quasi-biennial oscillation. *J. Atmos. Sci.*, IPRC-501.

Maximenko, N., P. Niiler, M.-H. Rio, O. Melnichenko, L. Centurioni, D. Chambers, V. Zlotnicki, and B. Galperin: Mean dynamic topography of the ocean derived from satellite and drifting buoy data using three different techniques. *J. Atmos. Oceanic Tech.*, IPRC-576.

Peng, J., T. Li, M.S. Peng, X. Ge: Barotropic instability in the tropical cyclone outer region. *Quart. J. Royal Met. Soc.*, IPRC-588.

Qu, T., S. Gao, I. Fukumori, R. A. Fine, and E. J. Lindstrom: Origin and pathway of equatorial 13°C water in the Pacific identified by a simulated passive tracer and its adjoint. *J. Phys. Oceanogr.*, IPRC-578.

Qu, T., and Y. T. Song: Mindoro Strait and Sibutu Passage transports estimated from satellite data. *Geophys. Res. Lett.*, IPRC-604.

Richards, K.J., S.-P. Xie, and T. Miyama: Vertical mixing in the ocean and its impact on the coupled ocean/atmosphere system in the Eastern Tropical Pacific. *J. Climate*, IPRC-560.

Small, R. J., K. J. Richards, S.-P. Xie, P. Dutrieux and T. Miyama: Damping of Tropical Instability Waves caused by the action of surface currents on stress. *J. Geophys. Res.-Oceans*, IPRC-605.

Souma, K. and Y. Wang: Improved simulation of the East-Asian summer monsoon rainfall with satellite-derived snow water equivalent data, *Mon. Wea. Rev.*, IPRC-575.

Stott, L., J. Southon, A. Timmermann, A. Koutavas: A Benthic Radiocarbon Age Anomaly at Intermediate Depth in the Pacific Ocean during the Last Deglaciation. *Paleoceanography*, IPRC-579.

Stowasser, M., H. Annamalai, and J. Hafner: Response of the South Asian Summer Monsoon to global warming: Mean and synoptic systems, *J. Climate*, IPRC-545.

Tanimoto, y., S.-P. Xie, K. Kai, H. Okajima, H. Tokinaga, T. Murayama, M. Nonaka, and H. Nakamura: Observations of marine atmospheric boundary layer transitions across the summer Kuroshio Extension. *J. Climate*, IPRC-553.

Timm, O. and H. F. Diaz: Synoptic-Statistical Approach to Regional Downscaling of IPCC 21st Century Climate Projections: Seasonal Rainfall over the Hawaiian Islands, *J. Climate*, IPRC-596.

Timmermann, A., O. Timm, L. Stott, and L. Menviel: The roles of CO_2 and orbital forcing in driving Southern Hemispheric temperature variations during the last 21,000 years. *J. Climate*, IPRC-555.

Tokinaga, H., Y. Tanimoto, S.-P. Xie, T. Sampe, H. Tomita, and H. Ichikawa: Ocean frontal effects on the vertical development of clouds over the western North Pacific: In situ and satellite observations. *J. Climate*, IPRC-599.

Wang, B., J. Liu, J. Yang, T.-J. Zhou and Z. W.-Wu: Distinct principal modes of early and late summer rainfall anomalies in East Asia. *J. Climate*, IPRC-589.

Wang B., F. Huang, Z. Wu, J. Yang, X. Fu, and K. Kikuchi: Multi-scale climate variability of the South China Sea monsoon: A Review. *Dyn. of Atmos. and Oceans*, IPRC-554.

Wang, B., Q. Ding, P. V. Joseph: Objective definition of the Indian summer monsoon onset. *J. Climate*, IPRC-561.

Wang, Y.: How do outer spiral rainbands affect tropical cyclone structure and intensity? *J. Atmos. Sci.*, IPRC-572.

Yaremchuk, M., D. Nechaev, and G. Panteleev: A method of successive corrections of the control subspace in the reduced-order variational data assimilation. *Mon. Wea. Rev.*, IPRC-583.

Yaremchuk, M., J. McCreary, Z. Yu, and R. Furue: The South China Sea throughflow retrieved from climatological data. *J. Phys. Oceanogr.*, IPRC-543.

Wu, B., T. Zhou, and T. Li: Contrast of rainfall-SST relationships in the western North Pacific between the ENSO developing and decaying summers. *J. Climate*, IPRC-600.

Wu, B., T. Zhou, and T. Li: Seasonally evolving dominant interannual variability modes of East Asian Climate. *J. Climate*, IPRC-601.

Zeng, L., Y. Du, and S.-P. Xie, D. Wang: Barrier Layer in the South China Sea during summer 2000. *Dyn. Atmos. and Oceans*, IPRC-544.

Zhou, X., and B. Wang: From concentric eyewall to annular hurricane: A numerical study with the cloud-resolved WRF model. *Geophys. Res. Lett.*, IPRC-575.

Zinke, J., M. Pfeiffer, O. Timm, W.-Ch. Dullo, and G.J.A. Brummer: Western Indian Ocean marine and terrestrial record of climate variability: A review and new concepts of land-ocean interactions since AD 1660. *Intern. J. Earth Sciences*, IPRC-547.

Book Chapters

Li, T., 2010: Monsoon climate variabilities. In D.-Z. Sun and F. Bryan (Eds.), *Climate Dynamics: Why Does Climate Vary?* American Geophysical Union, Washington DC. IPRC-665.

McCreary, J. P., R. Murtugudde, J. Vialard, P. N. Vinayachandran, J. D. Wiggert, R. R. Hood, D. Shankar, and S. R. Shetye, 2009: Biophysical processes in the Indian Ocean. In J.D. Wiggert, R.R. Hood, S.W.A. Naqvi, K.H. Brink, S.L. Smith (Eds.), *Indian Ocean Biogeochemical Processes and Ecological Variability*, American Geophysical Union, Washington DC. IPRC-584.

THE YEAR'S WORKSHOPS AND CONFERENCES

Date	Title
March 30, 2009	IPRC Mini Workshop on "Ocean Mixing"
March 12, 2009	Mini Symposium on "Climate Processes over the Asia-Pacific Region"
March 3 – 6, 2009	Joint IPCC-WCRP-IGBP Workshop: New Science Directions and Activities Relevant to the IPCC AR5
December 5, 2008	Minisymposium on High-Resolution Atmospheric Modeling
December 2–4, 2008	The Third International Workshop on High-Resolution and Cloud Modeling
June 14–23, 2008	Summer School: El Niño - Southern Oscillation: Dynamics and Predictability
May 16, 2008	IPRC Informal Annual Review Workshop
May 5–6, 2008	Annual IPRC Symposium - IPRC 10th Anniversary
April 22, 2008	Atmospheric Composition Minisymposium: JAMSTEC/IPRC/UH Research

THE YEAR'S SEMINARS

Date	Speaker	Affiliation	Title
March 11, 2009 Special Joint IPRC /Met Seminar	Sir Brian Hoskins	Grantham Institute for Climate Change, Imperial College, London	*Understanding of Storm Tracks from Idialized World GCM Simulations*
March 10, 2009*	Pascale Braconnot	IPSL/LSCE, Unité mixte CEA-CNRS-UVSQ, France	*Monsoon and Interannual Variability in Simulations of the Holocene*
March 5, 2009	Jon Reisner	Los Alamos National Laboratory, Los Alamos, New Mexico	*Los Alamos National Lab's Foray into Hurricane Lightning: Observations and Modeling*
March 2, 2009 Public Lecture	Susan Solomon	NOAA - Earth System Research Laboratory in Boulder, Colorado	*A Tale of Two Environmental Issues: How the World Solved the Ozone Problem, and Got Stuck in Gridlock on the Climate Problem*
February 25, 2009*	George Boer	Canadian Centre for Climate Modelling and Analysis, Victoria, Canada	*What are the Prospects for Decadal Climate Prediction?*
February 11, 2009*	Hiroki Tokinaga	IPRC	*Cloud Response to Mid-latitude SST Fronts*
February 4, 2009*	In-Sik Kang	School of Earth and Environmental Science, Seoul National University, Seoul, Korea	*Aspects of Dynamical Climate Prediction: Initialization and Model Development*
January 28, 2009*	Mototaka Nakamura	Frontier Research Center for Global Change, Yokohama, Japan, and IPRC, UH	*Impacts of SST Anomalies Along the Gulf Stream and Kuroshio/Oyashio on the Large-Scale Atmospheric State*
January 21, 2009*	H. Annamalai	IPRC	*Response of the South Asian Summer Monsoon to Global Warming: Inference from IPCC-AR4 models*
January 14, 2009*	Ralf Bennartz	Department of Atmospheric and Oceanic Sciences, University of Wisconsin, Madison, Wisconsin	*Cloud-Aerosol Interactions from a Satellite Perspective*
January 5, 2009	Hiroyuki Murakami	Advanced Earth Science and Technology Organization (AESTO)/ Meteorological Research Institute, Ibaraki, Japan	*Impact of Global Warming on Tropical Cyclones in a 20-km-mesh MRI/JMA High-resolution Global Model*
December 23, 2008	Andrei Zatsepin	P.P. Shirshov Institute of Oceanology, Russian Academy of Sciences, Moscow, Russia	*Black Sea Basinscale and Mesoscale Dynamics and their Dependence on Wind Forcing and Bottom Topography*
December 12, 2008**	Humio Mitsudera	Institute of Low Temperature Science, Hokkaido University, Sapporo, Japan	*Numerical Experiments on Wind- and Buoyancy-driven Overturning in the Sea of Okhotsk*
November 5, 2008*	Alan Plumb	Massachusetts Institute of Technology, Cambridge, Massachusetts	*Stratospheric impact on surface climate: Is it real, and how does it work?*

Date	Speaker	Affiliation	Title
October 29, 2008*	Hironori Fudeyasu	IPRC	*Multi-Scale Interactions During the Life Cycle of a Tropical Cyclone Simulated by a Global Cloud-System-Resolving Model*
October 27, 2008	Peter Baines	University of Bristol, Bristol, United Kingdom; and University of Melbourne, Australia	*Global Rainfall and the Classification of ENSO*
October 15, 2008*	Yuqing Wang	IPRC	*Effect of Mesoscale Topography over the Tibetan Plateau on Summer Precipitation in China: A Regional-Model Study*
September 29, 2008*	Jong-Ghap Jhun	Seoul National University, Seoul, Korea	*Variability and Teleconnection of East Asian Summer Monsoon*
September 17, 2008*	Bin Wang	IPRC	*Tibetan Plateau Warming and Precipitation Changes in East Asia*
September 11, 2008**	Andrei Natarov	IPRC	*SVS-Forming Instabilities in the Equatorial Ocean*
September 4, 2008**	Jay McCreary	IPRC	*Biophysical processes in the Indian Ocean*
April 30, 2008****	Markus Stowasser	d-fine GmbH, Munich, Germany	*Climate-related Opportunities and Risks in the Financial Sector*
April 29, 2008	Xiaopei Lin	Ocean University of China, Qingdao, China	*Explaining the Global Distribution of Peak-Spectrum Variability of Sea Surface Height*
April 28, 2008	Hezi Gildor	Department of Environmental Sciences, The Weizmann Institute of Science, Rehovot, Israel	*Submesoscale Barriers to Mixing in the Ocean from Current Measurements and Aerial-Photographs*
April 25, 2008	Takuya Hasegawa	JAMSTEC Institute of Observational Research and Global Change, JAPAN	*SST Cooling over the Western Part of the Pacific Warm Pool and Coastal Upwelling along the Papua New Guinea Coast Before the 2002/03 El Niño*
April 24, 2008**	Bo Qiu	Department of Oceanography, University of Hawai'i, Honolulu, Hawaii	*Eddy-Mean Flow and Eddy-Eddy Interaction: New Insights and Wide-Swath Satellite Altimeter Mission*
April 16, 2008*	Jaci Brown	Yale University, New Haven, Connecticut	*The Energetics of the Tropical Pacific Ocean and ENSO Dynamics*
April 2, 2008*	Bin Wang	IPRC	*Dynamical seasonal and intraseasonal predictability and prediction: Status, understanding and challenges*

* Joint IPRC UH Mānoa Meteorology Department Seminar
** Joint IPRC UH Mānoa Oceanography Department Seminar
*** Joint IPRC UH Mānoa Meteorology and Oceanography Department Seminar
****Joint IPRC-ICCS Seminar

LUNCHEON DISCUSSIONS

Date	Speaker	Affiliation	Title
March 20, 2009	Kohei Yoshida	Hokkaido University, Japan	*Role of Vertical Eddy Heat Flux in the Temperature Response of the Tropical Tropopause to Changes in Tropical Sea-surface Temperature*
March 17, 2009	Nikolai Maximenko, Konstantin Lebedev, Peter Hacker, Jim Potemra, & Sharon DeCarlo	IPRC	*Near-real Time Argo Products Developed at the APDRC and Available for Your Research*
February 17, 2009	Jürgen Sündermann	University of Hamburg, Hamburg, Germany	*Climate and Earth Rotation*
February 10, 2009	Tommy Jensen	QinetiQ North America, Stennis Space Center, Stennis, Mississippi	*Hurricane Katrina Simulations using the COAMPS-NCOM-SWAN Coupled Atmosphere-Ocean-Wave Modeling System*
January 20, 2009	Kunihiro Aoki	Graduate School and Faculty of Science Hokkaido University Japan	*The Oceanic Eddy Heat Transport in a Hhigh-resolution Ocean GCM Simulation*
January 7, 2009	Ted Durland	Oregon State University, Corvallis, Oregon	*Equatorial Basin Modes*
December 22, 2008	Takanori Horii	Institute of Observational Research for Global Change, JAMSTEC, Japan	*Mixed-layer Temperature Balance in the Eastern Indian Ocean during the 2006 Indian Ocean Dipole*
September 16, 2008	Jong-Seong Kug	Department of Meteorology, University of Hawai'i, Honolulu, Hawaii	*Cross-scale Interaction in the Tropics: ENSO and Intraseasonal Variability*
September 4, 2008	Kelvin Richards	IPRC	*A New View of the Equatorial Ocean*
September 2, 2008	Hae-Kyung Drbohlav	IPRC	*A Diagnostic Study of the Indian Ocean Dipole Mode during El Niño and Non-El Niño Years*
June 26, 2008	Chaoxia Yuan	University of Tokyo, Tokyo, Japan	*Influences of IOD and ENSO on the Snow Cover in Tibet during Early Winter*
June 25, 2008	Norman Barth	Member of the US Delegation to the Bali UN climate negotiations	*An Informal Exchange on Climate - a Personal Talk about the Bali Conference of the Parties to the UN Framework Convention on Climate Change, and Other Elements of the International Climate Discussion*
June 24, 2008	Yoshikazu Sasai	FRCGC/JAMSTEC, Yokohama, Japan	*Effects of Mesoscale Eddies on the Marine Biology in the Kuroshio Extension: An Eddy-resolving Physical-biological Model Analysis*
May 19, 2008	Zhiyong Meng	Peking University, Beijing, China	*Tests of an Ensemble Kalman Filter for Mesoscale and Regional Scale Data Assimilation*

IPRC VISITING SCHOLARS

The IPRC has a visiting scholar program. From April 2008 to March 2009, the following scholars visited the IPRC for one week or longer.

Name	Affiliation	Dates
Yoshikaza Sasai	Japan Agency for Marine-Earth Science & Technology, Yokohama, Japan	02/16/09–03/24/09
Tommy Jensen	Naval Research Laboratory, Stennis Space Center, Mississippi	02/09/09–02/13/09
George Boer	University of Victoria, Victoria, British Columbia, Canada	02/02/09–03/06/09
In-Sik Kang	Seoul National University, Seoul, Korea	01/17/09–02/16/09
Wataru Ohfuchi	Japan Agency for Marine-Earth Science & Technology, Yokohama, Japan	01/14/09–02/12/09
Hiroyuki Murakami	Advanced Earth Science & Technology Organization, Tokyo, Japan	12/01/08–02/25/09
Alan Plumb	Massachusetts Institute of Technology, Boston, Massachusetts	11/04/08–11/14/08
So-Young Yim	Seoul National University, Seoul, Korea	10/17/08–11/21/08
Jong-Ghap Jhun	Seoul National University, Seoul, Korea	09/01/08–11/30/08
Hyodae Seo	University Corporation for Atmospheric Research, Boulder, Colorado	08/05/08–12/17/09
Raleigh Hood	University of Maryland, Maryland	07/25/08–08/01/08
P.N. Vinayachandran	India Institute of Science, Bengaluru, India	07/21/08–08/03/08
Ai-Lan Lin	Institute of Tropical and Marine Meteorology, Guangzhou, China	04/13/08–07/14/08
Hitoshi Irie	Japan Agency for Marine-Earth Science & Technology, Yokohama, Japan	04/21/08–04/24/08

IPRC RESEARCH SUPPORT

Institutional Support

Title	PI and Co-PIs	Agency	Amount	Period
Enhancement of Data and Research Activities for Climate Studies at the International Pacific Research Center (IPRC)	K. Hamilton, P. Hacker & J. Potemra	NOAA	$1,218,000	10/01/08–09/30/09
JAMSTEC YR 12, (2008 – 2009)	K. Hamilton	JAMSTEC	$2,316,000	04/01/08–03/31/09
Support of Research at the International Pacific Research Center	Not applicable	*University of Hawai'i	$528,670	04/01/08–03/31/09
Data-Intensive Research and Model Development at the International Pacific Research Center	K. Hamilton, S.P. Xie & P. Hacker	NASA	$1,103,000	03/01/07–02/29/12

* The University of Hawai'i also provides approximately 16,500 sq. ft. of office space to the IPRC

Individual Grants

Title	PI and Co-PIs	Agency	Amount	Period
A Tropical Cyclone Genesis Forecast Model	T. Li	ONR	$176,400	02/16/09–05/31/12
Near-real time debris distribution in the North Pacific	N. Maximenko	NFWF/NOAA	$69,909	01/01/09–12/31/09
Dynamics of anisotropic mean and time-varying structure of ocean circulation	N. Maximenko, E. Di Lorenzo, & N. Schneider	NASA	$719,963	10/01/08–09/30/12
Arrangement of historical observation dataset for Phillipines Meteorological stations III	A. Timmermann	JAMSTEC/ IORGC	$5,139	09/16/08–12/26/08
Toward reducing climate model biases in the equatorial Atlantic and adjacent continents	S.P. Xie & I. Richter	NOAA/CPO	$342,124	07/01/08–06/30/11
Changes of tropical Pacific climate variability during the last millennium	A. Timmermann & O. Timm	NOAA	$191,851	07/01/08–06/30/13
Precipitation Climatology Projections for Mid and Late 21st Centuries for the Main Hawaiian Islands	K. Hamilton	USGS	$42,427	06/01/08–05/31/09
Application of multi satellite radiance products to NRL NAVDAS	T. Li & S. Zhang	DoD-PET	$74,500	06/01/08–04/30/09
Development of an Extended and Long-range Precipitation Prediction System over the Pacific Islands	H. Annamalai	NOAA	$443,586	05/01/08 - 04/30/11
Scale Interactions in the equatorial ocean	K. Richards & J. McCreary	NSF	$595,444	05/01/08–04/30/11
Quantifying the effects of vortical hot towers and vortex Rossby waves on tropical cyclone intensification	T. Li	NPS	$49,400	04/29/08–03/15/09
Development of long-lead coupled climate model prediction and intraseasonal prediction system	B. Wang	APCC	$158,618	04/01/08–12/31/08
Study of Processes Leading to Tropical Cyclone Structure and Intensity Changes	Y. Wang	NSF	$398,016	04/01/08–03/31/10
Analysis and High-Resolution Modeling of Tropical Cyclogenesis during TCS-08 and TPARC Field Campaign	T. Li & M. Peng	ONR	$231,243	01/01/08–12/31/10

Title	PI and Co-PIs	Agency	Amount	Period
Climate Change and Persistent Droughts: Impacts, Vulnerability and Adaptation in Rice Growing Subdivisions of India	H. Annamalai	Norwegian Embassy	$127,053	12/07/07–11/30/10
Collaborative Research: Impacts of ocean physics on the Arabian Sea oxygen minimum zone	J. McCreary, K. Richards, & Z. Yu	NSF	$385,570	10/01/07–09/30/10
UH/MHPCC Generation of Submesoscale	K. Richards	MHPCC-Engagement Grant	$35,174	08/25/07–06/30/09
Understanding Annual Cycle-ENSO Interactions in Climate Change Simulations	N. Schneider & A. Timmermann	DOE	$142,877	08/15/07–08/14/08
Measurements of the velocity field associated with interleaving	K. Richards	NSF	$117,330	08/01/07–01/31/09
Evaluation and Improvement of NOAA Climate GCM Air-Sea Interaction Physics: An EPIC/VOCALS Synthesis Project	Y. Wang, S.P. Xie, & S. de Szoeke	NOAA / OGP/ CPPA	$275,384	08/01/07–07/31/10
Future Projections of Mean and Variability of the Asian Summer Monsoon and Indian Ocean Climate Systems	H. Annamalai	DOE	$165,836	08/01/07–07/31/11
Understanding climate-biogeochemical feedbacks during the last glacial-interglacial transition: A systematic modeling and paleo-data synthesis approach	A. Timmermann	NSF	$314,100	07/01/07–06/30/10
PI-GCOS Server Reimbursement	J. Potemra	Bureau of Meteorology Australia	$20,000	06/01/07–05/31/09
Improving the COAMPS atmospheric variational data assimilation system with direct use of satellite radiances	T. Li & X. Zhang	DOD-PET / ONR	$68,000	06/01/07–05/31/08
Inter-annual variability and prediction on eddies in the Gulf of Aden and the Somali Current Region	J. McCreary	ONR	$103,050	05/01/07–09/30/09
Analysis of climate change in Korea and East Asia area and study of the atmospheric and ocean effects	B. Wang	Yonsei University	$121,279	04/01/07–12/31/09
Collaborative Research: Decadal Coupled Ocean-Atmosphere Interactions in the North Pacific	N. Schneider	NSF	$72,365	03/01/07–02/28/10
Dynamics of Boreal Summer Intraseasonal Oscillation	B. Wang & J. Fu	NSF	$342,883	03/01/07–02/28/09
Acceleration of the Last Glacial Termination Due to Climate-Carbon Cycle Feedbacks	A. Timmermann	NSF	$42,465	02/01/07–01/31/09
Western Pacific Tropical Cyclone Reanalysis with the NRL Atmospheric Variational Data Assimilation System (NAVDAS)	T. Li & X. Zhang	ONR	$180,957	01/01/07–08/31/10
Using a Digital Filter As a Weak Constraint in WRF 4D-VAR	T. Li & X. Zhang	NCAR	$105,816	11/01/06–07/31/08
Collaborative Research: Origin, Pathway and Fate of Equatorial 13°C Water in the Pacific	T. Qu & I. Fukumori	NSF	$486,210	09/01/06–08/31/10
Dynamics of Tropical Cyclone Intensity Change	T. Li	ONR / NRL	$91,000	09/01/06–08/31/09
Orographically Induced Ocean-Atmosphere Interaction: Satellite Observations and Numerical Modeling	S.P. Xie	NASA	$248,162	06/15/06–06/24/10

Title	PI and Co-PIs	Agency	Amount	Period
Effects of the Stratospheric Quasi-biennial Oscillation on Seasonal Predictability of Tropospheric Circulation in the Northern Hemisphere Extratropics	K. Hamilton	NOAA-CLIVAR	$166,355	06/01/06–05/31/09
Collaborative Research: Eddy Dynamics and Impacts of Low Frequency Variations in the California Current System	N. Schneider	NSF	$193,340	03/01/06–02/28/10
Validation of Alternating Zonal Jets Detected in Satellite Altimetry Using In-Situ Observations	N. Maximenko	NSF	$170,147	02/15/06–01/31/09
An adaptive food web model for the epipelagic and mesopelagic	K. Richards	LSU	$95,531	02/01/06–07/31/08
Tropical Cyclone Genesis and Sudden Changes of Track and Intensity in the Western Pacific	B. Wang, T. Li & Y. Wang	ONR	$643,500	01/01/06–09/30/08
Ship-board Atmospheric Sounding over the Kuroshio Extension: A Supplement to CLIVAR KESS	S.P. Xie & B. Qiu	NSF	$219,707	04/01/05–03/31/09
Dynamic Balance of the Oceanic Mixed Layer Observed by In Situ Measurements and Remote Sensing	N. Maximenko	NASA / Scripps	$332,614	01/01/05–03/31/09
Study of Processes Leading to Tropical Cyclone Intensity Change	Y. Wang	NSF	$278,840	10/15/04–09/30/08
Predictability and Diagnosis of Low Frequency Climate Processes in the Pacific	N. Schneider	DOE	$150,002	09/15/04–09/14/09
Application of Satellite Data to Improve the Simulation and Prediction of Tropical Intraseasonal Oscillation	J. Fu, B Wang, & X. Xie	NASA	$272,333	06/01/04–05/31/08
Analysis of Climate Change in Korea and East Asia Area and Study of the Atmospheric and Ocean Effects	B. Wang	Yonsei University	$149,199	06/01/04–12/31/09
Application of Comprehensive Global Models to Problems in the Dynamics of the Troposphere and Stratosphere	K. Hamilton	NSF	$322,809	09/01/02–05/31/08

IPRC STAFF*

FACULTY

HACKER, Peter
HAMILTON, Kevin
LI, Tim
McCREARY, Julian
POTEMRA, Jim
RICHARDS, Kelvin
SCHNEIDER, Niklas
TIMMERMANN, Axel
WANG, Bin
WANG, Yuqing
XIE, Shang-Ping

RESEARCHERS

ANNAMALAI, H.
FU, Joshua, Xiouhua
FURUE, Ryo
LEE, June-Yi
MAXIMENKO, Nikolai
NAKAMURA, Mototaka
NATAROV, Andrei
QU, Tangdong
YU, Zuojun

TECHNICAL STAFF

BURNS, Dave
DeCARLO, Sharon
HAFNER, Jan
JIA, Yanli
LEBEDEV, Konstantin
LIU, Ping
MERRILL, Ron
SHEN, Yingshuo

ADMINISTRATIVE SUPPORT

HO, Jeanie
NAKAJIMA, Aimee
WAKUMOTO, Lori

OUTREACH

SPEIDEL, Gisela
TOKINAGA, Keiko

POSTDOCTORAL FELLOWS

CHEN, Ju
CHOWDARY, Jasti
FRIEDRICH, Tobias
FUDEYASU, Hironori
GE, Xuyang
KADOTA, Minoru
KAJIKAWA, Yoshiyuki
KIKUCHI, Kazuyoshi
KIM, Hyung Jin
KWON, Min Ho
LAUER, Axel
McGREGOR, Shayne
MELNICHENKO, Oleg
MENVIEL, Laurie
RICHTER, Ingo
SAMPE, Takeaki
SASAKI, Yoshinori
SEO, Hyodae
SOMA, Kazuyoshi
SOORAJ, K.P. Veettil
TIMM, Oliver
TOKINAGA, Hiroki
WANG, Lei
XU, Jing
YOSHIDA, Sachiko
ZHANG, Shengjun

*As of March 31, 2009

A publication of the
International Pacific Research Center
School of Ocean and Earth Science and Technology
University of Hawai'i at Mānoa
1680 East-West Road, POST Bldg., Room 401
Honolulu, Hawai'i 96822

Tel: (808) 956-5019 Fax: (808) 956-9425
Web: http://iprc.soest.hawaii.edu

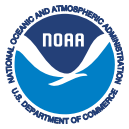

The IPRC is a climate research center funded by governmental agencies in Japan and the United States and by the University of Hawai'i.